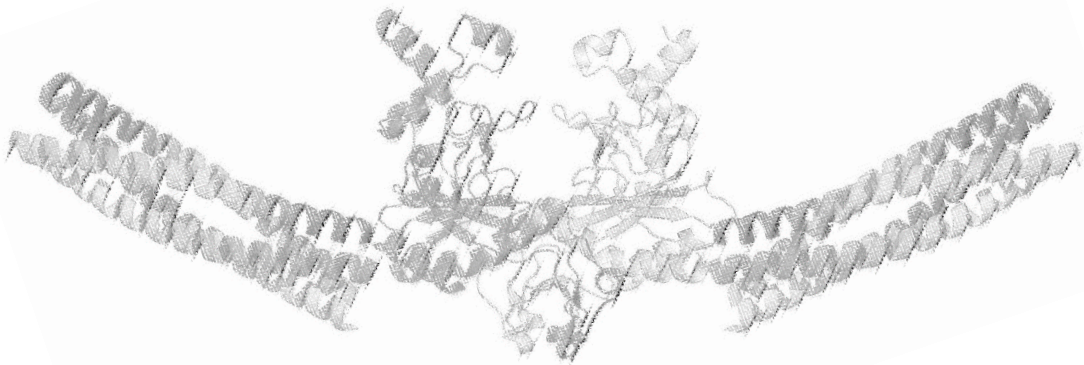


Analysis of the sliding process of restriction enzymes



Inauguraldissertation

zur Erlangung des Grades
Doktor der Naturwissenschaften

Dr. rer. nat.

Im Fachbereich Biologie und Chemie
der Justus-Liebig-Universität Gießen

vorgelegt von
Apothekerin

Carolin Menges

Gießen, 2015

Die vorliegende Arbeit wurde im Rahmen des Graduiertenkollegs „*Enzymes and Multienzyme Complexes Acting on Nucleic Acids*“ (GRK 1384) am Institut für Biochemie des Fachbereichs 08 der Justus-Liebig-Universität in Gießen in der Zeit von Februar 2010 bis Oktober 2013 unter der Leitung von Prof. Dr. Alfred Pingoud durchgeführt.

Erstgutachter: Apl. Prof. Dr. Peter Friedhoff
Institut für Biochemie
Fachbereich Biologie und Chemie
Heinrich-Buff-Ring 58
35392 Gießen

Zweitgutachter: Prof. Dr. Reinhard Dammann
Institut für Genetik
Fachbereich Biologie und Chemie
Heinrich-Buff-Ring 58-62
35392 Gießen

Erklärung

Hiermit versichere ich, die vorliegende Dissertation selbständig und ohne fremde Hilfe verfasst zu haben und keine anderen als die hier angegebenen Hilfsmittel benutzt zu haben. Alle Textstellen, die wörtlich oder sinngemäß aus veröffentlichten Schriften entnommen sind, und alle Angaben, die auf mündlichen Auskünften beruhen, sind als solche kenntlich gemacht.

Gießen, den 23. Juni 2015

(Carolin Menges)

Danksagung

Als aller erstes möchte ich mich sehr herzlich bei **Prof. Dr. Alfred Pingoud** bedanken, dafür dass er mich als „fachfremde“ Pharmazeutin in seine Arbeitsgruppe aufgenommen und mir dadurch die Möglichkeit zur Erstellung dieser Dissertation gegeben hat. Lieber Ping, ich danke Ihnen für Ihre engagierte und liebevolle Betreuung, für die vielen hilfreichen Ratschläge und natürlich für die unzähligen Fotos Ihrer Blümchen aus dem Garten, mit denen Sie mir immer eine Freude bereitet haben. Vielen Dank für Ihr Vertrauen in mich und meine Arbeit. Ich hätte mir keinen besseren Doktorvater vorstellen können.

Prof. Dr. Reinhard Dammann danke ich für die Übernahme des Zweitgutachtens.

Ich danke **Dr. Wolfgang Wende** für die hervorragend wissenschaftliche und liebevolle Betreuung meiner Arbeit. Wollte, Danke für Deine große Geduld und Dein immer offenes Ohr, für die stetige Motivation und Unterstützung und ganz besonders für die Momente in denen Du mit Deinen „Zauberhänden“ die Dinge wieder zum Laufen gebracht hast.

Ich danke **Prof. Dr. Peter Friedhoff** für die zahlreichen wissenschaftlichen Diskussionen (ob auf dem Flur oder vor dem Kaffeeautomaten), für die genialen Ideen und hilfreichen Ratschläge, für die konstruktive Kritik und natürlich für die Aufnahme ins IRTG.

Ein riesen Dank geht an das Sekretariat. **Ina** und **Karina**, Danke dass ihr euch um alle bürokratischen Belange gekümmert und zudem auch immer ein offenes Ohr für Probleme jeglicher Art gehabt habt. **Anja**, danke für die tolle Organisation aller IRTG Aktivitäten.

Ich danke **Ines** und **Jasmina** für die schöne und lustige Zeit im Labor 1. Danke, dass ich euren großen Schreibtisch bekommen habe nachdem ihr fertig wart ☺. Ines, Dir danke ich ganz besonders für die seelische und moralische Unterstützung, für die vielen Gespräche und hilfreichen Diskussion und für die lustigen Dart und Billardabende zusammen mit Roger. Von Dir kann man echt viel lernen!

Ich danke **Sabrina**, **Betty** und **Heike** für die technische Unterstützung im Labor. Sabrina, danke, dass Du mich an Anfang meiner Arbeit in alles eingewiesen und begleitet hast und dass man auch sonst mit Dir immer über alles quatschen konnte.

Darüber hinaus möchte ich mich beim Rest meiner Arbeitsgruppe am Institut für Biochemie bedanken. **Mert**, **Andi**, **Lilly**, **Laura**, **Fabian** und **Ping Ping**, Danke für die tolle Arbeitsatmosphäre und die lustigen Weihnachtsfeiern. Ich hatte mit euch eine wunderschöne und unvergessliche Zeit.

Ich danke allen Mitgliedern des **IRTG's** und des **GGL's** für die gute Zusammenarbeit und die angenehme Arbeitsatmosphäre, für die zahlreichen Diskussionen in Seminaren und für die interessanten Konferenzen.

Ich möchte ich mich bei meinen beiden **Kollaborationspartnern** aus Würzburg (Markus Sauer, Sören Doose und Sebastian Letschert) und Paris (Pierre Desbiolles und Jasmina Dikic) für die gute Zusammenarbeit, freundliche Aufnahme und Betreuung und vor allem für die Einweisung in Fluoreszenzmikroskopie und Einzelmolekülstudien bedanken.

Mein Dank gilt zudem allen Studenten, die mich im Rahmen meiner Arbeit unterstützt haben. Besonders zu nennen ist hier **Bianca**, die für mich unzählige Anisotropie Messungen durchgeführt hat.

Ich danke meinen liebsten Freundinnen **Isa**, **Romy** und **Elena** für ihr Interesse an meiner wissenschaftlichen Arbeit, auch wenn es manchmal über ihre Vorstellungskraft hinaus ging (nein Romy, die Proteine kann man nicht im Eppi sehen... ☺) Danke für eure aufbauenden Worte und dafür, dass ihr immer an mich geglaubt habt.

Ganz besonders möchte ich mich aber bei meiner **Familie** und meinem **Freund** bedanken. Danke für eure grenzenlose Unterstützung, für euer Verständnis und Vertrauen in allem was ich mache, für die vielen hilfreichen Ratschläge fernab der Wissenschaft und für die aufmunternden Worte, wenn's mal nicht so gut lief. Ohne euch wäre das alles nicht möglich gewesen. Danke, dass ihr immer für mich da seid. Ich liebe euch von ganzem Herzen!!!

Meinem Doktorvater

Prof. Dr. Alfred Pingoud

gewidmet



Publications

Dikić J., **Menges C.**, Clarke S., Kokkinidis M., Pingoud A., Wende W., Desbiolles P. *The rotation-coupled sliding of EcoRV*. Nucleic Acids Res. 2012 May; 40 (9):4064-70

Heller I., Sitters G., Broekmans O.D., Farge G., **Menges C.**, Wende W., Hell S.W., Peterman E.J.G., Wuite G.J.L. *STED nanoscopy combined with optical tweezers reveals protein dynamics on densely covered DNA*. Nature Methods. 2013 Sep; 10 (9):910-6

Menges C., Dikić J., Friedhoff P., Wende W., Pingoud A. *Facilitated diffusion of Type II restriction endonucleases depends on size, conformation and salt concentration*. In preparation.

Oral presentations

June 2010, **Moscow** (Russia)

Off-Spring Meeting IRTG 1384

“Analysis of protein DNA interactions by single molecule experiments”

September 2011, **Gießen** (Germany)

4th GGL Annual Conference

„Analysis of the sliding process of restriction enzymes“

→ **GGL Presentation Award for the best talk**

June 2012, **Bochum** (Germany)

19. Arbeitstagung “Mikromethoden in der Proteinchemie”

„Untersuchung des Sliding Prozesses von Restriktionsenzymen unter Verwendung von Einzelmolekültechniken“

→ **Thermo Fisher Scientific Price for the best talk**

Poster presentations

May 2010, **Vilnius** (Lithuania)

Workshop IRTG 1384 “Enzymes and multienzyme complexes acting on nucleic acids”

„Analysis of the sliding process of restriction enzymes by single molecule techniques“

August 2010, **Bremen** (Germany)

6th NEB Meeting on DNA Restriction and Modification

„Analysis of the sliding process of restriction enzymes by single molecule techniques“

September 2010, **Gießen** (Germany)

3th GGL Annual Conference

„Analysis of the sliding process of restriction enzymes by single molecule techniques“

September 2011, **Frankfurt am Main** (Germany)

GBM Tagung „Molecular Life Sciences“

„Analysis of the sliding process of restriction enzymes by single molecule techniques“

August 2012, **Oxford** (England)

73rd Harden Conference „Machines on genes II - The central dogma at the interface of biology, chemistry and physics“

„Analysis of the sliding process of restriction enzymes by single molecule techniques“

September 2012, **Gießen** (Germany)

5th GGL Annual Conference

„Analysis of the sliding process of restriction enzymes by single molecule techniques“

Abbreviations

α	alpha
aa	Amino acids
AdoMet	Adenosyl methionine
APS	Ammonium peroxide sulfate
ATP	Adenosine triphosphate
bp	Base pair
BHQ	Black hole quencher
BSA	Bovine serum albumin
CCD	Charge coupled device
CF	Correction factor
CIAP	Calf intestinal alkaline phosphatase
Δ	delta
D_1	one-dimensional diffusion coefficient
Da	Dalton
DMSO	Dimethylsulfoxid
DNA	Deoxyribonucleic acid
dNTP	Deoxyribonucleic triphosphate
DOL	Degree of labeling
DTT	1,4-Dithiotreitol
ε	Extinction coefficient
E	FRET efficiency
<i>E. coli</i>	<i>Escherichia coli</i>
e.g.	<i>Exempli gratia</i> (for example)
EDTA	Ethylenediaminetetraacetic acid
ξ	Friction coefficient
FCS	Fluorescence correlation spectroscopy
FP	Fusion protein scRM6 D54C – EcoRV C21S
FRET	Förster resonance energy transfer
g	gram
HEX	Hexachloro fluorescein
His	Histidin
HPLC	High performance liquid chromatography
i.e.	<i>It est</i> (such as)
IPTG	Isopropyl- β -D-1-thiogalactopyranoside
k	kilo
k_{cat}	turnover number
K_D	equilibrium dissociation constant
k_{diff}	diffusion constant
K_M	Michaelis-Menten constant
k_{on}	association rate constant
k_{off}	dissociation rate constant
KGB	Potassium glutamate buffer

λ	lambda (wavelength or sliding length)
l	liter
LB	Luria bertani
LEW	Lysis-, equilibration- and wash
lin	linear
μ	micro
m	milli
M	Molar
min	minute
MSD	Mean squared displacement
MT	Methyl transferase
MW	Molecular weight
n	nano
NTA	Nitrilotriacetic acid
o/n	over night
oc	open circle
OD	Optical density
p	pico
PAGE	Polyacrylamide gel electrophoresis
PBS	Phosphate buffered saline
PCR	Polymerase chain reaction
PEG	Polyethylene glycol
r	anisotropy
RE	Restriction endonuclease
rpm	rotations per minute
RT	Room temperature
s	second
sc	supercoiled or single chain
SDS	Sodium dodecyl sulfate
STE	Sodium-tris-EDTA
t	time
τ	dwel time
TBE	Tris-borate-EDTA
TCA	Trichlor acidic acid
TCEP	Tris(2-chlorethyl)phosphate
TEMED	N,N,N',N'-tetramethylethylenediamin
TIRFM	Total internal reflection fluorescence microscopy
TM	Temperature
TPE	Tris-phosphate-EDTA
Tris	Tris-(hydroxymethyl)-aminomethan
UV	ultraviolett
V	volume
vs.	versus
wt	wild type

Table of content

Abbreviations	9
Table of content.....	11
1 Introduction.....	14
1.1 <i>Restriction enzymes</i>	14
1.1.1 Type II restriction enzymes	15
1.1.1.1 Three dimensional structure of Type II restriction enzymes	16
1.1.1.2 Target site location of Type II restriction enzymes	24
1.2 <i>Single-molecule experiments</i>	28
1.2.1 Studying rotational motion by single-molecule experiments	33
1.3 <i>Aim</i>	35
2 Material and methods.....	37
2.1 <i>Material</i>	37
2.1.1 Chemicals.....	37
2.1.2 Buffers	38
2.1.3 Bacterial strains.....	40
2.1.4 Plasmids	41
2.1.5 Oligonucleotides	42
2.1.6 Enzymes and proteins	45
2.1.7 Markers	46
2.1.8 Fluorophores	46
2.2 <i>Methods</i>	48
2.2.1 Microbiological methods	48
2.2.1.1 Preparation of electro-competent cells	48
2.2.1.2 Electroporation.....	48
2.2.2 Molecular biology methods	49
2.2.2.1 Electrophoresis.....	49
2.2.2.2 Polymerase chain reaction (PCR)	50
2.2.2.3 Isolation of DNA	51
2.2.2.4 Ethanol precipitation.....	51

2.2.2.5	Determination of DNA concentration.....	52
2.2.2.6	Site-directed mutagenesis	52
2.2.2.7	Cloning.....	53
2.2.2.8	Screening	54
2.2.2.9	Protein overexpression.....	54
2.2.2.10	Protein purification	55
2.2.2.11	TCA precipitation	57
2.2.2.12	Determination of protein concentration	57
2.2.2.13	Determination of protein cleavage activity.....	57
2.2.2.14	PEG modification	58
2.2.3	Fluorescence spectroscopy based methods.....	58
2.2.3.1	Binding activity studied by fluorescence anisotropy	58
2.2.3.2	Michaelis-Menten kinetics.....	60
2.2.3.3	Competitive cleavage assay	62
2.2.3.4	Fluorescent labeling	63
2.2.3.5	Determination of the degree of labeling (DOL)	65
2.2.3.6	FRET measurements.....	65
2.2.3.7	Single-molecule experiments.....	70
3	Results	71
3.1	<i>Preparation of an elongated restriction enzyme to study rotational motion..</i>	<i>71</i>
3.1.1	Preparation of the scRM6-EcoRV fusion protein.....	73
3.1.1.1	Purification of the scRM6-EcoRV fusion protein	75
3.1.2	Biochemical characterization of the scRM6-EcoRV fusion protein	77
3.1.2.1	Determination of cleavage activity	77
3.1.2.2	Determination of binding activity.....	78
3.1.2.3	Michaelis-Menten kinetics.....	80
3.1.3	Studying the spatial expansion via FRET.....	81
3.1.4	Single-molecule experiments.....	85
3.2	<i>Comparison of structurally different restriction enzymes</i>	<i>88</i>
3.2.1	Preparation of single-cysteine variants	88
3.2.1.1	Determination of binding and cleavage activity	89
3.2.1.2	Testing the accessibility of single-cysteine residues	90
3.2.1.3	Site-specific labeling of single-cysteine variants.....	91

3.2.2	Studying the conformation of structurally different restriction enzymes ...	93
3.2.3	Studying linear diffusion of structurally different restriction enzymes	104
3.2.3.1	Substrate length dependence of linear diffusion	105
3.2.3.2	Salt dependence of linear diffusion	112
3.2.3.3	Structure dependence of linear diffusion	117
4	Discussion	120
4.1	<i>Preparation of an elongated restriction enzyme to study rotational motion</i>	120
4.1.1	Preparation of the scRM6-EcoRV fusion protein	121
4.1.2	Biochemical characterization of the scRM6-EcoRV fusion protein	123
4.1.3	Studying the spatial expansion via FRET	125
4.1.4	Single-molecule experiments	127
4.2	<i>Comparison of structurally different restriction enzymes</i>	<i>132</i>
4.2.1	Preparation of single-cysteine variants	132
4.2.2	Studying the conformation of structurally different restriction enzymes .	134
4.2.3	Studying linear diffusion of structurally different restriction enzymes	144
5	Summary.....	152
6	Zusammenfassung	154
7	References.....	156

1 Introduction

1.1 Restriction enzymes

Restriction enzymes are specific endonucleases and components of restriction modification (RM) systems that can be found among bacteria [1], archaea [2] and in certain viruses [3]. Their main function *in vivo* is the protection of their host against foreign DNA, e.g. phage DNA. However, restriction enzymes are also important *in vitro* tools for recombinant DNA work and widely-used in molecular biological and biochemical laboratories.

Restriction modification (RM) systems consist of a restriction endonuclease and a corresponding DNA-methyltransferase [4-6] (Figure 1). Both components recognize the same DNA sequence, usually 4 – 8 bp in length. The restriction endonuclease induces a double strand break at the recognition sequence whereas the methyltransferase adds a methyl group to adenine (N6) or cytosine (N4 or C5) in each strand of the recognition sequence. In order to defend the organism, the restriction endonuclease has to recognize and cleave the incoming foreign DNA. The host genome is modified by the methyltransferase and thereby protected from cleavage by the restriction endonuclease.

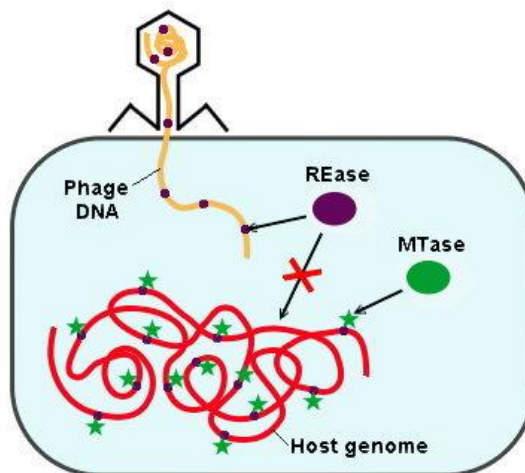


Figure 1: Schematic representation of bacterial phage infection and defense mechanism. The restriction endonuclease (REase, purple) cleaves the incoming foreign DNA (yellow) at the specific recognition site (purple dot). The host genome is modified at the specific recognition site (purple dot with green star) by the methyltransferase (MTase, green) and thereby protected from cleavage by the restriction endonuclease.

Bacteria and archaea exhibit numerous restriction modification (RM) systems. As a result, several different restriction enzymes were discovered over the years. Generally, four types of restriction endonucleases can be distinguished [7-9], based on their subunit composition, cofactor requirement and cleavage mechanism.

Type I restriction endonucleases consist of three different subunits, which are responsible for modification (HsdM), restriction (HsdR) and recognition (HsdS), respectively. Type I restriction endonucleases require ATP, Mg^{2+} and S-adenosyl methionine (AdoMet) for their activity and interact with two asymmetrical bi-partite recognition sites. The DNA is cleaved distal to the recognition site, approximately half-way between two sites [10,11].

Type II restriction endonucleases are the most frequently found enzymes and can be further divided into different subtypes [12]. Enzymes belonging to this type are used as powerful tools for genetic engineering processes. All restriction enzymes used in this work (EcoRV, PvuII and BsoBI) belong to this type and are further described in chapter 1.1.1.

Type III restriction endonucleases consist of two different subunits, which are responsible for recognition / modification (Mod) and cleavage (Res). Type III restriction endonucleases require ATP and Mg^{2+} for their activity and are stimulated by AdoMet. They interact with two asymmetrical head-to-head recognition sites and cleave the DNA close to one recognition site [13,14].

Type IV restriction endonucleases consist of two different subunits, which are responsible for recognition and cleavage. Type IV enzymes cleave methylated DNA, hence they are not part of a RM system. They require GTP and Mg^{2+} for their activity and interact with at least two recognition sequences at a variable distance. Cleavage of the DNA occurs close to one recognition site [15].

1.1.1 Type II restriction enzymes

Type II restriction enzymes are the biochemically and structurally best characterized specific nucleases [12,16-18]. In comparison to other types, Type II restriction endonucleases have a more simplified subunit organization, being usually homodimeric or homotetrameric. Cleavage of the DNA occurs within or close to their recognition site. Type II restriction endonucleases do not require ATP or GTP, but still require Mg^{2+} as cofactor. Because of their great diversity, they are further divided into 11 different subtypes, based on their properties.

Type **IIA** enzymes (e.g. Bpu10I) are dimers of non-identical subunits and recognize asymmetric sequences. Each subunit cleaves one strand of the DNA. Type **IIB** enzymes (e.g. BpII) cleave the DNA at both sides of the recognition sequence. Type **IIC** enzymes (e.g. BcgI) possess both cleavage and modification domains within one polypeptide. Type **IIE** enzymes (e.g. EcoRII, NaeI) interact with two copies of their recognition sequence, one being the target, the other being an allosteric effector. Type **IIF** enzymes (e.g. Cfr10I, SfiI) are homotetrameric, interact with two copies of their recognition sequence and cleave both of them. Type **IIG** enzymes (e.g. Eco57I) have both cleavage and modification domains within one polypeptide and are a subgroup of Type IIC enzymes. Most of them are also Type IIS enzymes. Type **IIH** enzymes (e.g. AhdI) behave like Type II enzymes but are genetically organized like Type I enzymes. Type **IIM** enzymes (e.g. DpnI) recognize a specific methylated sequence and cleave the DNA at a fixed site. Type **IIP** enzymes are homodimers, recognize palindromic sequences of 4 – 8 bp in length and cleave both strands within the recognition sequence producing 3'-hydroxyl and 5'-phosphate ends. Most enzymes used for genetic engineering processes are Type IIP enzymes. Some of the best-studied restriction endonucleases, as EcoRI and EcoRV, belong to this subtype. Type **IIS** enzymes (e.g. FokI, BfiI) recognize asymmetric sequences and cleave at least one strand of the DNA outside of the recognition site (cleavage site is shifted from the recognition site). Type **IIT** enzymes (e.g. BsII) are heterodimers with two different subunits.

1.1.1.1 Three dimensional structure of Type II restriction enzymes

Orthodox Type II restriction enzymes are homodimers of identical subunits. Each subunit consists of one domain (exceptions are Type IIE and IIS enzymes, which harbor two domains) which is again composed of three subdomains, each responsible for recognition, cleavage and dimerization. Although type II restriction enzymes exhibit low sequence similarity, they share common structural properties. All type II restriction enzymes possess a common core motif (CCM), which is highly conserved [17] (Figure 2). The core consists of a five-stranded mixed β -sheet, which is surrounded by two α -helices [19]. The catalytic residues of the PD...(D/E)xK motif (x represents a hydrophobic residue) are located on the second and third strand [20]. The fourth and the fifth strand can be either parallel (EcoRI) or antiparallel (EcoRV) to each other. Based on this, Type II restriction enzymes can be further divided into two different structural families, namely the EcoRI and the EcoRV family [1,21].

Enzymes belonging to the EcoRI family approach the DNA from the major groove and recognize the DNA via an α -helix and an α -loop. The resulting fragments have ‘sticky ends’ with 5’-overhangs. Well-known representatives of this family are FokI, BamHI and BsoBI. Enzymes from the EcoRV family attack the DNA from the minor groove, recognize the DNA via a β -strand and a β -turn and produce fragments with ‘blunt’ or 3’-staggered ‘sticky ends’. Representatives of this family are for example PvuII, BglI and NaeI.

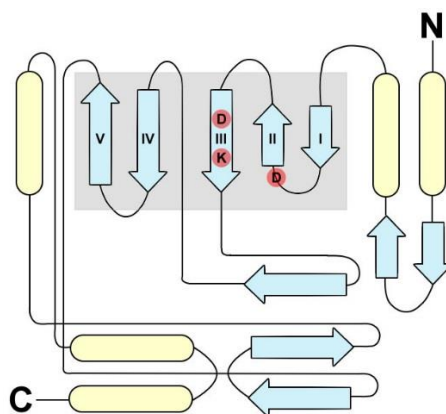


Figure 2: Topology of the Type II restriction endonuclease EcoRV. α -helices are indicated in light yellow, β -strands are indicated in light blue. The central five-stranded β -sheet is shaded grey. The location of the PD...D/ExK motif in the second and third strand is indicated in red. Note, that the fourth and fifth strand are antiparallel. C = C-terminal end of the polypeptide chain, N = N-terminal end of the polypeptide chain.

Several crystal and co-crystal structures of Type II restriction endonucleases are available in the protein data bank [22], most of them representing the free enzyme or the specific enzyme-DNA complex [18]. By comparing these two kind of structures, one can realize that restriction enzymes have to undergo large conformational changes in order to bind to DNA. And indeed, many studies revealed that binding to the specific recognition sequence is coupled to extensive changes in the conformation of the enzyme [23] (as well as changes in the conformation of the DNA). Two different types of conformational changes can be distinguished: On the one hand local conformational changes, like the structuring of regions, which are unstructured before (e.g. unfolding of α -helices to form ‘arms’ [24], folding of disordered regions [25], ordering of disordered loops [25]) and on the other hand quaternary conformational changes, like the repositioning or the rotation of subunits and subdomains. This repositioning can be achieved in a tongue-like movement [26], which means opening of the DNA-binding cleft by a motion of the two subunits perpendicular to the DNA-axis (e.g. BamHI and PvuII) or in a scissor-like movement, which means opening of the DNA-binding cleft by a motion of the subunits parallel to

the DNA-axis (e.g. EcoRV [27], BsoBI [27] and BglII [28]). Both types of conformational changes are interrelated, since local changes of flexible regions can trigger large quaternary changes of rigid regions.

As mentioned above, most structures are available for the free enzyme or the specific enzyme-DNA complex. However, the non-specific enzyme-DNA complex is an important intermediate step and it represents the structure of an enzyme diffusing along the DNA [29]. For this reason, the structure of the non-specific complex can provide important information on how the enzyme switches from non-specific to specific binding and it can give insight into what the structural basis for linear diffusion is. So far, structural information on the non-specific enzyme-DNA complex is available for two restriction enzymes only (EcoRV [30], BamHI [29]). Because of the similarities found in both systems, some general statements about the non-specific complex in comparison to the specific complex could be made: Nonspecific complexes are more hydrated at the protein-DNA interface, thus have a smaller protein-DNA contact surface and are less compact [29,30]. The DNA-binding cleft is more open and the catalytic centers are positioned far away from the phosphodiester backbone. A closing around the non-specific DNA would lead to sterical clashes, because of the non-complementarity. Additionally, a more open complex allows for more flexibility of some segments in order to scan the DNA for specific elements. The DNA is accommodated only loosely, no interactions with the bases can be observed [31]. Instead all contacts are formed to the phosphodiester backbone and are mainly electrostatic interactions and hydrogen bonds. A balance of attractive and repulsive forces holds the protein and the DNA together. In summary, the arrangement of enzyme and DNA in the non-specific complex shows up to be appropriate for preventing catalysis while allowing for sliding.

In addition to the similarities found in both systems, there is also one major difference. The crystal structure of the non-specific BamHI-DNA complex showed that the conformation was extensively rearranged compared to the specific complex [29]. For EcoRV, the non-specific complex instead revealed that the overall conformation is very similar to that of the specific complex [32]. This demonstrates, that large conformational adaptations are not necessarily required and that also small changes in the conformation are sufficient for the recognition process. The three dimensional structures of the restriction enzymes used in this study (EcoRV, PvuII and BsoBI) are described in more detail in the following section.

EcoRV restriction enzyme

EcoRV is one of the best characterized Type IIP restriction endonucleases. The name ‘Eco’ is derived from the gram-negative bacterium *Escherichia Coli* (*E. coli*), the organism from which the enzyme was firstly isolated. EcoRV forms a homodimer of two identical subunits. Each subunit contains 244 amino acids and has a molecular weight of 29.5 kDa. The enzyme recognizes the palindromic sequence 5'-GAT[↓]ATC-3' and cleaves within the central TA step, leaving ‘blunt ends’. Thus, it is numbered among the EcoRV family. For its activity, EcoRV requires Mg²⁺-ions. EcoRV is one of a few restriction enzymes, for which all relevant crystal structures are available. The free enzyme (1RVE), the non-specific complex (2RVE) and the specific complex (4RVE). Each subunit of the enzyme is organized into three different subdomains, the dimerization, the catalytic and the recognition subdomain (see Figure 3). The dimerization subdomain consists of a short α -helix and a two-stranded antiparallel β -sheet, followed by a long α -helix, which is already part of the catalytic subdomain. The catalytic subdomain consists of the common five-stranded β -sheet (two short and three long β -strands), two α -helices and a glutamine-rich-loop (Q-loop). The catalytic residues D74, D90 and K92 are located in the Q-loop and on the third β -strand, respectively and make contacts to the bases in the minor groove of the DNA. The recognition domain consists of two α -helices and two short β -strands which are connected by a loop (recognition-loop, R-loop). Residues located in the R-loop are responsible for all base-specific contacts in the major groove and contacts to the phosphodiester backbone.

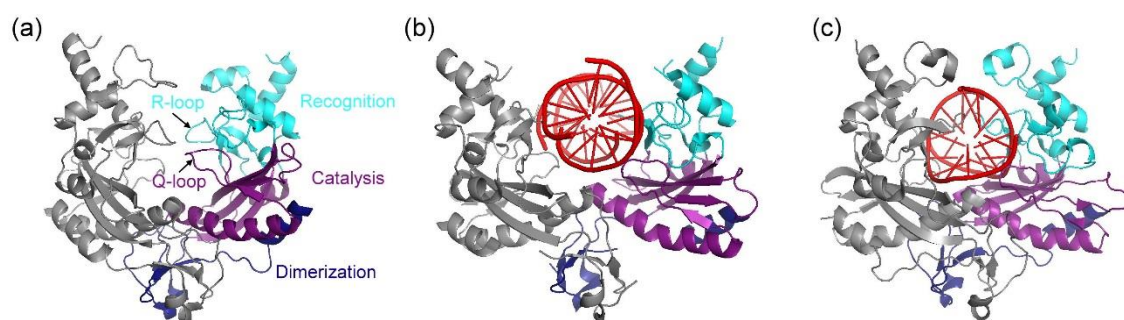


Figure 3: Crystal structures of the EcoRV restriction endonuclease. (a) Crystal structure of the free enzyme (1RVE), (b) Co-crystal structure of the non-specific EcoRV-DNA complex (2RVE), (c) Co-crystal structure of the specific EcoRV-DNA complex (4RVE). The different subdomains are marked in one subunit: blue = dimerization subdomain, purple = catalytic subdomain, cyan = recognition subdomain. The two loops (Q-loop and R-loop) are located in the catalytic and recognition subdomain, respectively. The DNA is shown in red.

The free EcoRV enzyme forms a U-shaped dimer whose cleft seems to be too narrow to accommodate DNA. The R- and the Q-loops are disordered and occupy the space in the cleft. Thus, the enzyme has to open the DNA-binding cleft to allow DNA entry. It was hypothesized, that the free restriction enzyme oscillates between an open and a closed state and that the opening is triggered by the association of the outer sides of the C-terminal arms of EcoRV with the DNA molecule [33]. The conformation of the non-specific complex seems to be more open in comparison to the free enzyme. The Q-loops, which are located at the bottom of the DNA-binding cleft become ordered [30], the R-loops instead, which are located at the top of the DNA-binding cleft stay partly disordered. They wrap over the DNA molecule, which allows them to make van der Waal's contacts with each other [30] but no contacts with the DNA bases. It was assumed, that the flexible R-loops can probe the local DNA sequence during linear diffusion [30]. The orientation of the subunits changes only slightly in the non-specific complex. The DNA is embedded in DNA-binding cleft with the minor groove facing the floor and the major groove facing the top of the cleft. It is close to B-form and no central bend of the DNA can be observed. The specific complex seems to be more closed compared to the non-specific complex. The R-loops become ordered and make contacts to the outer bases in the major groove of the DNA. The orientation of the subunits changes in a mainly scissor-like movement, which brings the two subunits closer together and allows EcoRV to embrace the DNA. In the specific complex also the conformation of the DNA changes. It becomes sharply bent by an angle of 55° , which locally unwinds the DNA, unstacks the central two base pairs of the recognition sequence and brings the scissile phosphate close to the active site. The major groove becomes narrower and deeper and the minor groove wider and shallower.

PvuII restriction enzyme

PvuII is a Type IIP restriction endonuclease and belongs to the EcoRV family. The enzyme was firstly isolated from the gram-negative bacterium *Proteus vulgaris* and is one of the smallest known restriction enzymes. It consists of two identical subunits with a molecular weight of 18.5 kDa and 157 amino acids. PvuII recognizes the palindromic sequence 5'-CAG[↓]CTG-3' and produces 'blunt ends' after the Mg^{2+} dependent hydrolysis. For PvuII, only the crystal structure of the free enzyme (1PVU) and the specific complex (1PVI) are available. Each subunit of the enzyme is organized into three different subdomains, the dimerization, the catalytic and the recognition subdomain (see Figure 4).

The dimerization subdomain consists of a long α -helix and a loop (L-AB loop), followed by a short α -helix, which is already part of the catalytic subdomain. Residues located in the L-AB loop make contacts in the minor groove of the DNA. The catalytic subdomain consists of the common five-stranded β -sheet (two short and three long β -strands), an additional short β -strands, two α -helices and a loop (L-12). The catalytic residues D58, E68 and K70 are located in the L-12 loop and on the third β -strand, respectively and make contacts to the bases in the minor groove of the DNA. The recognition subdomain is formed by two α -helices and two antiparallel β -strands. Each α -helix- β -strand pair is connected by a loop, which contains on the one hand a histidine-triplet (L-4C loop) and on the other hand an asparagine-duplet (L-7D loop), both being responsible for the specific interactions with the bases in the major groove and contacts to the phosphodiester backbone. PvuII shows an extensive structural homology to EcoRV regarding the catalytic and the recognition subdomain. The L-12 loop for example is equivalent to the Q-loop, the histidine-triplet and the asparagine-duplet (located in the L-4C and L7D loops) can also be found in the R-loop of EcoRV. The dimerization subdomains of both enzymes are instead unrelated [34].

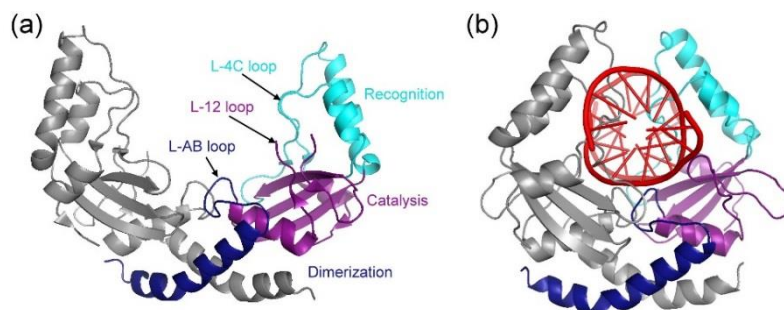


Figure 4: Crystal structures of the PvuII restriction endonuclease. (a) Crystal structure of the free enzyme (1PVU), (b) Co-crystal structure of the specific PvuII-DNA complex (1PVI). The different subdomains are marked in one subunit: blue = dimerization subdomain, purple = catalytic subdomain, cyan = recognition subdomain. The three loops (L-AB, L-12 and L-4C) are located in the dimerization, catalytic and recognition subdomain, respectively. The DNA is shown in red.

The free PvuII enzyme forms a U-shaped dimer, whose cleft is considerably more open than it could be found in other crystal structures of restriction enzymes [34]. This open conformation does not allow a complete binding to the DNA with both subunits. Only a small region at the bottom of the DNA-binding cleft (L-AB loop) could contact the DNA with both subunits simultaneously.

Since the L-AB loop is positioned at the interface between the dimerization and catalytic subdomain, it was assumed that interactions of the L-AB loop with the DNA induce motions of the subdomains, thereby bringing the enzyme in a more closed conformation [34]. Indeed, in the specific complex the two subunits approach each other, thereby closing the DNA-binding cleft in a tongue-like movement [35]. The protein wraps around the central G-C base pairs and an additional hydrogen bond is formed between the side chains of His85, which is located in the L-4C loop in the recognition subdomain of each subunit. The distance between these two histidine residues decreases by more than 20 Å during the transition from the free enzyme to the specific complex [35]. So far, it is unclear whether this hydrogen bond is also formed in the non-specific complex in order to keep the protein on the DNA while scanning for the specific recognition sequence. The DNA is located in the cleft between the two subunits with the minor groove facing the bottom and the major groove facing the top of the cleft. It retains its characteristic B-form.

BsoBI restriction enzyme

BsoBI is a thermostable Type IIP restriction endonuclease, which belongs in contrast to EcoRV and PvuII to the EcoRI family. It was isolated from the thermophilic gram-positive bacterium *Bacillus stearothermophilus* and has therefore a temperature optimum of 65°C. Each subunit of the homodimer has a molecular weight of 36.7 kDa and contains 323 amino acids. The enzyme recognizes the palindromic sequence 5'-C[↓]YCGRG-3' (Y represents a pyrimidine, and R represents a purine) and cleaves between the first and second base, leaving 'sticky ends' with 5'-overhangs. Like EcoRV and PvuII, it requires Mg²⁺-ions for DNA cleavage. For BsoBI only the crystal structure of the specific complex (1DC1) is available, which revealed that the enzyme forms a tunnel around the DNA [36]. Each subunit of the enzyme is organized into two different subdomains, the helical and the catalytic subdomain (see Figure 5). The helical subdomain consists of a total of five α -helices, beginning and ending with two very long α -helices, which cross each other and form the side walls of the tunnel. Residues located in this domain mainly form hydrogen-bonds to bases in the minor groove of the DNA. The catalytic subdomain consists of the common five-stranded β -sheet, which harbors the catalytic residues D212, E240 and K242 and is enlarged by three additional β -strands. Residues located in this domain make contacts to the bases in the major groove. Both subdomains are associated and partially wrapped around each other, resulting in the largest subunit-subunit interface among the dimeric enzymes.

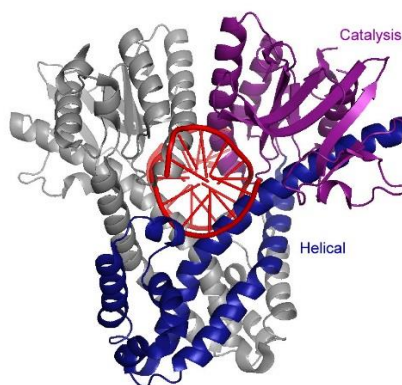


Figure 5: Crystal structure of the *BsoBI* restriction endonuclease. Co-crystal structure of the specific BsoBI-DNA complex (1DC1). The different subdomains are marked in one subunit: blue = helical subdomain, purple = catalytic subdomain. The DNA is shown in red.

The tunnel around the DNA has a length of ~ 20 Å and is formed by only α -helices from both subdomains. It has a close steric complementarity to the BsoBI recognition site, allowing a perfect alignment of enzyme and DNA. Also the electrostatic field inside the tunnel, which is positive, enhances the binding to the phosphodiester backbone. Since the gap between the two subunits is too small to allow DNA entry, it was hypothesized, that BsoBI has to undergo large conformational changes to bind to the DNA [36]. Because the interface of the catalytic domain is weaker than that of the helical domain, it is likely, that the catalytic subdomain moves apart, while the helical subdomain stays fixed. The residues Arg131 and Asn132, which are located in the helical subdomain, are supposed to be involved in the closing of the catalytic subdomain around the DNA [36]. The formation of a tunnel around the DNA could be a strategy to promote linear diffusion, because it prevents the protein from falling off the DNA. Otherwise, such a close position of enzyme and DNA and the numerous H-bonds would not favor a rapid movement along the DNA. It was therefore postulated that the enzyme forms a more open complex with non-specific DNA [36]. The DNA itself is located in the tunnel with the major groove facing the bottom and the minor groove facing the top. It shows only slight deviations from the canonical B-form. No bending is observed but the DNA is somehow extended and undertwisted, which makes the major groove wider and the minor groove shallower.

1.1.1.2 Target site location of Type II restriction enzymes

To fulfil their biological function, restriction endonucleases must locate their target site on the foreign DNA before it becomes methylated by the corresponding methyltransferase and before it is transcribed or replicated. This is a challenging task, since the enzyme has to find the specific site within a large excess of non-specific sites. A normal three-dimensional (3D) diffusion in solution, that involves association and dissociation events on the DNA, would be too slow to be effective [37]. To this end, restriction enzymes have developed a strategy, called **facilitated diffusion**, to accelerate the location of the target site [38]. This mechanism (see Figure 6) involves an initial non-specific binding anywhere on the DNA, followed by a scanning process, which is a thermally driven one-dimensional (1D) diffusion of the restriction enzyme along the DNA molecule, best described as a random walk and distinct from the ATP-driven directional translocation along the DNA (of for example Type I restriction endonucleases). Due to the reduction in dimensionality, it requires much less time than a three-dimensional (3D) search to locate the target sequence [103].

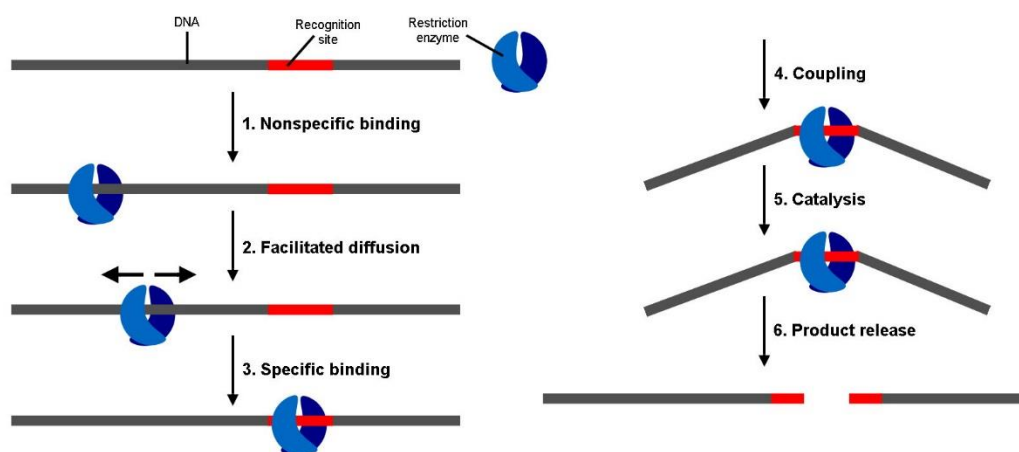


Figure 6: Schematic representation of the reaction pathway of restriction endonucleases. The restriction enzyme first binds nonspecifically to the DNA (1), which is followed by a process of facilitated diffusion along the DNA (2) until the recognition site is located and specific binding occurs (3). Subsequently, conformational changes in the protein as well as in the DNA occur (4). After the phosphodiester bond cleavage in both strands (5) the product is released (6).

Three different types of facilitated diffusion were postulated, dependent on the degree of preserving the contact between protein and DNA during the movement: (i) sliding, (ii) hopping or jumping and (iii) intersegment transfer [37-39] (see Figure 7):

Sliding, is a one-dimensional (1D) diffusion (it is 2-3 orders of magnitude slower than three-dimensional (3D) diffusion) and is also called linear diffusion. During sliding, the enzyme remains bound to the DNA, which implies that the non-specific binding mode persists during linear diffusion and that the water layer around DNA and protein remains intact. Sliding has the advantage that it prevents the enzyme from potentially missing a target site in case of following the helical pitch of the DNA. A disadvantage of sliding is that small ligands bound to the major or minor groove of the DNA represent obstacles for linear diffusion [40].

Hopping or jumping is a three-dimensional (3D) diffusion, during which the enzyme first dissociates from the DNA molecule and subsequently re-associates. The difference between hopping and jumping is based on the location of the re-association site, which can be either close to the dissociation site (hopping) or far from it (jumping). In contrast to sliding, the non-specific binding mode is transiently given up, which means that each component can associate with water molecules and counter ions. Hopping or jumping is well-suited to rapidly reach DNA sites which are far away from the initial binding site or to bypass obstacles bound to the DNA. A disadvantage is that specific sites can be overlooked, since the enzyme does not stay in continuous contact with the DNA.

Intersegment transfer takes place when an enzyme (often a tetramer), which is bound to a DNA molecule by one DNA-binding site, binds simultaneously to the same DNA molecule at a distant location via another DNA-binding site. This double binding will produce loops in the DNA. Consequently, intersegment transfer is only possible for enzymes which possess two DNA-binding sites. Intersegment transfer is well-suited to cover large distances on the DNA and is unlikely to be inhibited by obstacles.

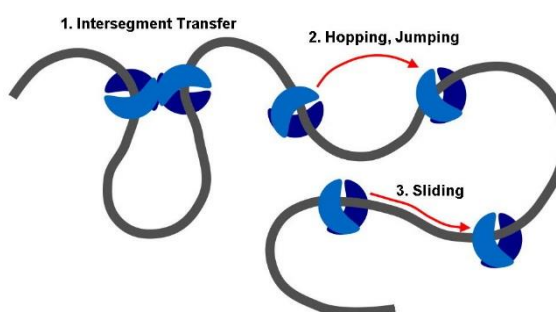


Figure 7: Schematic illustration of different types of facilitated diffusion. (1) Intersegment transfer, which involves simultaneous binding of the DNA molecule via two DNA-binding sites, (2) hopping or jumping, which involves dissociation and re-association events and (3) sliding, during which the enzyme remains bound to the DNA. The DNA molecule is indicated in grey, the two subunits of the homodimeric protein are indicated in light and dark blue.

The concept of facilitated diffusion was originally proposed in 1968 by Adam and Delbrück in order to describe the interactions between membrane receptors and their ligands [103]. In 1974, Richter and Eigen transferred the concept to specific DNA-binding proteins, which have to locate their target site on a DNA molecule [104]. The first experimental evidence of facilitated diffusion was presented in the early 1980s for the lac repressor [41] and for the restriction enzyme EcoRI [40,42,43]. It could be shown that facilitated diffusion speeds up target site location by a factor of > 10 compared to a three-dimensional (3D) diffusion [40] and that restriction endonucleases scan $\approx 10^6$ bp in one binding event, which results in an effective scanning distance of ≈ 1000 bp [40]. In the following years, facilitated diffusion was extensively examined by conventional kinetic methods [31,38,44-47], which are based on the measurement of the cleavage rate as a function of the DNA length. The experiments focused mainly on sliding (linear diffusion) rather than on hopping/jumping or intersegment transfer. It could be shown that several other type II restriction enzymes make use of facilitated diffusion for target site location [39]. The most detailed kinetic studies have been carried out with the restriction endonucleases EcoRI and EcoRV. The following observations could be made:

Dependency on the DNA length. Long DNA substrates are cleaved much faster than short DNA substrates [45], which can be easily explained by the fact that long DNA substrates can be explored not only by three-dimensional diffusion but additionally by one-dimensional diffusion.

Dependency on the Mg^{2+} - and the salt-concentration. Since linear diffusion takes place on non-specific DNA it should be dependent on the concentration of mono- and divalent metal ions. Whereas in the presence of high Mg^{2+} -concentrations (10 mM) linear diffusion was decreased for EcoRI [40], linear diffusion was increased for EcoRV [45]. The contrary behavior could be explained by the fact that EcoRI needs Mg -ions only for catalysis but EcoRV for catalysis and recognition, thus the specific sites could be better recognized at high Mg^{2+} -concentrations. Regarding the salt concentration, linear diffusion showed a maximum at 50 mM NaCl for EcoRV [45]. Higher as well as lower concentrations of NaCl decreased linear diffusion, which perfectly correlated with the tendency of the non-specific binding affinity. At high salt concentrations non-specific DNA binding is too weak, at low salt concentrations non-specific DNA binding is too tight, both prevents linear diffusion.

Overlooking of specific sites. Specific sites are not overlooked by EcoRI [44] and EcoRV [45], which means that there is a high probability that a specific site is recognized and cleaved after binding to it. This suggested that restriction enzymes stay in close contact to the DNA and scan continuously the major groove, thereby following the helical pitch [44] and that sliding is the major process of facilitated diffusion rather than hopping or jumping. Overlooking was found to be dependent on mono- and divalent metal ions. With higher concentrations of both, NaCl and Mg^{2+} -ions, the specific site was more efficiently recognized than with lower concentrations [45].

Pausing at star sites. EcoRI pauses at star sites, which means that linear diffusion is slowed down when the enzyme encounters a site on the DNA which resembles the recognition site [44]. The higher the binding affinity to the star site, the longer the pausing time and the bigger the inhibitory effect on linear diffusion [44]. This can be explained by the fact that, in contrast to non-specific sites, with star sites some base-specific contacts can be formed, as it could be demonstrated for BstYI [48]. These stronger probing interactions must be loosened again before linear diffusion can continue. The inhibitory effect of one star site could be amplified by a second star site [44]. The data suggested that restriction enzymes can adopt two different binding modes: (i) a specific binding mode, which is tight and dominated by many specific contacts between the enzyme and the bases of the DNA. The friction coefficient for linear diffusion is high, therefore the enzyme is immobile, (ii) a non-specific binding mode, which is loose and dominated by electrostatic interactions between the enzyme and the phosphodiester backbone of the DNA. The friction coefficient for linear diffusion is low and allows for sliding [44].

Influence of obstacles on the DNA. Obstacles on the DNA slow down or block linear diffusion. This could be demonstrated for obstacles in the major groove (e.g. triple helix forming oligonucleotides [44]) and in the minor groove (e.g. intercalating drugs like distamycin or netropsin [40]) as well as for non-specific [40] and specific binding proteins [44]. The question arose whether facilitated diffusion takes place also *in vivo*, since the DNA in a cell is usually associated with a variety of different proteins. It was shown that the efficiency of linear diffusion is strongly correlated with the ability to protect the cell against phage infection [31]. Thus it was assumed that linear diffusion indeed is of importance also *in vivo*. Additionally, one has to keep in mind that the biological target of restriction endonucleases is phage DNA which isn't supposed to be occupied by many proteins.

Reflection at the ends of linear DNA. It could be shown that EcoRV is reflected at the ends of a linear DNA rather than falling off from it [45]. The electrostatic potential at the ends of a linear DNA is different from that in the middle. Since linear diffusion strongly depends on the electrostatic interaction between the protein and the DNA [31], it might be difficult for the protein to approach the end by linear diffusion.

Mechanism of product dissociation. For EcoRI it could be shown that it leaves the cleavage site by linear diffusion before it dissociates from the cleavage products [42]. EcoRV instead directly dissociates from the cleavage products without using linear diffusion [45]. The different behavior was attributed to the different cleavage modes. EcoRV produces blunt ends, whereas EcoRI produces sticky ends. Blunt ends produce two additional negative charges at the 5'-phosphates, thereby pushing the cleavage products directly out of the DNA-binding tunnel of the enzyme due to electrostatic repulsion. Sticky ends remain temporary double-stranded, allowing the enzyme to diffuse to non-specific DNA.

Facilitated diffusion is a general phenomenon that could be observed not only for restriction enzymes but also for many other proteins that interact with DNA. Examples are the RNA polymerase [49,50], DNA-methyltransferases [51,52], the lac repressor [41,53] and transcription factors [54,55].

1.2 Single-molecule experiments

The target search mechanism of specific DNA-binding proteins was studied intensively by conventional kinetic methods (see 1.1.1.2). However, these bulk ensemble measurements have some major disadvantages, since they represent only an average of all different subpopulations present in the ensemble. Consequently, they cannot provide any dynamic information and therefore tend to mask rare but potentially important molecular trajectories in a given process. Regarding the target search mechanism of type II restriction enzymes, bulk ensemble methods could only show whether or not facilitated diffusion contributed to the searching process, but they could not provide detailed information regarding the mechanism itself. It became obvious that new experimental methods are required to characterize the dynamics of structures in general and specifically to elucidate the mechanism of facilitated diffusion.

A few decades ago, single-molecule methods were introduced in biochemical research [56-58]. These methods are based on optical (microscopic) techniques, which allow the direct time-resolved visualization of proteins interacting with DNA molecules. The term single-molecule experiments covers numerous different techniques, which are often combined. There are for example **fluorescence spectroscopic detection methods** [59], which can be further divided into FRET-based methods [60,61] that can probe the dynamic intra- and intermolecular interactions of proteins and nucleic acids and single-molecule tracking methods [62] that can measure the molecular position (translocation) and molecular orientation (rotational motion, see also 1.2.1). Another example are **mechanical manipulation methods** in which a defined force is applied in order to affect the dynamics of a molecule or to induce conformational changes. Examples are optical tweezers [63,64], magnetic tweezers [65,66] and laminar flow [67]. Single-molecule experiments necessitate extremely low concentrations of the interacting components (in the pM range) in order to observe only a single molecule at a given time.

To study the mechanism of facilitated diffusion of various DNA-binding proteins, **single-molecule tracking** is the method of choice, because it allows tracking the protein over many microns along the DNA molecule. To visualize the protein it has to be modified with a fluorophore (2.2.3.4). To optically resolve the motion of the labeled protein along the DNA molecule, the DNA has to be converted from the naturally occurring supercoiled into an elongated conformation. For this purpose a long DNA fragment is needed whose both ends are modified with biotin. Two different mechanical manipulation methods can be used for 'DNA stretching'. The first approach comprises the attachment of the DNA molecule to a streptavidin-coated microscope slide (or coverslip) with the aid of a laminar flow (see Figure 8) [67]. After the attachment by both ends, the DNA should retain a transversal movability so that protein binding is still possible. Also the surface of the microscope slide should not allow non-specific protein binding. The stretched DNA molecule is visualized by incubating it with a DNA groove binding dye (e.g. SYBR®gold).

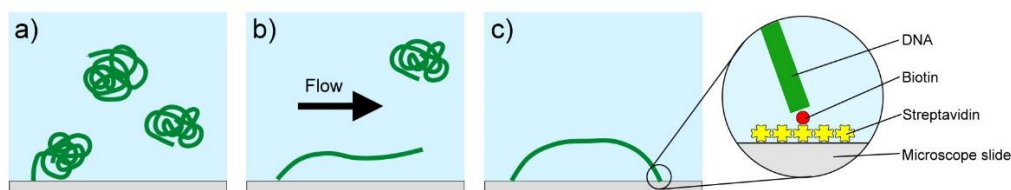


Figure 8: Elongation of DNA molecules. (a) The incubation of a streptavidin-coated microscope slide with biotinylated DNA molecules leads to the attachment of the DNA molecule by one end. (b) The application of a fast buffer flow elongates the DNA molecule and (c) leads to the attachment of the second end of the DNA molecule.

An alternative approach for ‘DNA stretching’ is the use of optical tweezers [64]. In this case both biotinylated ends of the DNA molecule are attached to streptavidin-coated polystyrol beads, which are held in position in solution by optical tweezers. This system has some advantages over the previous mentioned method. The stretching of the DNA molecule can be easily adjusted, the distance between surface and DNA is much larger ($> 3\mu\text{m}$ compared to $< 100\text{ nm}$) and the position of the DNA can be located without the use of DNA groove binding dyes.

The interaction of the labeled protein with the stretched DNA molecule is visualized by total internal reflection fluorescence microscopy (TIRFM, see Figure 9). In this technique, the excitation light is reflected off the interface between the microscope slide and the aqueous sample. Due to this special illumination geometry only a small part of the excitation light is able to enter the sample. Consequently, only proteins which are close to the surface are illuminated. This spatially limited excitation allows the detection of single fluorophores. The interaction of the protein with the DNA molecule can be seen as a short fluorescent signal within the coordinates of the stretched DNA.

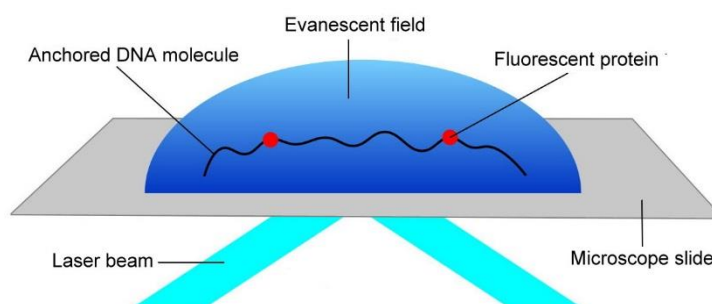


Figure 9: Total internal reflection fluorescence microscopy (TIRFM). A laser beam used for excitation of the labeled proteins is reflected off the interface between the microscope slide and the aqueous sample. The reflection generates an evanescent field, which decays exponentially into the aqueous sample. Only labeled proteins with a distance of a few hundred nanometer to the surface are illuminated.

The fluorescent signal is imaged using a charge-coupled device (CCD) camera and movies of the interaction can be recorded. One movie usually contains several interaction events between the protein and the DNA molecule. To further analyze the interaction, all images that belong to one interaction event are identified (Figure 10A). For each image, the longitudinal and transversal position of the protein on the DNA molecule has to be determined (Figure 10B). This can be done with the aid of a computer program, which fits the point spread function of the fluorophore emission with a two dimensional Gaussian function. The localization accuracy of the fluorescent spot is limited by the number of photons accumulated during the exposure time of the CCD camera. Taking all images of one interaction event together, the protein trajectory on the DNA molecule can be reconstructed. Typical protein trajectories display both the longitudinal and transversal position of the protein as a function of time (Figure 10C). From the protein trajectories the mean squared displacement (MSD) can be derived (Figure 10D).

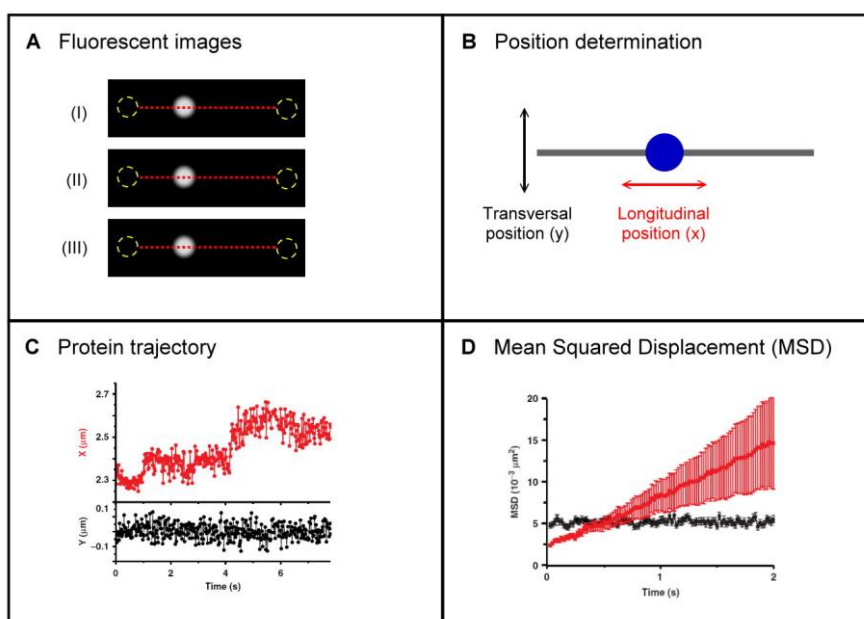


Figure 10: Analysis of the protein-DNA interaction. (A) Example of three consecutive fluorescent images. The position of the DNA is indicated by the red dashed line, the ends of the DNA are indicated by yellow dashed circles. The white spot corresponds to the fluorescent signal of the labeled protein. (B) For each fluorescent image, the transversal (y) and the longitudinal (x) position of the protein (blue spot) on the DNA (grey line) has to be determined. (C) Example of a typical trajectory of a diffusing protein. The transversal (black) and the longitudinal (red) position is plotted against the time. (D) Example of a typical MSD of a diffusing protein. The transversal (black) and the longitudinal (red) MSD is plotted against the time. *Note: Figures 10C and 10D are adopted from [67].*

The transversal MSD function is approximately constant, since the transversal motion of the protein is restricted. Fluctuations of the signal are only attributed to the thermal fluctuations of the DNA molecule. For diffusive motion, the longitudinal MSD function is expected to yield a linear graph, displaying sliding movement of the protein. The slope of the graph can be used to calculate the one-dimensional diffusion coefficient (D_1) which resembles the velocity of the protein on the DNA molecule.

$$D_1 = \frac{MSD_x(t)}{2 \cdot t}$$

By using single-molecule tracking techniques, facilitated diffusion has been visualized for various DNA-binding proteins, like T7 RNA polymerase [68], the lac repressor [69], Rad51 [70], the human oxoguanine DNA-glycosylase I [71], Msh2-Msh6 [72], tumor suppressor p53 [73] and the type II restriction endonuclease EcoRV [64,67]. In case of EcoRV it has been shown that the restriction enzyme slides along the DNA with a one-dimensional diffusion coefficient of $D_1 = 0.01 \mu\text{m}^2\text{s}^{-1}$ and that the sliding motion was interrupted by occasional jumps (translocations $> 200 \text{ nm}$) of the enzyme [67]. This led to the conclusion that an optimal searching process consists of a balanced combination of both, sliding and jumping [67]. It has further been shown that sliding was not influenced by a buffer flow whereas the number of large jumps was reduced [67]. Increasing salt concentrations (up to 60 mM NaCl) strongly reduced the interaction time of the protein with the DNA molecule whereas the mean one-dimensional diffusion coefficient (D_1) increased with increasing salt concentration [67]. In another study it was possible to directly visualize the cleavage of a specific recognition site on the DNA by EcoRV [64]. The experimental setup, based on optical tweezers, also allowed the adjustment of the DNA length. It was shown that under-stretching of the DNA ($< 100 \%$ compared to the contour length of the DNA) did not influence D_1 , whereas only 5 % overstretching of the DNA led to a decrease in D_1 by 30 %. This observation was attributed to a changed energy landscape of the DNA molecule. The one-dimensional diffusion coefficient of EcoRV was found to be $D_1 = 0.003 \mu\text{m}^2\text{s}^{-1}$, which was one order of magnitude smaller than estimated by Bonnet et al. [67]. The difference was ascribed to the larger hydrodynamic radius due to labeling with quantum dots instead of organic fluorophores [64].

1.2.1 Studying rotational motion by single-molecule experiments

Because of the helical nature of DNA, specific DNA-binding proteins are supposed to rotate around the DNA double helix during linear diffusion. This makes sense, since many proteins make non-specific contacts with the DNA backbone through electrostatic interactions [29]. In order to maintain correct register with the DNA and to sense directly the base pair sequence, translational diffusion would require a 360° rotation per helical turn. A first theoretical analysis of such a ‘rotation-coupled diffusion’ was made already in the 1970s by Schurr [74]. The one-dimensional diffusion coefficient (D_1) of a sliding protein is strongly dependent on the friction between the protein and the DNA molecule and is related to the friction coefficient (ξ) by Einstein’s equation:

$$D_1 = \frac{k_B T}{\xi}$$

where k_B is the Boltzmann constant and T the temperature. Dependent on the type of motion, friction can be translational (ξ_{trans}) or rotational (ξ_{rot}) and depends on the viscosity η of the medium and the hydrodynamic radius r of the protein (Stoke’s equation):

$$\xi_{\text{trans}} = 6\pi\eta r \quad \xi_{\text{rot}} = 8\pi\eta r^3 \left(\frac{2\pi}{10bp} \right)^2$$

From these two equations it can be deduced that in a pure translational diffusion of the protein along the DNA molecule (ξ_{trans}), D_1 decreases proportionally with increasing radius r of the protein. On the other hand, in a pure rotational diffusion of the protein around the DNA molecule, ξ is much more affected by the radius of the protein and D_1 decreases to the power of three with increasing radius r of the protein. In a rotation-coupled translational diffusion, the total friction can be easily described by the sum of the translational and the rotational friction ($\xi_{\text{total}} = \xi_{\text{trans}} + \xi_{\text{rot}}$) [74]. Since the rotational contribution to the total friction is 2 orders of magnitude larger than the translational contribution, rotation-coupled translational diffusion is expected to be substantially slower than a pure translational diffusion. For this reason, the order of magnitude of the measured one-dimensional diffusion coefficient in single-molecule experiments can provide information on whether or not rotation is involved in the sliding mechanism [74].

The Schurr rotational model has later been generalized by considering that the distance between the protein center of mass and the DNA axis can be larger than zero [75]. This so-called off-axis rotation generates slightly smaller diffusion coefficients than the on-axis rotation of the Schurr model.

The dependency of the one-dimensional diffusion coefficient on the protein radius (translational diffusion depends on r^{-1} , rotational diffusion depends on r^{-3}) can serve as a tool for identifying the basic mechanism of protein motion along a DNA molecule. Several studies have been performed which either investigated the impact of the protein size (different proteins, same label) [76] or the impact of the label size (same protein, different label) [77] on D_1 . The experimental results were compared to theoretical predictions for pure translational and rotation-coupled translational diffusion. In both studies it could be shown that D_1 decreased with increasing size of the protein or label in a way which is consistent with a rotation-coupled translational diffusion [76,77]. In addition to the verification of rotational motion by determining the one-dimensional diffusion coefficient and comparing it to theoretical models, two methodologically different approaches have been developed to determine the average orientation and thereby rotational motion of individual biomolecules. The first approach uses fluorescence polarization, the second approach is based on torque measurements.

Fluorescence polarization. Exciting a fluorophore with linear polarized light will result in the emission of linear polarized light. The intensity of the emitted polarized light is strongly dependent on the orientation of the fluorophore. If the fluorophore is coupled to a macromolecule, changes in the orientation of the macromolecule (e.g. rotation) would lead to changes in the orientation of the fluorophore and can be monitored via a change of the fluorescence intensity over time. Fluorescence polarization was first applied to study the axial rotation of myosin around the actin helix [78]. In this study the actin filament was sparsely labeled with a fluorophore and excited with linear polarized light. Myosin was bound to the glass surface of a microscope slide. When the actin filament started to slide on myosin, the orientation of labeled actin molecules was monitored via a change in fluorescence intensity, which has been separated into vertically and horizontally polarized components. The intensities of the vertically and horizontally polarized light alternated periodically showing rotational movement of actin along myosin [78]. Combination with single molecule tracking revealed that the actin filament completed a full rotation after $\sim 1 \mu\text{m}$ translocation.

Since actin has a helical pitch of ~ 72 nm, it was concluded that myosin did not follow the helical pitch but rather skipped many protomers [78]. In contrast, for the formin mDia1, a protein which regulates the polymerization of actin filaments, it has been shown that it completed a full rotation after ~ 72 nm, which is consistent with a rotational movement that follows the helical pitch of actin filaments [79].

Torque measurements. By attaching to a biomolecule a labeled tag that is huge compared to the size of the biomolecule, rotations of the biomolecule would lead to rotations of the huge labeled tag which can be imaged in real time under an optical microscope. With this technique rotational motion could be directly demonstrated for RNAP [80,81] and F_1 -ATPase [82,83]. In the former studies, RNAP was attached to the surface of a microscope slide and the DNA molecule was attached to a huge streptavidin-coated bead (diameter ~ 900 nm), which was asymmetrically labeled with a fluorophore. The DNA molecule was dragged towards the protein with the aid of optical [80] or magnetic [81] tweezers. The interaction of RNAP with the DNA molecule lead to a rotation of the DNA molecule and thereby to a rotation of the huge labeled bead. In the latter studies the continuous rotation of the central gamma subunit of the rotary motor protein F_1 -ATPase was revealed under an optical microscope by attaching to the protein either an actin filament [82] or a bead-duplex [83] as a huge labeled tag. Rotation of the protein led to rotation of the huge tag and could be visualized directly.

1.3 Aim

The location of the specific recognition sequence by restriction endonucleases is a complex process. It has been studied intensively by bulk ensemble measurements (1.1.1.2) as well as by single-molecule experiments (1.2). Nevertheless, there are still some open questions which so far have not been investigated. Two of these questions, which are related to the sliding mechanism of restriction enzymes, will be addressed in this work.

Is linear diffusion coupled to rotation?

Type II restriction enzymes slide along the DNA in the process of searching for their recognition site [64,67]. Because of the helical nature of DNA, the question arises whether sliding proteins follow the pitch of the DNA double helix or not. Several studies exist which support the hypothesis of such a rotation-coupled sliding indirectly [74-77].

However, rotational motion coupled to lateral sliding has not been directly visualized for a diffusing restriction enzyme so far, because of the restricted spatial and temporal resolution of single-molecule detection systems. To partially circumvent these limitations, an elongated restriction enzyme will be produced by extending the homodimeric restriction enzyme EcoRV with the quasi-linear protein scRM6. Initially, the prepared protein-protein fusions will be characterized extensively by biochemical and biophysical techniques. Finally, the protein-protein fusions will be fluorescently labeled at their distal ends in order to study the interaction with DNA using single-molecule techniques. On the one hand, rotational movement will be shown indirectly by measuring the one-dimensional diffusion coefficient of the fusion protein and comparing it to theoretical models. On the other hand, rotational movement will be shown directly by following the movement of the widely separated fluorescent labels by TIRFM with superior spatial resolution.

Does the structure of an enzyme influence the degree of linear diffusion?

The structure of the DNA-binding cleft and the degree of surrounding the DNA varies among different restriction enzymes. By comparing the crystal structures of PvuII, EcoRV and BsoBI (see 1.1.1.1), it can be seen that the DNA-binding cleft is open, half-closed and fully-closed, respectively. The question arises whether enzymes with a different structure of the DNA-binding cleft make use of linear diffusion to different extents, for example more for enzymes with a closed DNA-binding cleft. In this context, the structure of the non-specific complex is of particular interest since it reflects the structure of an enzyme that slides along the DNA [29]. Because structural information on the non-specific complex is only available for EcoRV [30] a direct comparison of the three enzymes on the basis of their co-crystal structures has not been possible so far. To still obtain an estimation which conformation the enzyme adopts in the non-specific complex, a FRET analysis will be performed at first. This allows measuring the relative distance of the two subunits and thereby to estimate the degree of DNA-binding cleft opening. Subsequently, the three enzymes are subjected to a comparison of their sliding ability. This can easily be tested with conventional kinetic methods by measuring the dependence of the cleavage rate on the length of the DNA substrate [40,44,45]. It is to be found, whether the above mentioned hypothesis, namely the more closed the complex the more sliding is used, can be confirmed and thereby whether one can derive from the structure of an enzyme the degree of linear diffusion.

2 Material and methods

2.1 Material

2.1.1 Chemicals

All chemicals listed in Table 1 were of high purity grade.

Table 1: Chemicals

Name	Company
2-Mercaptoethanol	Merck
Acetic acid	Merck
Acrylamide:bisacrylamide solution 19:1 (40 %)	AppliChem
Acrylamide:bisacrylamide solution 29:1 (40 %)	AppliChem
Agar	AppliChem
Agarose Ultra Pure TM	Invitrogen
Aluminiumsulfate	AppliChem
Ammoniumsulfate	AppliChem
Ampicillin	AppliChem
Boric acid	Merck
Bromphenol blue	Merck
BSA	NEB
Calcium chloride	Merck
Chloramphenicol	AppliChem
Coomassie® Brilliant blue G250	AppliChem
Disodium hydrogen phosphate	Merck
dNTPs	Fermentas
DTT	AppliChem
EDTA	AppliChem
Ethanol	Merck
Ethidium bromide	Roth
Formamide	Merck
Glycerol	AppliChem
Glycine	Merck
HCl	Merck
HEPES	AppliChem

Imidazole	Merck
IPTG	AppliChem
Kanamycin Sulfate	AppliChem
KOH	Roth
Lubrol	Sigma
Magnesium Acetate	Merck
Magnesium Chloride	Merck
Magnesium Sulfate	Merck
NaOH	Roth
Ni ²⁺ -NTA-agarose	Qiagen
o- Phosphoric acid 87 %	Roth
Potassium Chloride	Merck
Potassium dihydrogen Phosphate	Merck
Potassium Glutamate	Merck
SDS	AppliChem
Sodium Acetate	AppliChem
Sodium Chloride	Merck
TCEP	Pierce
TEMED	Merck
Trichloroacetic acid	Roth
Tris	Merck
Triton X-100	Merck
Tryptone	AppliChem
Tween20	Merck
Urea	AppliChem
Xylene cyanol	Merck
Yeast extract	AppliChem

2.1.2 Buffers

All buffers were prepared with water from the Milli-Q Synthesis (Millipore) water purification system. Buffers listed in Table 2 – 4 were used for protein purification (2.2.2.10). The buffer listed in Table 5 was used for all kinds of assays. The buffer was supplemented with either 10 mM MgCl₂, 5 mM CaCl₂ or 1 mM EDTA, when indicated. Also the NaCl concentration was altered to 20, 100 and 200 mM for the competitive cleavage assay (2.2.3.3). The buffer listed in Table 6 was used for single-molecule experiments (2.2.3.7). Buffers listed in Table 7 were used for modification reactions (2.2.2.14 and 2.2.3.4).

The high salt PBS buffer was used for the fusion protein variants only. The composition of all other buffers is directly indicated in the chapter of the corresponding method.

Table 2: Purification buffers (EcoRV variants, PvuII variants, scPvuII)

Name	Components
Lysis, Equilibration buffer	30 mM KH ₂ PO ₄ -KOH pH 7.2, 800 mM NaCl, 0.5 mM EDTA, 1 mM DTT, 0.01 % (v/v) Lubrol, 10 mM Imidazole
Wash buffer	30 mM KH ₂ PO ₄ -KOH pH 7.2, 500 mM NaCl, 0.5 mM EDTA, 1 mM DTT, 0.01 % (v/v) Lubrol, 15 mM Imidazole
Elution buffer	30 mM KH ₂ PO ₄ -KOH pH 7.2, 0.5 mM EDTA, 1 mM DTT, 0.01 % (v/v) Lubrol, 250 mM Imidazole
Dialysis buffer	30 mM KH ₂ PO ₄ -KOH pH 7.4, 100 mM NaCl, 0.5 mM EDTA, 1 mM DTT, 0.01 % (v/v) Lubrol, 60 % (v/v) glycerol
Low-salt buffer	20 mM KH ₂ PO ₄ -KOH pH 7.4, 0.5 mM EDTA
High-salt buffer	20 mM KH ₂ PO ₄ -KOH pH 7.4, 0.5 mM EDTA, 1 M KCl

Table 3: Purification buffers (scRM6 D54C-L_(x)-EcoRV C21S, scRM6 D54C)

Name	Components
Lysis, Equilibration, Wash buffer	20 mM Hepes pH 8.0, 0.1 mM DTT, 10% (v/v) glycerol, 500 mM NaCl, 10 mM Imidazole
Elution buffer	20 mM Hepes pH 8.0, 5 mM DTT, 10% (v/v) glycerol, 500 mM NaCl, 250 mM Imidazole, 0.5 mM EDTA
Dialysis buffer	20 mM Hepes pH 8.0, 5 mM DTT, 60% (v/v) glycerol, 400 mM NaCl, 0.5 mM EDTA
Low-salt buffer	20 mM Hepes pH 8.0, 5 mM DTT, 250 mM NaCl, 0.5 mM EDTA
High-salt buffer	20 mM Hepes pH 8.0, 5 mM DTT, 1 M NaCl, 0.5 mM EDTA

Table 4: Purification buffers (BsoBI)

Name	Components
Lysis, Equilibration buffer	10 mM Tris-HCl pH 8.0, 500 mM NaCl, 15 mM Imidazole, 0.5 mM EDTA
Wash buffer	10 mM Tris-HCl pH 8.0, 200 mM NaCl, 15 mM Imidazole, 0.5 mM EDTA
Elution buffer	10 mM Tris-HCl pH 8.0, 200 mM NaCl, 200 mM Imidazole, 0.5 mM EDTA
Dialysis buffer	30 mM KH ₂ PO ₄ -KOH pH 7.2, 300 mM NaCl, 0.1 mM 2-mercaptoethanol, 0.01 % (v/v) Lubrol, 0.5 mM EDTA, 50 % Glycerol

Table 5: Reaction buffer

Name	Components
Reaction buffer	20 mM Tris-HCl pH 7.5, 50 mM NaCl, 5 mM DTT, 0.1 mg/mL BSA

Table 6: Single-molecule buffer

Name	Components
KGB	25 mM Tris-Acetate pH 7.4, 100 mM K-glutamate, 20 mM NaCl, 10 mM Mg-Acetate, 1 mM DTT, 0.1 mg/mL BSA

Table 7: Modification buffers

Name	Components
PBS	10 mM Na ₂ HPO ₄ *2 H ₂ O, 1.7 mM KH ₂ PO ₄ , 137 mM NaCl, 2.7 mM KCl
PBS high salt	10 mM Na ₂ HPO ₄ *2 H ₂ O, 1.7 mM KH ₂ PO ₄ , 1 M NaCl, 2.7 mM KCl

2.1.3 Bacterial strains

Different *E. coli* strains are listed in Table 8. The strains LK111λ and BL21DE3 contained an additional plasmid coding for the EcoRV methyltransferase (pLBM), which protects the genome from cleavage. The strain XL10 Gold contained the plasmid PLGM, which encodes for the PvuII methyltransferase and the strain XL1-Blue contained the plasmid pACYC, which encodes for the BsoBI methyltransferase. The indicated resistance refers to the plasmids coding for the corresponding methyltransferase.

Table 8: Bacterial strains

Name	Application	Resistance
DH5α	Amplification of the plasmids pAT-PEB and pMK-RQ	-
LK111λ pLBM	Amplification of the plasmid pHisRV and expression of all EcoRV variants	Chloramphenicol
BL21DE3 pLBM	Amplification of the plasmid pET28a and expression of all scRM6-EcoRV fusion protein variants (L _(x)) and scRM6 D54C	Chloramphenicol
XL10-Gold pLGM	Amplification of the plasmid pRIZ' and expression of all PvuII variants	Kanamycin
XL1-Blue pACYC	Amplification of the plasmid pQE2 and expression of BsoBI A153C	Chloramphenicol

2.1.4 Plasmids

Table 9: Plasmids and expression vectors.

Name	Application	Resistance
pAT-PEB	Plasmid used in the cleavage assay of EcoRV and PvuII; Template for the amplification of different PCR products	Ampicillin
pMK-RQ	Plasmid carrying the synthetic gene coding for scRM6 D54C	Kanamycin
pHisRV	Expression vector carrying the gene coding for different EcoRV variants (C21S, D214C, N154C)	Ampicillin
pET28a	Expression vector carrying the gene coding for all scRM6-EcoRV fusion protein variants (L _(x)) and scRM6 D54C	Kanamycin
pQE2	Expression vector carrying the gene coding for BsoBI A153C	Ampicillin
pRIZ'	Expression vector carrying the gene coding for different PvuII variants (wild type, D125C)	Ampicillin

2.1.5 Oligonucleotides

Oligonucleotides listed in Table 10 were obtained from Biomers (Ulm, Germany) and used for site directed mutagenesis (2.2.2.6).

Table 10: Oligonucleotides used for site-directed mutagenesis

Name	Sequence (5'→3')	Mutation	REase site
Oligo_515	CTAGAATTCTACTATTGCAAATGGGAAAGG	PvuII D125C	+ EcoRI
Oligo_464	GAGGATGAATTCTTATGCTATTGGAG	EcoRV D214C	+ EcoRI
Oligo_386	GCTTTATCGTCCGCTCTCGCGAGGTTCCCTC GAAGTGATTTAATTAATG	L ₍₀₎	- HindIII
Oligo_387	CCGCTCTCGCGAGGTTCAATGCTCTTCGAA GTGATTTAATTAATGC	L _(NA)	+ EarI
Oligo_412	CGTTCCGCTCTCGCGCGTTTCG- GACTTCGAAGTGATTTAATTAATGC	L _(G)	- HindIII
Oligo_413	CGTTCCGCTCTCGCGCGTTTCAAC- CTTCGAAGTGATTTAATTAATGC	L _(N)	- HindIII
Oligo_414	CGTCCGCTCTCGCGCGTCCG- CATCCCTTCGAAGGATTAATTAATGC	L _(NAS)	- HindIII

Oligonucleotides listed in Table 11 were obtained from Biomers (Ulm, Germany) and used for cloning approaches (2.2.2.7).

Table 11: Oligonucleotides used for cloning approaches

Name	Sequence (5'→3')	Application	Restriction site
Oligo_110	CCATCACGGGAGCTTCGAAGTGAT- TTAATTAATG	EcoRV C21S insert	+ HindIII
Oligo_111	GGGATTAAACACTCGAGC- TATTGCTTATTTTC	EcoRV C21S insert	+ XhoI

Oligonucleotides listed in Table 12 were obtained from Biomers (Ulm, Germany) and used for screening (2.2.2.8).

Table 12: Oligonucleotide used for screening

Name	Sequence (5'→3')	Application
Oligo_073	CACCATCATGACTAAGCAAGA-GAAGAC	Mutagenesis L _(x) -variants
RV_S183C	TTGTGTGTTTCCACAGCCGGCCAAATCTCCAGC	Mutagenesis L _(x) -variants
Oligo_036	CCCGCGAAATTAATACGACTC	Cloning of scRM6 D54C and EcoRV C21S
Oligo_037	TAGAGGCCCAAGGGGTTAT	Cloning of scRM6 D54C and EcoRV C21S
Oligo_208	CTTTATAAACCAAGCGAAC-CAAATAAAAAAATTGC	Mutagenesis EcoRV variants
Oligo_068	CATTACTGGATCTATCAACAG-GAG	Mutagenesis EcoRV variants
Oligo_048	CTTCTAATTGGAGGGTTAACAG-TACTACCAGGACG	Mutagenesis PvuII variants
Oligo_024	CCGTTACCCACCTACTAGC	Mutagenesis PvuII variants

HPLC-purified oligonucleotides listed in Table 13 were obtained from Biomers (Ulm, Germany) and used in the competitive cleavage assay (2.2.3.3). The desired double-stranded oligonucleotides were prepared by annealing the single-stranded upper oligonucleotide with the corresponding single-stranded lower oligonucleotide. Both strands were mixed in a 1:1 molar ratio, heated up for 5 min at 95°C and slowly cooled down to room temperature. Single-stranded oligonucleotides, which were modified with a fluorophore, were mixed in a 1:1.3 molar ratio with the complementary unmodified oligonucleotide.

Table 13: Oligonucleotides used in the competitive cleavage assay

Name	Sequence (5'→3')	Description	5' modification
Oligo_546	CGTCCGGCCTCGACTCGAGAGCTGAC	BsoBI 26 back	
Oligo_544	GTCAGCTCTCGAGTCGAGGCCGGACG	BsoBI 26 for	Atto 488
Oligo_545	GTCAGCTCTCGAGTCGAGGCCGGACG	BsoBI 26 for	Atto 647N
Oligo_351	CGTCCGGCCTCGAGATATCAGCTGAC	EcoRV 26 back	
Oligo_349	GTCAGCTGATATCTCGAGGCCGGACG	EcoRV 26 for	Atto 488
Oligo_350	GTCAGCTGATATCTCGAGGCCGGACG	EcoRV 26 for	Atto 647N
Oligo_356	CGTCCGGCCTCGACAGCTGAGCTGAC	PvuII 26 back	

Oligo_355	GTCAGCTCAGCTGTCGAGGCCGGACG	PvuII 26 for	Atto 488
Oligo_543	GTCAGCTCAGCTGTCGAGGCCGGACG	PvuII 26 for	Atto 647N
Oligo_352	CACCATACCCACGCCGAAACAAGCGC	153 back	
Oligo_353	GGCGTGCAAGATTCCGAATACCGCAA	498 back	
Oligo_354	CCAATTCTTGGAGTGGTGAATCCGTT	958 back	
Oligo_562	GTCAGGGGGGCGGAGCCTATGGAAAAAC	1488 back	

HPLC-purified oligonucleotides listed in Table 14 were obtained from Biomers (Ulm, Germany) and used for fluorescence anisotropy measurements (2.2.3.1). The corresponding unmodified oligonucleotides were used for FRET measurements (2.2.3.6).

Table 14: Oligonucleotides used for fluorescence anisotropy and FRET measurements

Name	Sequence (5'→3')	Description	5' modification
Oligo_030	CAGACGATATCCGTAC	EcoRV cognate upper	HEX
Oligo_251	CAGACGATATCCGTAC	EcoRV cognate upper	
Oligo_548	CAGACCTATAGCGTAC	EcoRV nonspecific upper	HEX
Oligo_549	CAGACCTATAGCGTAC	EcoRV nonspecific upper	
Oligo_031	GTACGGATATCGTCTG	EcoRV cognate lower	
Oligo_550	GTACGCTATAGGTCTG	EcoRV nonspecific lower	
Oligo_163	GTCCGCAGCTGACCTA	PvuII cognate upper	HEX
Oligo_551	GTCCGCAGCTGACCTA	PvuII cognate upper	
Oligo_552	GTCCGGTCGACACCTA	PvuII nonspecific upper	HEX
Oligo_553	GTCCGGTCGACACCTA	PvuII nonspecific upper	
Oligo_164	TAGGTCAGCTGCGGAC	PvuII cognate lower	
Oligo_554	TAGGTGTCGACCGGAC	PvuII nonspecific lower	
Oligo_581	CGTTGCTCGAGACATC	BsoBI cognate upper	HEX
Oligo_582	CGTTGCTCGAGACATC	BsoBI cognate upper	
Oligo_583	CGTTGGAGCTCACATC	BsoBI nonspecific upper	HEX
Oligo_584	CGTTGGAGCTCACATC	BsoBI nonspecific upper	
Oligo_585	GATGTCTCGAGCAACG	BsoBI cognate lower	
Oligo_586	GATGTGAGCTCCAACG	BsoBI nonspecific lower	

2.1.6 Enzymes and proteins

All enzymes and proteins listed in Table 15 were used with the recommended buffers according to the manufacturer's manual.

Table 15: Commercially available enzymes and proteins

Name	Application	Company
BSA	Buffer preparation	NEB
CIAP	Dephosphorylation	Fermentas
DpnI	Digest of "rolling circle" PCR products	Fermentas
EatI	Screening	NEB
EcoRI	Screening	NEB
HaeIII	Competitive cleavage assay	Fermentas
HindIII	Cloning, Screening	Fermentas
Lysozyme	Cell lysis	Pierce
MscI	Screening	NEB
NdeI	Cloning	Fermentas
NotI	Screening	NEB
<i>Pfu</i> -polymerase	PCR	H. Büngen, Giessen
T4 DNA ligase	Ligation	Fermentas
<i>Taq</i> -polymerase	PCR	H. Büngen, Giessen
XhoI	Cloning	NEB

All proteins listed in Table 16 were purified as described in chapter 2.2.2.10.

Table 16: Purified proteins

Name	Extinction coefficient mono-mers (ϵ) [$\text{L cm}^{-1} \text{mol}^{-1}$]	$A_{[280]} \rightarrow \text{mg/mL}$ correction factor
EcoRV C21S	48360	0.61
EcoRV C21S D214C	48480	0.61
EcoRV C21S N154C	48480	0.61
scRM6 D54C-EcoRV C21S	54880	1.05
scRM6 D54C-L ₍₀₎ -EcoRV C21S	53600	1.04

scRM6 D54C-L _(NA) -EcoRV C21S	53600	1.04
scRM6 D54C-L _(G) -EcoRV C21S	53600	1.04
scRM6 D54C-L _(N) -EcoRV C21S	53600	1.04
scRM6 D54C-L _(NAS) -EcoRV C21S	53600	1.05
scRM6 D54C	6520	4.35
PvuII	35560	0.54
PvuII D125C	35680	0.54
scPvuII	71240	0.53
BsoBI A153C	49620	0.77

2.1.7 Markers

Markers listed in Table 17 were used for protein and DNA electrophoresis (2.2.2.1)

Table 17: Markers

Name	Application	Company
PageRuler™ Unstained Protein Ladder	SDS-PAGE	Fermentas
GeneRuler™ 1 kb Ladder	Agarose gel electrophoresis	Fermentas
pUC8 mix Marker	PAGE	Fermentas

2.1.8 Fluorophores

Fluorescent dyes were used for different purposes. Atto488- and Atto647N-5'-modified oligonucleotides (Table 13) were used in the competitive cleavage assay (2.2.3.3). HEX 5'-modified oligonucleotides (Table 14) were used to determine the protein binding activity by fluorescence anisotropy (2.2.3.1). Atto488- and Atto647N-maleimide (purchased from AttoTEC) were used to label the single-cysteine variant EcoRV N154C and all scRM6-EcoRV fusion protein variants (2.2.3.4). Cy3- and Cy5-maleimide (purchased from GE healthcare) were used to label the single-cysteine variants EcoRV D214C, PvuII D125C and BsoBI A153C (2.2.3.4). Cy3B-maleimide (purchased from GE healthcare) was used to label the single-cysteine fusion protein variant scRM6 D54C-EcoRV C21S for single-molecule experiments (2.2.3.4). The chemical structures of all fluorophores are shown in Figure 11.

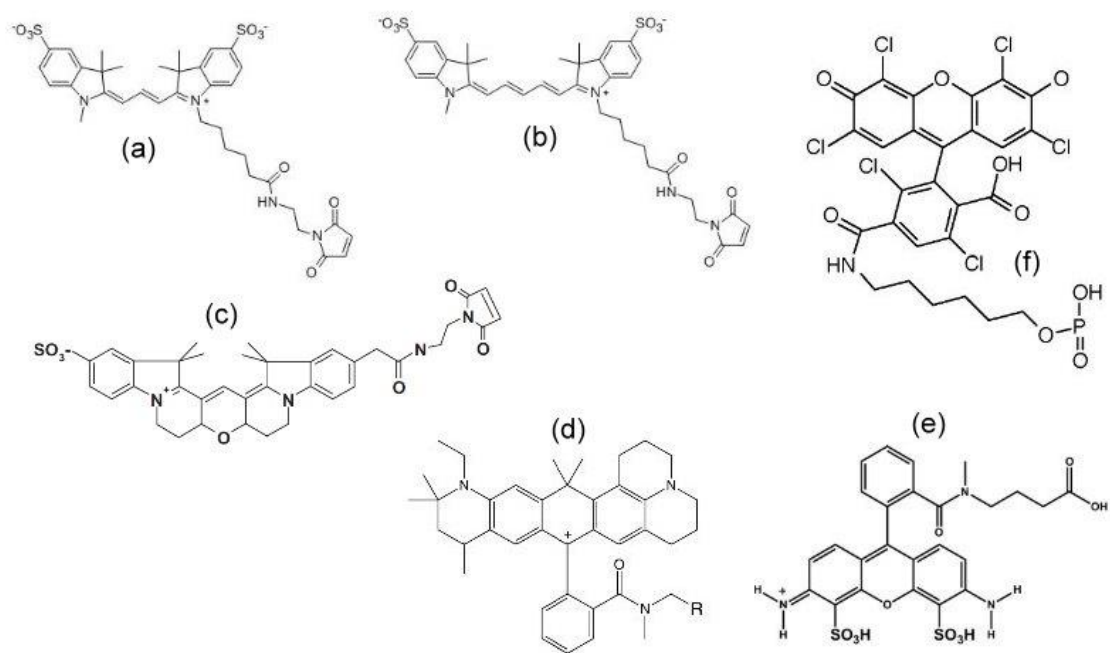


Figure 11: Chemical structures of used fluorophores. Cyanine dyes (a) Cy3-maleimide, (b) Cy5-maleimide and (c) Cy3B-maleimide. Carborhodamine dyes (d) Atto647N and (e) Atto488. Fluorescein dye (f) HEX. (Structure of Atto647N from Eggeling et al. 2008)

Spectral properties of the fluorophores are summarized in Table 18.

Table 18: Physical characteristics of used fluorophores. Absorption maximum (λ_{abs}), emission maximum (λ_{em}), extinction coefficient (ϵ) and correction factor for the absorbance at 260 nm (CF_{260}) or 280 nm (CF_{280}).

Name	λ_{abs} (nm)	λ_{em} (nm)	ϵ (L cm ⁻¹ mol ⁻¹)	CF_{260}	CF_{280}
Atto488	501	523	90,000	0.25	0.10
Atto647N	644	669	150,000	0.06	0.05
Cy3	550	570	150,000	0.08	0.08
Cy3B	559	570	130,000	0.08	0.08
Cy5	649	670	250,000	0.05	0.05
HEX	535	556	73,000	0.43	-

2.2 Methods

2.2.1 Microbiological methods

For bacterial cell growth, LB-medium (10 g/L tryptone, 5 g/L yeast extract, 5 g/L NaCl, pH 7.5) or LB-agar plates (LB-medium supplemented with 1.5 % (w/v) agar) were used. Corresponding antibiotics were added after sterilization, immediately before use.

2.2.1.1 Preparation of electro-competent cells

For the preparation of electro-competent *E. coli* cells (2.1.3), a 500 mL LB-medium culture was inoculated with 10 mL of a pre-culture of the desired cells and grown at 37°C until the OD₆₀₀ reached a value of 0.6 – 0.8. The culture was first stored on ice for 15 min and then centrifuged for further 15 min at 4200 rpm and 4°C (Beckman, J6-HC). The supernatant was discarded, the cell pellet was re-suspended in 250 mL cold and sterile 10 % (v/v) glycerol and centrifuged again. This step was repeated with 150 and 20 mL glycerol. After the last centrifugation step, the pellet was re-suspended in 2 mL glycerol, and separated in 80 µL aliquots. Aliquots were frozen in liquid nitrogen and stored at -80 °C.

2.2.1.2 Electroporation

Electro-competent cells (80 µL) (Table 8) were thawed on ice and mixed with 5 µL plasmid DNA, “rolling circle” PCR products or ligation products. The mixture was transferred into a cold electroporation cuvette and transformation was performed in an electroporator (Easyject, EquiBio) at 1250 V, 25 mA and 25 Ω. The transfected cells were re-suspended in 800 µL LB-medium, transferred into a micro-centrifuge tube and incubated for 1 h at 37 °C. 50 µL of the cells were either spread on an LB-agar plate in order to screen for positive clones (2.2.2.8) or directly used for inoculation of a pre-culture.

2.2.2 Molecular biology methods

2.2.2.1 Electrophoresis

Agarose gel electrophoresis

Agarose gel electrophoresis was used to analyze large DNA fragments from 800 - 10000 bp in size. The samples were mixed with 5x loading buffer (250 mM EDTA pH 8, 30 % (v/v) glycerol, 1.2 % SDS, 0.3 mg/mL bromphenol blue, 0.3 mg/mL xylencyanol) and loaded on the gel (0.8 % (w/v) agarose in 1x TPE buffer). The run was performed in 1x TPE buffer (0.9 M Tris-H₃PO₄ pH 8.2, 2 mM EDTA) for 1 h at 90 V. The gel was stained with ethidium bromide and the bands were visualized and documented using the BioDoc Analyze (Biometra) gel documentation system.

Polyacrylamide gel electrophoresis (PAGE)

Polyacrylamide gel electrophoresis was used to analyze small DNA fragments up to 800 bp in size. The samples were mixed with 5x loading buffer and loaded on the gel (6 % (v/v) polyacrylamide (29:1) in 1 x TPE buffer). The run was performed in 1x TPE buffer for 1 h at 45 mA. The gel was stained with ethidium bromide and the bands were visualized and documented using the BioDocAnalyze (Biometra) gel documentation system.

Denaturing PAGE

Denaturing polyacrylamide gel electrophoresis was used to analyze fluorescently labeled DNA fragments, which were generated in the competitive cleavage assay (2.2.3.3). Samples were mixed with 2x Urea stop buffer (100 mM EDTA, 80 % (v/v) formamide) and loaded onto the gel (20 % (v/v) polyacrylamide (19:1), 7 M urea in 1x TBE buffer). Prior to the sample loading, the gel was pre-run for 1 h in 1x TBE buffer (100 mM Tris-H₃BO₃ pH 8.3, 2.5 mM EDTA) until the electric current stabilizes at a value of 15 mA. The main run was performed under the same conditions for an additional hour. The fluorescent bands were visualized using the VersaDoc™ Imaging System (Bio-Rad) and quantitatively analyzed with the program GelAnalyzer.

SDS-PAGE

SDS polyacrylamide gel electrophoresis was used to analyze protein molecules. The SDS-gel is composed of a stacking gel (6 % (v/v) polyacrylamide (29:1) in 130 mM Tris-HCl pH 6.8, 0.1 % SDS) and a separating gel (10 - 15 % (v/v) polyacrylamide (29:1) in 420 mM Tris-HCl pH 8.8, 0.1 % SDS). The samples were mixed with 2x Laemmli loading buffer (160 mM Tris-HCl pH 6.8, 2 % SDS, 5 % 2-mercaptoethanol, 40 % (v/v) glycerol, 0.1 % bromophenol blue), loaded on the gel and separated for 1 h at 35 mA in 1x Laemmli SDS-buffer (25 mM Tris, 0.19 M glycine, 0.1 % SDS). After the run, the gel was washed with hot water (2 x 15 min) and stained with Colloidal Coomassie Staining Solution (0.1 % Coomassie® Brilliant Blue G250, 2 % (v/v) H₃PO₄, 5 % aluminum sulfate, 10 % ethanol). The bands were documented using the BioDocAnalyze (Biometra) gel documentation system.

2.2.2.2 Polymerase chain reaction (PCR)

The polymerase chain reaction was used for site directed mutagenesis (2.2.2.6), to amplify genes for cloning approaches (2.2.2.7), for screening (2.2.2.8) or for the amplification of DNA fragments used in the competitive cleavage assay (2.2.3.3).

Two different types of polymerases were used: (i) The *Pfu*-polymerase possess proof-reading activity and was used for all purposes where genetic integrity of the PCR-product was important. (ii) The *Taq*-polymerase does not possess proof-reading activity and was used for screening purposes only. The reaction profile for both polymerases is shown in Table 19.

Table 19: PCR profile

	<i>Taq</i> -polymerase	<i>Pfu</i> -polymerase
1. Initial step	3 min at 95 °C	5 min at 93 °C
2. Denaturation	30 s at 95 °C	30 s at 93 °C
3. Primer annealing	45 s at 3 °C above TM of primer with lowest TM	45 s at 3 °C above TM of primer with lowest TM
4. Extension	1 min/1000 bp at 72 °C	1 min/500 bp at 68 °C
5. Final step	5 min at 72 °C	5 min at 68 °C

The steps 2 – 4 were repeated 29-times.

The reaction mixture for both polymerases is shown in Table 20. For screening purposes also a single re-suspended colony has been used as template. The activity buffer of the *Taq* polymerase contained 10 mM Tris-HCl pH 8.8, 50 mM KCl, 0.1 % Triton X-100 and 1.5 mM MgCl₂, the activity buffer of the *Pfu* polymerase contained 20 mM Tris-HCl pH 9.0, 10 mM (NH₄)SO₄, 10 mM KCl, 0.1 % Triton X-100 and 2.5 mM MgSO₄.

Table 20: PCR mixture

	<i>Taq</i> -polymerase	<i>Pfu</i> -polymerase
dNTPs	250 µM	250 µM
Buffer	1x <i>Taq</i> activity buffer	1x <i>Pfu</i> activity buffer
Forward primer	400 nM	400 nM
Backward primer	400 nM	400 nM
Template	10 – 50 ng DNA	10 – 50 ng DNA
Polymerase	3 U	10 U
Total volume	30 µL	100 µL

The resulting PCR-products were either purified using the Promega Wizard® SV Gel and PCR Clean-Up System according to the manual or directly analyzed by gel electrophoresis (2.2.2.1).

2.2.2.3 Isolation of DNA

Isolation of plasmid-DNA was done either low-scale with the Promega PureYield™ Plasmid Miniprep System or high-scale with the Promega PureYield™ Plasmid Midiprep System according to the manufacturer's instruction.

2.2.2.4 Ethanol precipitation

Ethanol precipitation was used to purify digested plasmid-DNA or PCR products and ligation products. The following protocol was used: the sample with the volume (vol.) was mixed with 1/3 vol. of sodium acetate and 3 vol. of 100 % (v/v) ethanol and incubated for 30 min on ice. Subsequently the sample was centrifuged for 30 min with 12000 rpm at 4 °C. The supernatant was removed and the pellet was re-suspended with the same volume of 70 % (v/v) ethanol. After a second centrifugation step and the removal of the supernatant the pellet was dried for 15 min on a heating block and dissolved in 15 – 20 µL water.

2.2.2.5 Determination of DNA concentration

The concentration of single- and double-stranded oligonucleotides, PCR-fragments or plasmid-DNA was determined using the spectrophotometer NanoDrop® 1000 (Thermo Scientific) and the Lambert-Beer law $A = \varepsilon \cdot c \cdot d$, where A = absorption at 260 nm, ε = molar extinction coefficient and d = optical path length. The molar extinction coefficient was calculated on the webpage <http://biophysics.idtdna.com>.

2.2.2.6 Site-directed mutagenesis

Site-directed mutagenesis was used to substitute certain amino acids in a protein, especially to create single-cysteine variants (3.2.1) and the different linker variants of the fusion protein scRM6-EcoRV (3.1.1). To this end, a PCR primer, carrying the desired mutation and an additional restriction site for screening, was designed (Table 10). The second primer was chosen in order to yield a fragment of approximately 300 bp in size. A *Pfu*-PCR was performed with the plasmid coding for the protein to be mutated as template (2.2.2.2). The PCR product, the so-called ‘megaprimer’, was purified and the correct size was confirmed by PAGE. The generated megaprimer was used as primer together with the same plasmid as template in a second PCR (so-called ‘rolling circle’ PCR [84]). The reaction profile of the rolling circle PCR is shown in Table 21.

Table 21: Rolling circle PCR profile

	<i>Pfu</i> -polymerase
1. Initial step	5 min at 93 °C
2. Denaturation	1 min at 93 °C
3. Primer annealing	50 s at 60 °C
4. Extension	15 min at 68 °C
5. Final step	20 min at 68 °C

The steps 2 – 4 were repeated 15-times.

The rolling circle PCR yielded a circular PCR product, which was incubated with DpnI for 3 h at 37 °C. DpnI cleaves only methylated sites, thereby only the original plasmid lacking the mutation was digested. After ethanol precipitation (2.2.2.4), appropriate electro-competent cells were transfected with the circular plasmid (2.2.1.2). The transformation was spread on an LB-agar plate and screened for positive clones (2.2.2.8).

2.2.2.7 Cloning

Cloning was used to generate the fusion protein consisting of scRM6 and EcoRV. To this end, the gene coding for the single-cysteine variant scRM6 D54C and the gene coding for the cysteine-free variant EcoRV C21S had to be transferred from their original plasmids (pMK-RQ and pHisRV, respectively) to the expression vector pET28a, coding for an N-terminal His₆-Tag. The genes were cloned consecutively (see Figure 12).

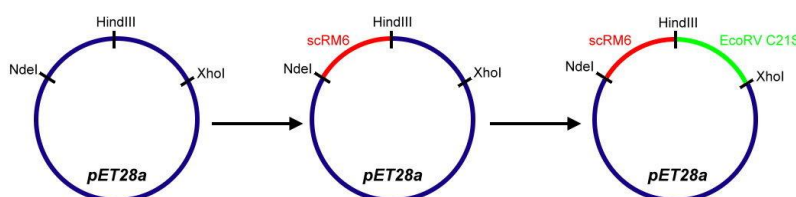


Figure 12: Cloning strategy for the fusion protein scRM6-EcoRV. Cloning was performed in a 2-step reaction. First, the gene coding for scRM6 D54C (red) was transferred to pET28a (blue) via NdeI and HindIII restriction sites. Second, the gene coding for EcoRV C21S (green) was transferred to the plasmid pET28a_scRM6 D54C via HindIII and XhoI restriction sites.

First, the plasmid pMK-RQ containing the synthetic gene coding for the single-cysteine variant scRM6 D54C and the vector plasmid pET28a were digested with NdeI and HindIII according to the company's manual. The digests were purified (2.2.2.4) and the concentration was determined (2.2.2.5). To prevent re-ligation of the vector plasmid pET28a with the original insert, a dephosphorylation of DNA 5'-termini was performed. Therefore, 1 µg of linearized vector DNA was mixed with 10x Dephosphorylation Buffer (Fermentas) and 1 U CIAP (Calf Intestinal Alkaline Phosphatase) in a total reaction volume of 20 µL and incubated for 30 min at 37 °C. The dephosphorylated vector was purified again. In the following ligation, 100 ng of the vector plasmid and a 5-fold molar excess of the insert were mixed with 10x T4 DNA Ligase Buffer (Fermentas) and 5 U T4 DNA Ligase in a total reaction volume of 20 µL and incubated overnight at 16 °C. The ligation product was purified, transferred into electro-competent cells (BL21DE3 pLBM), spread on an LB-agar plate and screened for positive clones (2.2.2.8).

Second, the gene coding for EcoRV C21S was amplified via *Pfu*-PCR using the plasmid pHisRV as template and primers covering the 5' and 3' region of the gene and carrying defined restriction sites (see Table 11). The PCR product was purified as describe before. After this, the PCR product with the gene coding for EcoRV C21S and the vector plasmid pET28a_scRM6 D54C were digested with HindIII and XhoI according to the company's manual. The digests were purified, the vector plasmid was dephosphorylated and vector and insert were ligated as described above. The ligation product was purified and transferred into electro-competent cells (BL21DE3 pLBM), spread on an LB-agar plate and screened for positive clones (2.2.2.8).

2.2.2.8 Screening

Screening was used to analyze the success of site-directed mutagenesis (2.2.2.6) or cloning (2.2.2.7). Several colonies were picked from an LB-agar plate and served as a template in a subsequent PCR performed with *Taq*-polymerase (2.2.2.2). The primers were chosen in order to cover the region of interest and are shown in Table 12. The PCR products were separated on a polyacrylamide or agarose gel (depending on the size of the DNA fragment) and analyzed either for the correct size of the fragment (successful insertion increased the size of the fragment) or the presence or absence of a restriction site after digesting the fragment with the desired enzyme. Positive clones were used for inoculation of a LB-medium culture. Plasmids were isolated low scale as described in 2.2.2.3 and sent for sequencing to confirm the correctness of the changed gene.

2.2.2.9 Protein overexpression

For the expression of proteins either a single colony from a LB-agar plate or freshly transformed *E. coli* cells containing the plasmid coding for the protein were used to inoculate a 50 mL pre-culture. After incubation overnight at 37 °C in an air shaker, 10 mL of the pre-culture were used to inoculate a 500 mL main-culture. The cells were grown at 37 °C until the OD₆₀₀ reached a value of 0.8. Protein expression was induced by adding 5 mL 100 mM IPTG to give a final concentration of 1 mM. The cells were further grown for 2 h at 37°C (BsoBI), 3 h at 37°C (scPvuII), overnight at 30°C (PvuII) or overnight at 20 °C (all other variants). To control the expression of the protein, samples were taken before and after induction. The volume taken depended on the OD₆₀₀ before and after induction in order to load the same amount of cells, allowing for comparison of the expression.

The samples for the expression test were centrifuged for 1 min at 13400 rpm (BioFuge Ependorf) and the pellet was re-suspended in 20 μ L 2x Laemmli loading buffer. After heating the samples at 95 °C for 5 min, they were loaded on an SDS gel and analyzed. The cells containing the desired protein were harvested by centrifugation for 15 min at 4200 rpm (Beckman JC-H6). The cell pellet was washed with 40 mL 1x STE buffer (10 mM Tris/HCl pH 8, 100 mM NaCl, 0.1 mM EDTA) and centrifuged again under the same conditions. The pellet was either stored at -20 °C or directly purified (2.2.2.10).

2.2.2.10 Protein purification

The buffers used for protein purification are listed in Table 2, Table 3 and Table 4.

Ni-NTA agarose purification. All protein variants carry an N-terminal Histidine-Tag and were therefore well-suited for the purification via Ni-NTA agarose beads. The principle is based on the binding to immobilized Ni^{2+} -ions via the imidazole group of the histidine residue. This process is reversible and the proteins can be eluted by addition of free imidazole. The structure of NTA (nitrilotriacetic acid) in complex with Ni^{2+} is shown in Figure 13.

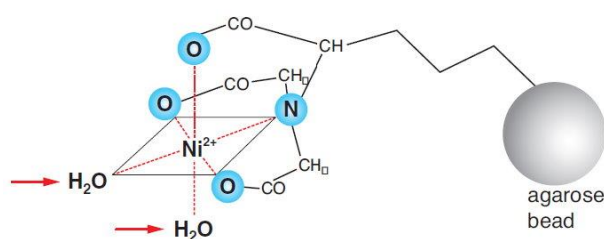


Figure 13: Structure of NTA in complex with Ni^{2+} : Ni-NTA agarose consists of the chelating ligand nitrilotriacetic acid (NTA) immobilized on agarose beads. Binding of proteins is based on the interaction between the polyhistidine-tag of the recombinant protein and the complexed Ni^{2+} -ions (adopted from: User's Manual Macherey-Nagel).

The cell pellet was thawed on ice and re-suspended in 30 mL LEW or LE buffer. The cells were lysed by ultrasonification with the Branson sonifier (12 x 30 s with 15 s break, duty cycle 50 %, output control 5). All fusion proteins were subjected to an additional step prior to ultrasonification. They were incubated with 1 mg/mL lysozyme (Sigma Aldrich) for 30 min at 4°C in order to decrease the amount of proteins stuck in the pellet. Also the time for ultrasonification was duplicated.

The cell suspension was centrifuged for 30 min at 20000 rpm and 4 °C (Beckman, JA20) to separate the soluble fraction containing the protein from the cell debris. 500 µL Ni-NTA suspension (Quiagen) were equilibrated with 20 mL LEW or LE buffer for 15 min. The soluble fraction was added to the Ni-beads and incubated for 2 h at 4 °C. After washing twice with 30 mL LEW or W buffer, the proteins were eluted with elution buffer and 3 fractions of 500 µL were collected. The purity and size of the proteins was analyzed by SDS-PAGE (2.2.2.1). Fractions containing the protein were dialyzed overnight in dialysis buffer or directly used for further purification steps.

Heparin purification. Heparin is a negatively charged macromolecule and has a high structural similarity to DNA. Therefore it is well suited for the purification of DNA-binding proteins. The binding is reversible and the proteins can be eluted by increasing the salt concentration of the buffer, thereby weakening electrostatic interactions. The structure of Heparin is shown in Figure 14.

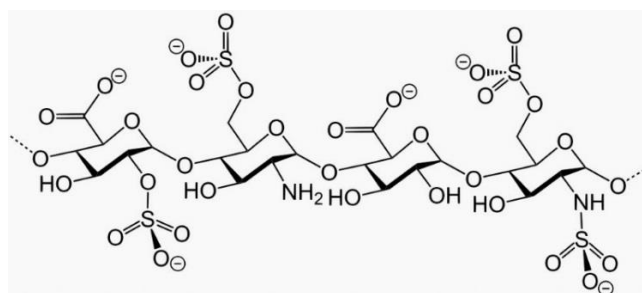


Figure 14: Detail of the structure of Heparin. Heparin is a highly sulfated glucosaminoglycan. Because of the high number of anionic sulfate groups it can be used either as a cation exchanger by capturing proteins with an overall positive charge. On the other hand it is suited for the purification of DNA-binding proteins, such as restriction enzymes, by taking advantage of the structural similarity to DNA being a negatively charged, sugar-containing macromolecule (adopted from Wikipedia).

Purification via Heparin was done only for scRM6-EcoRV fusion protein variants to separate them from other proteins that could be found in the eluates of the Ni-NTA agarose purification. Therefore, all eluates were pooled and reduced to a volume of 500 µL using Vivaspin 500 (10K) columns (GE Healthcare). The concentrated proteins were mixed in a 1:1 ratio with low-salt buffer and loaded onto a HiTrapTM Heparin HP column (GE Healthcare) connected to the ÄKTApurifierTM (GE Healthcare). Elution of the proteins was achieved by increasing the concentration of high-salt buffer by a linear gradient. The elution fractions were collected in tubes and analyzed by SDS-PAGE (2.2.2.1). Fractions containing the protein were dialyzed overnight in dialysis buffer.

2.2.2.11 TCA precipitation

TCA precipitation was applied after Heparin purification, if the protein concentration of collected fractions was too low to load it directly on a SDS-gel. Depending on the size of the peak in the chromatogram of the Heparin purification, a sample of the volume (vol.) was taken, mixed with 1/10 vol. TCA and incubated for 15 min on ice. Subsequently the sample was centrifuged for 15 min with 12000 rpm at 4 °C. The supernatant was discarded and the pellet was re-suspended in 20 µL 2x Laemmli loading buffer resulting in an orange color of the solution. After the addition of 1 µL 2M Tris the color of the solution changed to blue and samples were heated to 95 °C for 5 min. Finally, the samples were analyzed by SDS-PAGE (2.2.2.1).

2.2.2.12 Determination of protein concentration

The concentration of protein was determined using the spectrophotometer NanoDrop® 1000 (Thermo Scientific) and the Lambert-Beer law $A = \varepsilon \cdot c \cdot d$, where A = absorption at 280 nm, ε = molar extinction coefficient (see Table 16) and d = optical path length. The molar extinction coefficient ε was calculated based on the amino acid content [85] and are summarized in Table 16.

2.2.2.13 Determination of protein cleavage activity

The activity assay was performed to compare the activity of wild type EcoRV and wild type PvuII with the corresponding single-cysteine variants or fluorescently-labeled variants (3.2.1.1) and to compare wild type EcoRV with different scRM6-EcoRV fusion protein variants (3.1.2.1). In the activity assay, different concentrations of the protein were mixed with 6 nM plasmid-DNA (pAT-PEB), containing only one recognition site for PvuII and EcoRV, respectively. The samples were incubated for 1 h at 37 °C in reaction buffer, supplemented with 10 mM MgCl₂ (Table 5). The reaction was stopped by adding 5x loading buffer and fragments were analyzed on a 0.8 % agarose gel. The gel was stained with ethidium bromide and bands were visualized using the BioDocAnalyze (Biometa) gel documentation system.

2.2.2.14 PEG modification

PEG modification was used to test the accessibility of newly introduced cysteine residues at the surface of a protein before labeling it with a fluorophore. The chemistry of the modification reaction is explained in more detail in chapter 2.2.3.4. Polyethylene glycol increases the hydrodynamic radius as well as the molecular weight of a protein, thereby influencing the running behavior. A successful modification can be detected by a shifted band in the SDS-gel. After reduction of the cysteine residues by incubating the protein with 5 mM DTT for 1 h on ice, the proteins were transferred in 1x PBS buffer (Table 7) using Vivaspin 500 (10K) columns (GE Healthcare). In the modification reaction, 5 μ M protein were incubated with a 10-fold molar excess of PEG maleimide (Fluka) for 1 min or for 1 h at 37 °C. The structure of the modification reagent is shown in Figure 15.

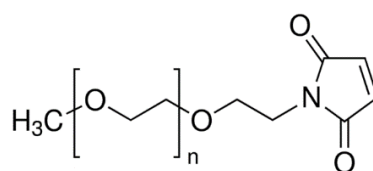


Figure 15: Chemical structure of PEG maleimide. Mono-Methyl polyethylene glycol 2-maleimidoethyl has a molecular weight of 5,000 g/mol (adopted from www.sigmaaldrich.com)

After the modification, the samples were mixed with 10 μ L 2x Laemmli loading buffer and separated on a SDS polyacrylamide gel (2.2.2.1).

2.2.3 Fluorescence spectroscopy based methods

2.2.3.1 Binding activity studied by fluorescence anisotropy

Fluorescence anisotropy is a powerful tool to determine the binding affinity of proteins to DNA. The principle of this method is shown in Figure 16. Exciting a fluorophore with linear polarized light leads to the emission of polarized light as well. If the fluorophore is coupled to a short DNA, e.g. an oligonucleotide, and excited with linear polarized light, the emitted light will be depolarized, because of the fast motion of the DNA and consequently of the fluorophore. Binding of a protein to the DNA leads to a slower motion of the DNA, because of an increase in mass, thus more of the emitted light stays polarized. The anisotropy describes the ratio of the emitted polarized light compared to the polarized light used for excitation. With other words: the more protein binds to the DNA, the slower the motion, the less emitted light is depolarized, the higher the anisotropy.

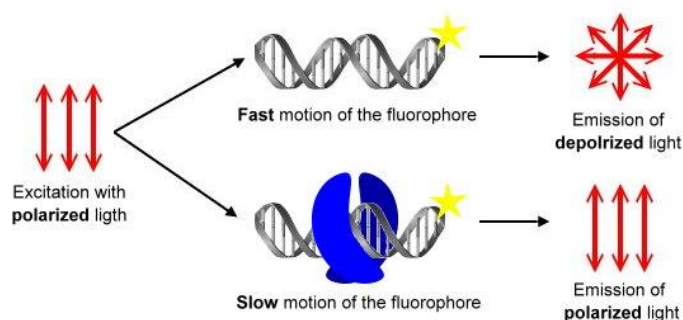


Figure 16: Principle of fluorescence anisotropy. A fluorophore (yellow star) coupled to a short DNA, is excited with linear polarized light (left). The fluorophore coupled to free DNA (middle, upper) will emit depolarized light (right, upper), because of the fast motion of the DNA. The fluorophore coupled to a protein-bound DNA (middle, lower) will emit polarized light (right, lower) because of a slower motion of the DNA.

The DNA used for fluorescence anisotropy measurements was prepared by annealing the 5'-HEX labeled upper strand with the complementary lower strand (see Table 14). The 16 bp long oligonucleotide was either a specific one, with the recognition site located in a central position (GAT↓ATC for EcoRV, CAG↓CTG for PvuII, and C↓TCGAG for BsoBI) or a non-specific one with the corresponding recognition site in a reverse orientation. The flanking base pairs were identical for each specific/non-specific DNA pair.

Fluorescence anisotropy measurements were used for two different purposes. In the first set of experiments, the dissociation constant (K_D) of six different scRM6-EcoRV fusion protein variants (scRM6 D54C-L_(x)-EcoRV C21S) was determined in comparison to the wild type protein EcoRV C21S (3.1.2.2). In these experiments only the K_D of the specific oligonucleotide was determined in the presence of Ca^{2+} -ions. In the second set of experiments, the dissociation constant (K_D) of EcoRV D214C, PvuII D125C and BsoBI A153C was determined in the presence of either Ca^{2+} -ions, Mg^{2+} -ions or EDTA (3.2.2). The K_D was determined for the specific as well as for the non-specific oligonucleotide. All steady-state ensemble anisotropy measurements were carried out at 24 °C using the FluoroMax®4 spectrofluorimeter (HORIBA Jobin-Yvon).

In the first set of experiments the excitation wavelength was set at 535 nm (slit width 5 nm) and the emission was detected at 556 nm (slit width 5 nm). In the second set of experiments the excitation wavelength was set at 530 nm (slit width 6 nm) and the emission was detected at 556 nm (slit width 6 nm). Initially, the cuvette (Quartz Ultra-Micro Cell, Hellma) was filled with 99 μL reaction buffer (supplemented with either 5 mM CaCl_2 , 10 mM MgCl_2 or 1 mM EDTA) and the intensities of the emitted polarized light were measured through vertical and horizontal polarization filters (I_{VV} , I_{VH} , I_{HV} , I_{HH}).

Next, 1 μL HEX-labeled oligonucleotide was added, resulting in a final concentration of 2 nM DNA (if not otherwise stated) and the intensities of the emitted polarized light were measured again. Finally 1 μL aliquots of increasing concentrations of protein were added to the cuvette, incubated for 1 min and the intensities of the emitted polarized light were measured after each addition. Each protein concentration was measured 5-times and subsequently averaged. The change of the volume due to the addition of protein never exceeded 8 % of the total binding reaction.

Afterwards, the respectively measured intensities of the emitted polarized light were corrected by subtraction the intensities of the buffer from the intensities of the DNA and each protein concentration. The anisotropy was recalculated using the following equation:

$$\text{anisotropy} = \frac{\left(\frac{I_{VV} \cdot I_{HH}}{I_{VH} \cdot I_{HV}}\right) - 1}{\left(\frac{I_{VV} \cdot I_{HH}}{I_{VH} \cdot I_{HV}}\right) + 2}$$

where I_{VV} and I_{VH} are the intensities of the vertical and horizontal components of the emitted light using vertical polarized excitation and I_{HV} and I_{HH} are the intensities of the vertical and horizontal components of the emitted light using horizontal polarized excitation. The anisotropy was then plotted against the protein concentration and a simple bimolecular binding model was fitted by non-linear regression to the data.

2.2.3.2 Michaelis-Menten kinetics

The Michaelis-Menten theory is a mathematical model, which describes enzyme catalyzed reactions. It is defined by the Michaelis-Menten equation (Figure 17, right), where v_0 is the initial velocity, v_{\max} is the maximum velocity, $[S]$ is the substrate concentration and K_M is the Michaelis-Menten constant, which represents the substrate concentration at half maximum velocity ($1/2 v_{\max}$).

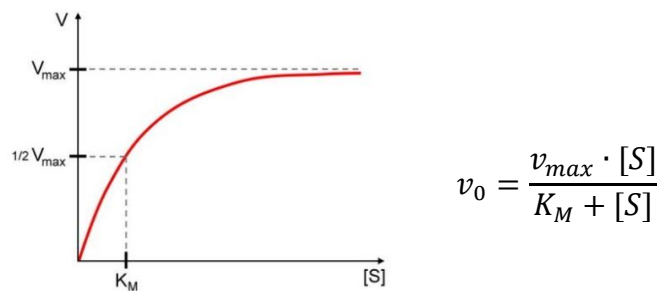


Figure 17: Michaelis-Menten kinetics. (Left) Typical curve according to Michaelis-Menten. Plotted is the substrate concentration ($[S]$) against the velocity (v). The characteristic kinetic parameters v_{\max} and $1/2 v_{\max}$ are marked on the y-axis, K_M is marked on the x-axis. (Right) Michaelis-Menten equation.

The K_M is a measure of the affinity of an enzyme for its substrate. Dividing the maximum velocity v_{\max} by the enzyme concentration $[E]$ yields k_{cat} , which is also known as the turnover number. The catalytic efficiency, given by the ratio k_{cat}/K_M , allows comparing different enzymes. The resulting graph (Figure 17, left) is a hyperbola, which asymptotically reaches the maximum velocity.

Michaelis-Menten kinetics were performed with the molecular beacon assay [86]. A molecular beacon is a short oligonucleotide with a hairpin structure, which carries at one end a fluorophore and at the other end a quencher. The principle of this assay is shown in Figure 18.

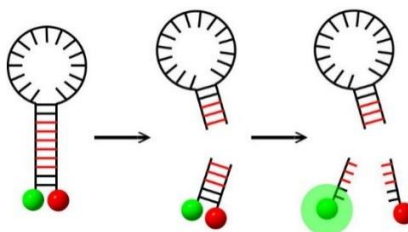


Figure 18: Principle of the molecular beacon assay. The fluorescence of the HEX-fluorophore (green) is quenched by the BHQ quencher (red) as long as the beacon is uncleaved. Cleavage of the beacon by a restriction endonuclease leads to the dissociation of the terminal end and the subsequent melting of the strands, thereby fluorophore and quencher get separated and an increase in fluorescence can be measured.

The molecular beacon 5'– (HEX) – CGGATATCGGACTTTTTTTTTTTTTTTT–GTCCGATATCCG – (BHQ) – 3' used in this assay was purchased from Biomers (Oligo_006). It is composed of a T_{16} -loop and a 12 bp duplex, which contains a specific recognition site for EcoRV (GATATC). Steady-state measurements were carried out under multiple turnover conditions at 37 °C with the InfiniteF200Pro plate-reader (Tecan). The following filter set for the HEX fluorophore was used: excitation at 535 nm (25 nm bandwidth), emission at 590 nm (20nm bandwidth). A mastermix, containing reaction buffer and either 100 pM (EcoRV C21S), 500 pM (scRM6 D54C-EcoRV C21S) or 1 nM (scRM6 D54C- $L_{(x)}$ -EcoRV C21S) protein, respectively, was prepared and 80 μ L aliquots were pipetted into eight wells of a microtiter plate. Immediately before measuring, 10 μ L molecular beacon with concentrations ranging from 1 – 50 nM (EcoRV C21S and scRM6 D54C-EcoRV C21S) or 6 – 300 nM (scRM6 D54C- $L_{(x)}$ -EcoRV C21S) were added to one well of the microtiter plate, respectively. The reaction was started by the addition of 10 μ L $MgCl_2$ (via the inject function of the device), resulting in a final concentration of 10 mM. The increase in fluorescence was recorded over a period of 10 min every 3 s.

The gain was set at 90. The initial velocity was calculated by linear regression of the first 20 data points and plotted against the beacon concentration. From the resulting curve, K_M and v_{max} were determined by non-linear regression using the Michaelis-Menten equation.

2.2.3.3 Competitive cleavage assay

To investigate the influence of linear diffusion on the rate of cleavage, a competitive cleavage assay was employed. A similar assay had been described in detail [87] and had already been applied for EcoRI [44] and EcoRV [31,45]. In the assay, two DNA substrates – a short oligonucleotide and a long PCR fragment – each containing one specific recognition site for either BsoBI, EcoRV or PvuII, were cleaved in competition. The short oligonucleotide was generated by annealing a 5'-Atto647N-labeled 26mer with the complementary oligonucleotide (see Table 13). To amplify the long PCR fragment, the same 26mer, but 5'-Atto488-labeled, was used as the upper PCR primer together with different lower primers to amplify fragments of 158, 498, 958 and 1488 bp in length (see 2.2.2.2). As PCR template the plasmid pAT-PEB was used. The correct size of the fragments was confirmed by PAGE (see 2.2.2.1). This procedure ensured, that the specific recognition site is embedded in an identical sequence context of 26 bp, flanked by a short arm of 7 bp and a long arm comprising 145 – 1480 bp (Figure 19).

For control experiments, also a 5'-Atto488 26mer was generated by annealing. The labeling with different fluorophores allows determining the cleavage rate of the short and the long substrate independently but in one reaction mixture.

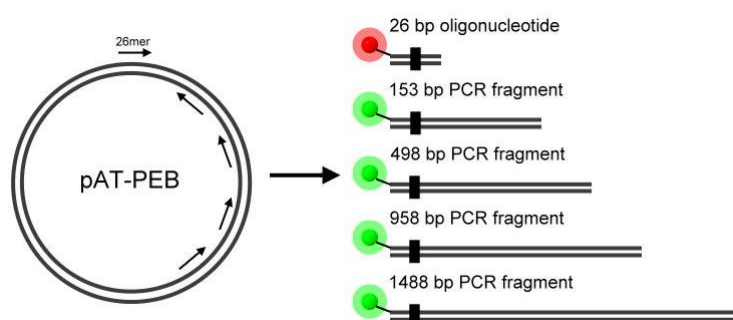


Figure 19: Scheme of substrate design. Different PCR fragments were generated by PCR using the pAT-PEB plasmid as template and a 5'-Atto488 (green) labeled 26mer oligonucleotide as upper primer. The lower primers were chosen to amplify fragments of 153, 498, 958 and 1488 bp in length. The 26 bp oligonucleotide was generated by either annealing the same 5'-Atto488 labeled upper primer or a 5'-Atto647N (red) labeled 26mer oligonucleotide with the complementary strand (DNA fragments are not drawn to scale). Adopted from [45].

In the cleavage reaction, 20 nM of the short oligonucleotide and 20 nM of one of the long PCR fragments were incubated with either 600 pM (BsoBI A153C, EcoRV D214C, PvuII D125C, scPvuII) or 10 nM (scRM6 D54C-EcoRV) protein in reaction buffer (Table 5, supplemented with 10 mM MgCl₂) at 37°C. At defined time intervals, 10 µL aliquots were withdrawn and mixed with 10 µL of 2x Urea stop buffer to stop the reaction. The resulting fragments were separated by denaturing PAGE (2.2.2.1). The fluorescent bands were visualized using the VersaDocTM Imaging System (Bio-Rad) and quantitatively analyzed with the program GelAnalyzer. The amount of substrate cleavage was plotted against the time and a single exponential function was fitted to the data points.

In experiments, in which the salt dependence was investigated, the NaCl concentration of the reaction buffer was altered to 20, 100 and 200 mM, respectively. In order to test whether the effect of linear diffusion can be abolished, experiments were carried out with 20 nM of the 26mer oligonucleotide and 20 nM of the 958mer PCR fragment predigested with the 4 bp-cutter HaeIII for 2 h at 37 °C, similarly as described by Ehbrecht et al. [40]. The predigested substrates were used without further treatment as described above.

2.2.3.4 Fluorescent labeling

A wide commonly used technique to modify proteins at defined sites is the modification via maleimide chemistry. The reactive maleimide group of the modification reagent (e.g. a fluorophore or PEG) reacts specifically with the functional sulfhydryl group of the protein to form a stable covalent bond (see Figure 20). Since the sulfhydryl group is only present in the side chain of the amino acid cysteine, the reaction is highly specific.

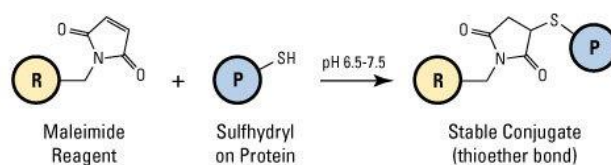


Figure 20: Reaction scheme for chemical conjugation. (R) represents a labeling reagent that carries the reactive maleimide group, e.g. a fluorophore, (P) represents a protein that carries the functional sulfhydryl group. The maleimide groups reacts with sulfhydryl group under formation of a stable covalent thioether bond (adopted from www.pierce-net.com)

For site-specific labeling, cysteine residues located at the surface of the protein had to be removed by mutagenesis and a single cysteine residue had to be introduced at the desired position. For an efficient labeling the sulfhydryl group must be kept in a reduced state.

Thus, proteins were incubated with 5 mM reducing agent (e.g. DTT) prior to the labeling reaction. The next step was a buffer exchange, on the one hand to create optimal buffer conditions for the chemical reaction (e.g. pH value), on the other hand to remove substances that can disturb the reaction (e.g. DTT). For this purpose Vivaspin 500 (10K) columns (GE Healthcare) were used following the manufacturer's instruction to transfer the protein in 1x PBS buffer (Table 7). For random double labeling reactions, 20 – 30 μM protein were first mixed with a 1:1 molar ratio (over dimer protein concentration) of donor fluorophore (Atto488, Cy3 or Cy3B) and shortly after a 10-fold molar excess (over dimer protein concentration) of acceptor fluorophore (Atto647N or Cy5) was added. Protein and fluorophores were incubated for 2 h at room temperature in 1x PBS buffer. For single labeling reactions, 20 – 30 μM proteins were mixed with a 10-fold molar excess (over dimer protein concentration) of either donor or acceptor fluorophore and also incubated for 2 h at room temperature in 1x PBS buffer. Since the fluorophores were dissolved in DMSO, the amount of the organic solvent never exceeded 10 % (v/v) of the total reaction volume. To remove the excess of unreacted, free fluorophore, Dynabeads® His-tag Isolation & Pulldown (Invitrogen) were used. The principle is shown in Figure 21.

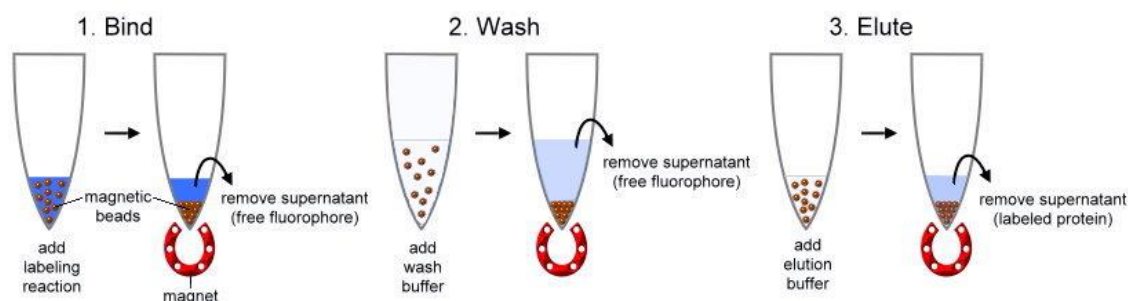


Figure 21: Principle of free fluorophore removal via Dynabeads®. (1) The labeling reaction was incubated with the magnetic beads allowing the labeled proteins (His-tagged) to bind to the magnetic beads (Ni^{2+} -coated). By applying a magnet, labeled proteins (bound to the beads) were separated from the free fluorophore (supernatant) (2) By adding 3-times wash buffer further free fluorophore was removed (3) The addition of elution buffer (containing imidazole) detached the labeled proteins from the beads.

Dynabeads® are coated in a cobalt-based Immobilized Metal Affinity Chromatography (IMAC) chemistry and are well-suited to isolate histidine-tagged proteins. The beads were first re-suspended and transferred to a microcentrifuge tube. The tube was placed on a magnet for 2min and the supernatant was discarded. Then the labeling reaction (30 μL) was added and incubated for 30 min allowing the labeled His-tagged proteins to bind to the beads.

The application of a magnet for 2 min separated the labeled proteins from the free fluorophore. Subsequently the beads were 3-times washed with 100 μ L wash buffer (1x PBS buffer supplemented with 0.05 % Tween20) by placing the tube on a magnet and discarding the supernatant. To obtain the labeled proteins, 20 – 30 μ L elution buffer (1x PBS buffer supplemented with 300 mM imidazole) were added and incubated for 15 min. After the application of a magnet for 2 min the supernatant, containing the labeled proteins, was transferred to a clean tube. In order to remove imidazole and to transfer the protein in dialysis buffer, ZebaTMSpin Desalting columns (7K) (Thermo Scientific) were used following the manufacturer's instruction. The single and double labeled proteins were used for FRET measurements (2.2.3.6).

2.2.3.5 Determination of the degree of labeling (DOL)

After modifying a protein with a fluorophore, the degree of labeling (DOL) was determined. For this purpose, the absorbance of the protein at 280 nm and the absorbance of the fluorophore at the absorbance maximum of the dye (Table 18) was recorded with the spectrophotometer NanoDrop® 1000 (Thermo Scientific). To correctly calculate the protein concentration, the absorbance at 280 nm had to be corrected using correction factors (CF) provided by the supplier (Table 18). The correction factor compensates for the absorption of the dye at 280 nm. The DOL was then calculated using the following equation:

$$DOL = \frac{\frac{A_F}{\epsilon_F}}{\frac{A_P - (A_F \cdot CF_{280})}{\epsilon_P}}$$

where A_F is the absorbance of the fluorophore at the absorbance maximum, ϵ_F is the molar extinction coefficient of the fluorophore (Table 18), A_P is the absorbance of the protein at 280 nm, ϵ_P is the molar extinction coefficient of the protein (Table 16) and CF_{280} is the correction factor of the fluorophore at 280 nm.

2.2.3.6 FRET measurements

Förster resonance energy transfer (FRET) is a powerful tool to study distances or small distance changes within biomolecules [88]. Because of the distance dependence it is also denotes as spectroscopic ruler. FRET requires the presence of two fluorophores, a donor fluorophore and an acceptor fluorophore. Both fluorophores can be attached to the same biomolecule (intramolecular FRET) or to different biomolecules (intermolecular FRET).

During FRET donor and acceptor fluorophore are coupled by dipole-dipole interactions and the energy is transferred from the donor to the acceptor fluorophore without radiation, which means that no photon is transferred. FRET depends on the following criteria:

- (i) The emission spectrum of the donor fluorophore has to overlap with absorption spectrum of the acceptor fluorophore
- (ii) Donor and acceptor dipole moments have to be in a suitable orientation to each other
- (iii) The distance of donor and acceptor should be in the range of 1 – 10 nm, which is a typical distance in biomolecules

The FRET efficiency (E) strongly depends on the distance of donor and acceptor fluorophore (Figure 22a) and can be described by the Förster equation:

$$E = \frac{R_0^6}{R_0^6 + r^6}$$

where r is the distance between donor and acceptor fluorophore and R_0 is the Förster radius. R_0 is characteristic for each fluorophore pair and describes the distance of donor and acceptor at which energy transfer is 50 % efficient. Around R_0 , small changes in the distance of donor and acceptor cause a large change in the FRET efficiency.

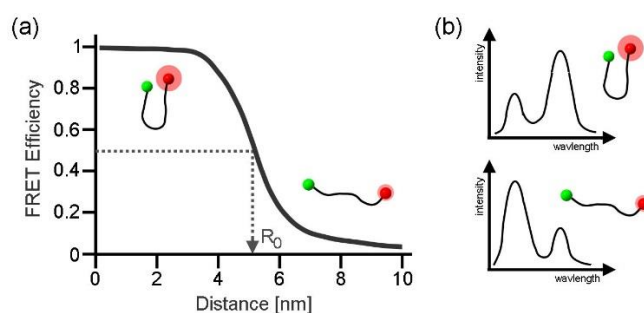


Figure 22: Principle of FRET. (a) Relationship between FRET efficiency and the distance of donor (green) and acceptor (red) fluorophore. The FRET efficiency is high, if the distance between donor and acceptor is short and it is low, if the distance between donor and acceptor is large. (b) Emission spectra of a biomolecule double labeled with donor and acceptor. Lower: the distance between donor and acceptor is large, thus the donor emission is high whereas the acceptor emission is low. Upper: the distance between donor and acceptor is short, thus the donor emission decreases whereas the acceptor emission increases.

FRET measurements were used for two different purposes. In the first set of experiments the spatial expansion of the fusion protein scRM6 D54C-EcoRV C21S and different linker variants (scRM6 D54C-L_(x)-EcoRV C21S) was studied in comparison to the wild type EcoRV C21S N154C and a DNA molecule (3.1.3). In the second set of experiments the conformation of the structurally different restriction enzymes EcoRV D214C, PvuII D125C and BsoBI A153 was studied in complex with specific and non-specific DNA as well as for the apoenzyme (3.2.2). All steady-state ensemble FRET measurements were carried out at 24 °C using the FluoroMax®4 spectrofluorimeter (HORIBA Jobin-Yvon).

Studying the spatial expansion of different fusion protein variants

Proteins were either double-labeled with Atto488 as donor fluorophore and Atto647N as acceptor fluorophore or single-labeled with Atto488 or Atto647N, respectively (see 2.2.3.4). Emission spectra were recorded for the donor fluorophore by scanning between 490 – 800 nm (slit width 4 nm) with excitation wavelength set at 470 nm (slit width 4 nm) and for the acceptor fluorophore by scanning between 640 – 800 nm (slit width 4 nm) with excitation wavelength set at 630 nm (slit width 4 nm). Initially, the cuvette (Quartz Ultra-Micro Cell, Hellma) was filled with 90 µL reaction buffer (supplemented with 5 mM CaCl₂) and emission spectra were recorded. Finally, 10 µL double-labeled protein (or double-labeled DNA) was added to the cuvette, resulting in a final concentration of 50 nM protein dimer concentration (or 25 nM DNA concentration) and emission spectra were recorded again. In control experiments, 5 µL donor only and 5 µL acceptor only labeled protein were added together to the cuvette and incubated for 5 min, resulting in a total protein concentration of either 50 nM. In experiments where the influence of the presence of DNA was investigated, an excess of either a 16 bp or 60 bp long specific oligonucleotide (see Table 14) was added to the cuvette, incubated for 5 min and emission spectra were recorded again. The spectra were corrected for background signal by subtracting the spectra of the buffer from the spectra of the protein or protein-DNA complexes. Finally the corrected spectra were normalized to the maximum donor emission at 520 nm and the FRET efficiency was calculated by dividing the emission intensity of the acceptor signal at 664 nm by the emission intensity of the donor signal at 520 nm.

Studying the conformation of structurally different restriction enzymes

Proteins were either double labeled with Cy3 as donor fluorophore and Cy5 as acceptor fluorophore or single labeled with Cy3 or Cy5, respectively (see 2.2.3.4). Emission spectra of double labeled proteins (F_{DA}) were recorded for the donor fluorophore by scanning between 552 – 800 nm (slit width 3 nm) with the excitation wavelength set at 546 nm (slit width 3 nm) and for the acceptor fluorophore by scanning between 650 – 800 nm (slit width 3 nm) with the excitation wavelength set at 644 nm (slit width 3 nm). Initially, the cuvette was filled with 90 μ L reaction buffer (supplemented with either 5 mM CaCl_2 , 10 mM MgCl_2 or 1 mM EDTA) and emission spectra were recorded. Next, 10 μ L double labeled protein were added to the cuvette, resulting in a final protein concentration of 50 nM. After recording the emission spectrum of the apoenzyme, an excess of unlabeled non-specific or specific DNA (see Table 14) was added to the cuvette and emission spectra were recorded after 5 min incubation. Subsequently, emission spectra were corrected for background signal by subtracting the spectrum of the buffer from the spectrum of the apoenzyme or enzyme-DNA complexes. Corrected emission spectra were normalized to the maximum donor emission and the FRET efficiency (E) was calculated directly by dividing the emission intensity of the acceptor at 666 nm (emA) by the emission intensity of the donor at 564 nm (emD), both resulting from direct excitation of the donor fluorophore (exD) [equation adopted from [89]].

$$E = \frac{F_{DA}^{exD,emA}}{F_{DA}^{exD,emD}}$$

Additionally, the FRET efficiency was calculated by an alternative method that considers the correction of the acceptor emission intensity for donor bleed-through and excitation crosstalk in accordance with the ‘Three-Cube Method’ [89]. To this end, additional measurements of single labeled proteins were performed.

First, the degree of donor bleed-through was determined with a protein sample single labeled with donor fluorophore (F_D). The donor fluorophore was excited with the excitation wavelength set at 546 nm and the emission intensity was measured for either donor at 564 nm or acceptor at 666 nm. The donor bleed-through correction factor β was calculated by dividing the emission intensity of the acceptor at 666 nm (emA) by the emission intensity of the donor at 564 nm (emD), both resulting from direct excitation of the donor fluorophore (exD).

$$\beta = \frac{F_D^{exD,emA}}{F_D^{exD,emD}}$$

Second, the degree of excitation crosstalk was determined with a protein sample single labeled with acceptor fluorophore (F_A). The acceptor fluorophore was either excited with the excitation wavelength set at 546 nm or 644 nm and the emission intensity was measured for the acceptor at 666 nm. The excitation crosstalk correction factor α was calculated by dividing the emission intensity of the acceptor at 666 nm (emA), resulting from excitation of the donor (exD) by the emission intensity of the acceptor at 666 nm (emA) resulting from excitation of the acceptor fluorophore (exA).

$$\alpha = \frac{F_A^{exD,emA}}{F_A^{exA,emA}}$$

Finally, double labeled proteins were measured as described above. The acceptor fluorophore was excited with the excitation wavelength set at 546 nm (exD) or 644 nm (exA) and the emission intensity of the acceptor was measured at 666 nm (emA). The donor fluorophore was excited with the excitation wavelength set at 546 nm (exD) and the emission intensity of the donor was measured at 564 nm (emD). The corrected FRET efficiency was calculated using the following equation:

$$E_{corr} = \frac{F_{DA}^{exD,emA} - \alpha \cdot F_{DA}^{exA,emA} - \beta \cdot F_{DA}^{exD,emD}}{F_{DA}^{exD,emD}}$$

2.2.3.7 Single-molecule experiments

Single-molecule experiments were performed with the fusion protein variant scRM6 D54C-EcoRV C21S to determine the one-dimensional diffusion coefficient (D_1) and to verify a rotational movement by comparing D_1 to mathematical models (3.1.4). The fusion protein was purified and labeled with Cy3B as described in chapter 2.2.2.10 and 2.2.3.4 with the exception that the second purification step via Heparin column was conducted after the labeling reaction. DNA molecules (~ 9.2 kbp in size and without any recognition site for EcoRV) were stretched to about 70 % of their contour length by attaching them to a streptavidin coated coverslip via their biotinylated ends as described previously [67,90]. To prevent non-specific interactions between the protein and the surface, residual streptavidin was passivated with casein blocking reagent (Roche Diagnostics) for 15 min. The stretched DNA molecules were stained with SybrGold (Invitrogen) and visualized through excitation and emission filters (Omega Optical) after excitation with a mercury lamp [67,90]. Transverse fluctuations of the DNA molecules ensured that most of the DNA was free accessible in solution. After recording the position of the DNA molecules, SybrGold was removed using a buffer containing 20 mM $MgCl_2$. The flow-cell was flushed with the KGB reaction buffer (Table 6) and the Cy3B-labeled fusion proteins were injected. For detection of individual fluorophores a TIRF microscopy setup was used as previously described [67]. Briefly, Cy3B-labeled fusion proteins were excited using a laser at 532 nm with a light intensity of 100 W/cm². The fluorescent light was collected through a dichroic mirror and a bandpass filter and imaged on an EMCCD camera (Ixon, Andor Technology) with an exposure time of 20 ms. The resulting point-spread function of the fluorescent spots in each frame was fitted with a 2D Gaussian function, thereby locating the position of the fusion protein on the DNA molecule with an accuracy of 30 nm. The one-dimensional diffusion coefficient (D_1) of the scRM6-EcoRV fusion protein was derived from the longitudinal mean squared displacement (MSD) calculated from 45 enzyme trajectories that were longer than 20 successive frames (> 400 ms).

3 Results

3.1 Preparation of an elongated restriction enzyme to study rotational motion

It has been proposed that restriction enzymes follow the helical pitch of the DNA during sliding and thereby complementing translational diffusion by a rotational motion [44]. So far, rotational motion of restriction enzymes during linear diffusion has only been demonstrated **indirectly** by single-molecule experiments via the size dependence of the one-dimensional diffusion coefficient (D_1) [75-77]. To determine D_1 , fluorescently labeled restriction enzymes are tracked using total internal reflection fluorescence microscopy. Images are recorded by an EMCCD camera every 20 ms. On each image the longitudinal and transversal position of the enzyme on the DNA is determined, thereby reconstructing the enzyme trajectory. From the enzyme trajectory the mean squared displacement (MSD) can be derived and from the slope of the longitudinal MSD the one-dimensional diffusion coefficient (D_1) can be deduced (for more details see 1.2 and Figure 10). The question arises whether a rotational motion can also be **directly** demonstrated in the same experimental setup used for the determination of D_1 . Usually, only the longitudinal position of the fluorescent spot is supposed to change over time if the motion of the enzyme is considered as simple translational diffusion (Figure 10D).

If rotational motion of the enzyme is involved in the translocation process, also the transversal position of the fluorescent spot is supposed to change in a periodic manner. This means in more detail that the fluorescent spot is expected to appear more below the DNA molecule in one fluorescent image and to appear more above the DNA molecule in another fluorescent image (indicative of a half-rotation of the enzyme) (see Figure 23a). The question arises whether such a transversal position change can be resolved in the experimental setup. For a conventional restriction enzyme (diameter of ~ 5 nm, directly labeled with a fluorophore) the transversal position of the fluorophore is expected to change by 5 nm while turning 180° around the DNA molecule (Figure 23a). Also the most sophisticated cameras would not be able to resolve this small transversal distance change of the fluorescent spot, which makes the visualization of a rotational motion with a conventional restriction enzyme impossible.

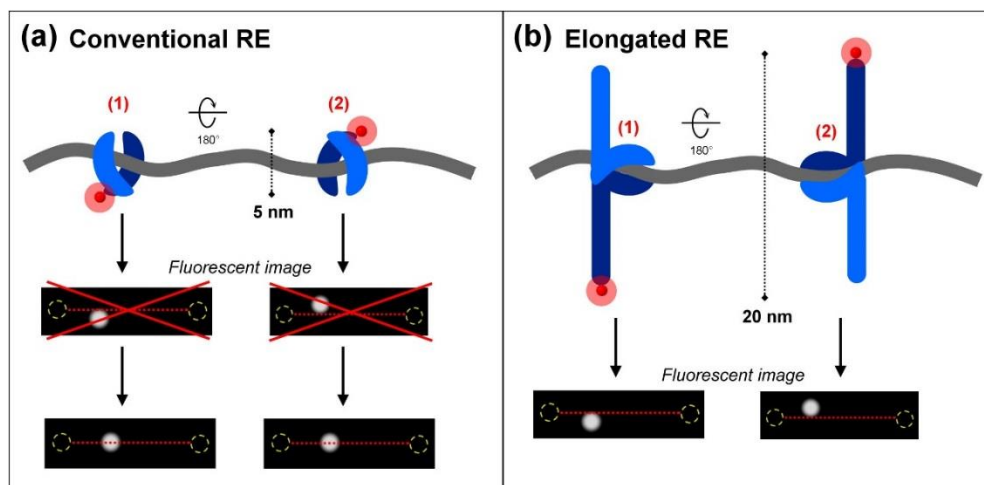


Figure 23: Rational design to visualize rotational movement of a restriction enzyme. (a) Conventional restriction enzyme, directly labeled with a fluorophore (b) Elongated restriction enzyme, labeled at the terminal end of the extension component scRM6. The DNA molecule is indicated in grey, each subunit of the homodimeric restriction enzyme is colored in light and dark blue, the fluorophore is indicated by a red sphere. The fluorescent images are explained in Figure 10A.

It becomes obvious that in order to circumvent the spatial resolution limit, the distance between the fluorophore and the DNA axis needs to be increased. To this end, an elongated restriction enzyme has been prepared (3.1.1). As restriction enzyme component the well-characterized Type IIP restriction enzyme EcoRV and as extension component the engineered Rop (repressor of primer) protein scRM6 has been used [91]. scRM6 is a homotetramer, which consist of a left-handed, all-antiparallel four-helix bundle with a hydrophobic core [91]. It has a heptad sequence periodicity (a periodicity of seven residues in the primary sequence) with the first and fourth residue being hydrophobic, which leads to the association of α -helices and the formation of a stable coiled coil [91]. The fusion protein scRM6-EcoRV was created by fusing the single-cysteine variant scRM6 D54C via its C-terminal α -helix to the N-terminal α -helix of the cysteine-free variant EcoRV C21S (2.2.2.7), resulting in two scRM6 proteins that were fused to one EcoRV homodimer (Figure 24). The position of the single-cysteine residue is located in a loop at the tip of the four-helix bundle, whereby the distance between the fluorophore and the DNA axis could be increased considerably. If we consider this elongated restriction enzyme (diameter of ~ 20 nm, labeled at the tip of scRM6) turning 180° around the DNA molecule, the transversal position of the fluorophore is expected to change by ~ 20 nm (Figure 23b). Using super-resolution fluorescence microscopy imaging techniques [92], this larger distance change should be resolvable, thereby visualizing a rotational motion.

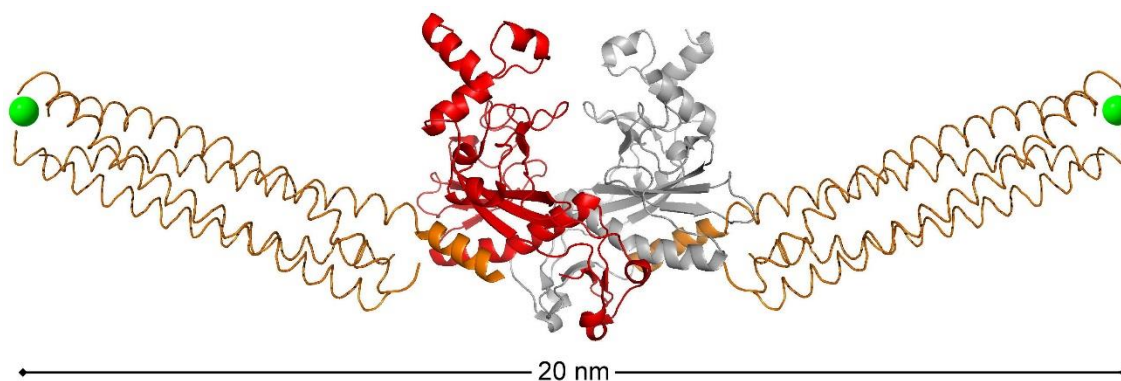


Figure 24: Model of the scRM6-EcoRV fusion protein. *Middle:* restriction enzyme EcoRV (4RVE without specific DNA), the two subunits of the homodimeric protein are colored in red and grey, the N-terminal α -helix in each subunit is colored in orange. *Left and right:* engineered Rop protein scRM6 (1QX8), all subunits of the homotetrameric protein are colored in orange. The C-terminal α -helix of scRM6 is directly fused to the N-terminal α -helix of EcoRV. The green spheres indicate the position of the single-cysteine residues and the fluorescent label.

After the preparation of the scRM6-EcoRV fusion protein (3.1.1), it was initially tested if the extension component scRM6 has an influence on the binding or cleavage activity of the restriction enzyme component EcoRV (3.1.2). Next, the spatial expansion of the scRM6-EcoRV fusion protein was investigated applying FRET measurements (3.1.3). Finally, single-molecule experiments were performed to demonstrate rotational movement indirectly by measuring D_1 of the scRM6-EcoRV fusion protein and comparing it to theoretical models (3.1.4) as well as to directly visualize the rotation with super-resolution fluorescence microscopy [92].

3.1.1 Preparation of the scRM6-EcoRV fusion protein

The scRM6-EcoRV fusion protein, consisting of the homodimeric restriction enzyme EcoRV and the homotetrameric engineered Rop protein scRM6, was cloned as described in 2.2.2.7. In order to specifically label the scRM6-EcoRV fusion protein with a fluorophore (2.2.3.4), a modified gene coding for the **single-cysteine variant** scRM6 D54C was synthesized by GeneArt. Eight native cysteine residues at position 33, 47, 90, 104, 147, 161, 204 and 218 were replaced by alanine residues and a single cysteine residue was introduced at position 54 in the first loop, which is located at the outside of the protein (see Figure 25).

TKQEK TALNMARFIRSQTLTLLEKLNELADI AESLHDHADELYRS ALARF GD CGENL
 TKQEK TALNMARFIRSQTLTLLEKLNELADI AESLHDHADELYRS ALARF GDDGENL
 TKQEK TALNMARFIRSQTLTLLEKLNELADI AESLHDHADELYRS ALARF GDDGENL
 TKQEK TALNMARFIRSQTLTLLEKLNELADI AESLHDHADELYRS ALARF GDDGENL

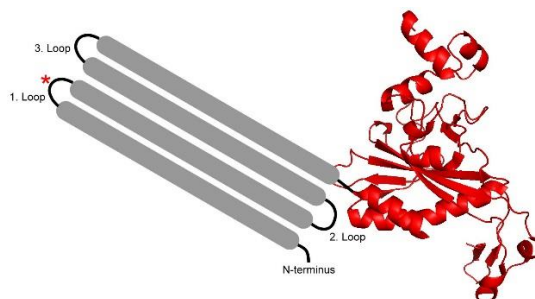


Figure 25: Single cysteine variant of the fusion protein scRM6-EcoRV. Upper: Amino acid sequence of the homotetramer scRM6. The eight native cysteine residues were exchanged for alanine residues (indicated in green) and a single cysteine residue was introduced in the first loop at position 54. Lower: Schematic representation of one subunit of the dimeric fusion protein. EcoRV is indicated in red, scRM6 is indicated in grey. The position of the single cysteine residue in the first loop is indicated by a red star.

In the scRM6-EcoRV fusion protein, the C-terminal α -helix of scRM6 D54C should be fused to the N-terminal α -helix of EcoRV C21S in a way that an elongated α -helix and a rigid connection between the two proteins is generated (Figure 24). In order to evaluate the optimal connection between the two proteins (with regard to binding- and cleavage activity and spatial expansion), **different linker variants** of the scRM6-EcoRV fusion protein were prepared by site directed mutagenesis (2.2.2.6). The gene coding for the single-cysteine variant scRM6 D54C-EcoRV C21S (containing a 15 amino acids long peptide linker between the two proteins) was used as template and five different variants with peptide linkers of 0, 1, 2 and 3 amino acids in length were prepared (Table 22).

Table 22: Different linker variants of the scRM6-EcoRV fusion protein.

Protein variant	Amino acid sequence of the peptide linker	Linker Length
scRM6 D54C-EcoRV C21S	α -helix-GDDGENLENLYFQGK- α -helix	15
scRM6 D54C-L ₍₀₎ -EcoRV C21S	α -helix- α -helix	0
scRM6 D54C-L _(G) -EcoRV C21S	α -helix-G- α -helix	1
scRM6 D54C-L _(N) -EcoRV C21S	α -helix-N- α -helix	1
scRM6 D54C-L _(NA) -EcoRV C21S	α -helix-NA- α -helix	2
scRM6 D54C-L _(NAS) -EcoRV C21S	α -helix-NAS- α -helix	3

3.1.1.1 Purification of the scRM6-EcoRV fusion protein

The single-cysteine variant scRM6 D54-EcoRV C21S and the different single-cysteine linker variants scRM6 D54-L_(x)-EcoRV C21S have been purified via Ni-NTA agarose as described in 2.2.2.10 using the purification buffers listed in Table 3. A representative SDS gel with the different fractions of the purification procedure is shown in Figure 26 for the variant scRM6 D54C-EcoRV C21S.

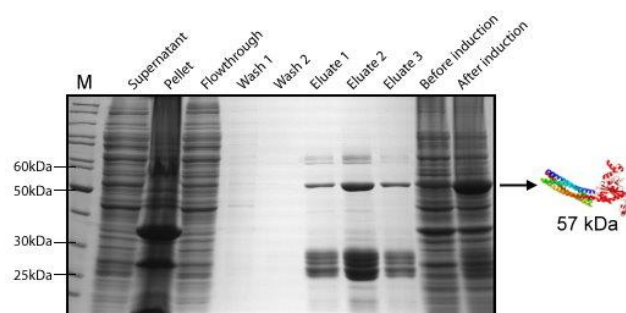


Figure 26: Purification of scRM6 D54C-EcoRV C21S via Ni-NTA agarose. 12 % (v/v) SDS gel, stained with Coomassie Brilliant Blue. M = marker (PageRuler™ Protein Ladder, Fermentas). According to the sum of the molecular mass of the individual components, the fusion protein is supposed to have a size of 57 kDa.

By comparing the lanes before and after induction (last two lanes) it can be seen that the fusion protein shows a strong expression. The three lanes of the eluates (eluate 1, 2, 3) show various bands; one defined band with a size of ~ 57 kDa, which corresponds to the size of the fusion protein, lots of smaller bands between 25 to 30 kDa, which correspond to the size of the individual components (indicated that the fusion protein could have been broken apart during purification) and also bands between 70 and 85 kDa. In order to separate the fusion protein from other proteins that could be found in the eluates, a second purification step was conducted using a Heparin column (HiTrap™ Heparin HP 1mL) connected to the ÄKTA purifier (2.2.2.10). Heparin is negatively charged and allows for purification of DNA-binding proteins. The fusion proteins were eluted via a linear salt gradient using the low and high salt buffer given in Table 3. The results of the Heparin purification are shown in Figure 27 for the variant scRM6 D54-EcoRV C21S.

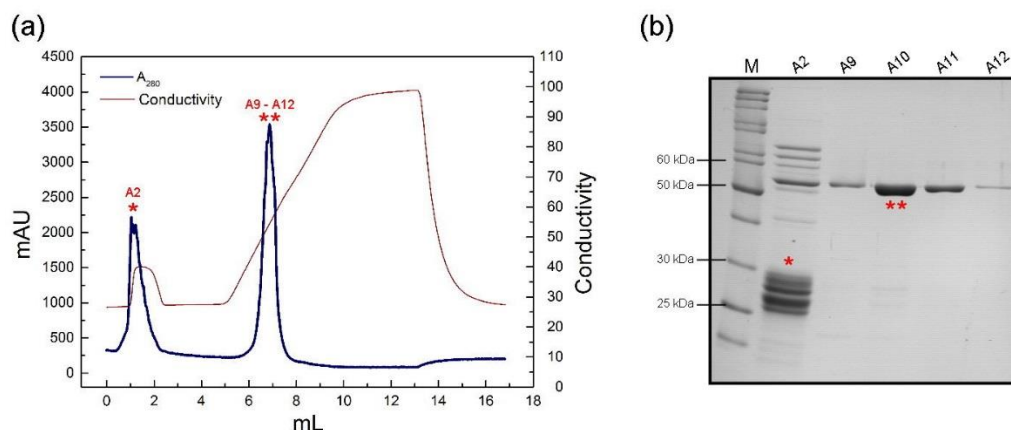


Figure 27: Purification of *scRM6 D54C-EcoRV C21S* via Heparin column. (a) Chromatogram of the purification. blue = absorption at 280 nm, brown = conductivity, * = first peak, ** = second peak (b) 12 % (v/v) SDS-gel, stained with Coomassie Brilliant Blue. M = marker (PageRuler™ Protein Ladder, Fermentas), A2 = fraction, which corresponds to the first peak, A9 – A12 = fractions, which correspond to the second peak.

On the chromatogram (Figure 27a) it can be seen that the conductivity starts at a value of 26 mS/cm, which corresponds to the salt concentration of the low salt buffer only (250 mM NaCl). After injection of the protein sample, the conductivity shortly increases up to a value of 40 mS/cm and decreases subsequently to the initial value of 26 mS/cm. It can be seen that after injection of the protein sample the absorption at 280 nm increases, indicative for the elution of unbound protein. After increasing the salt concentration linearly by mixing low salt with high salt buffer, the conductivity starts to increase again. This leads to the elution of further proteins, which can be seen by an increase in the absorption at 280 nm. The second peak appears at a conductivity of 55 mS/cm, which corresponds to a salt concentration of 530 mM NaCl. 3 μ L of fraction A2 (which corresponds to the first peak) and 2 μ L of fractions A9 – A12 (which correspond to the second peak) were analyzed on a SDS-gel (Figure 27b). The analysis of the gel shows that the fusion protein could be successfully separated from the individual components. Fractions corresponding to the second peak contained the desired fusion proteins with a size of 57 kDa. Fractions corresponding to the first peak contained the individual components with a size of 25 – 30 kDa and 70 – 85 kDa, but also a small amount of the fusion protein.

3.1.2 Biochemical characterization of the scRM6-EcoRV fusion protein

After the successful preparation and purification of the different scRM6-EcoRV fusion protein variants, it has been analyzed whether the extension component scRM6 has any influence on the binding or cleavage activity of the restriction enzyme component EcoRV. The activity was always compared to that of the wild type enzyme EcoRV C21S.

3.1.2.1 Determination of cleavage activity

The cleavage activity of different scRM6-EcoRV fusion protein variants was tested as described in chapter 2.2.2.13. The plasmid pAT-PEB contains a single recognition site for EcoRV, thus the conversion from supercoiled to linearized form is correlated with cleavage and can be detected on a gel. The results of the assay are shown in Figure 28.

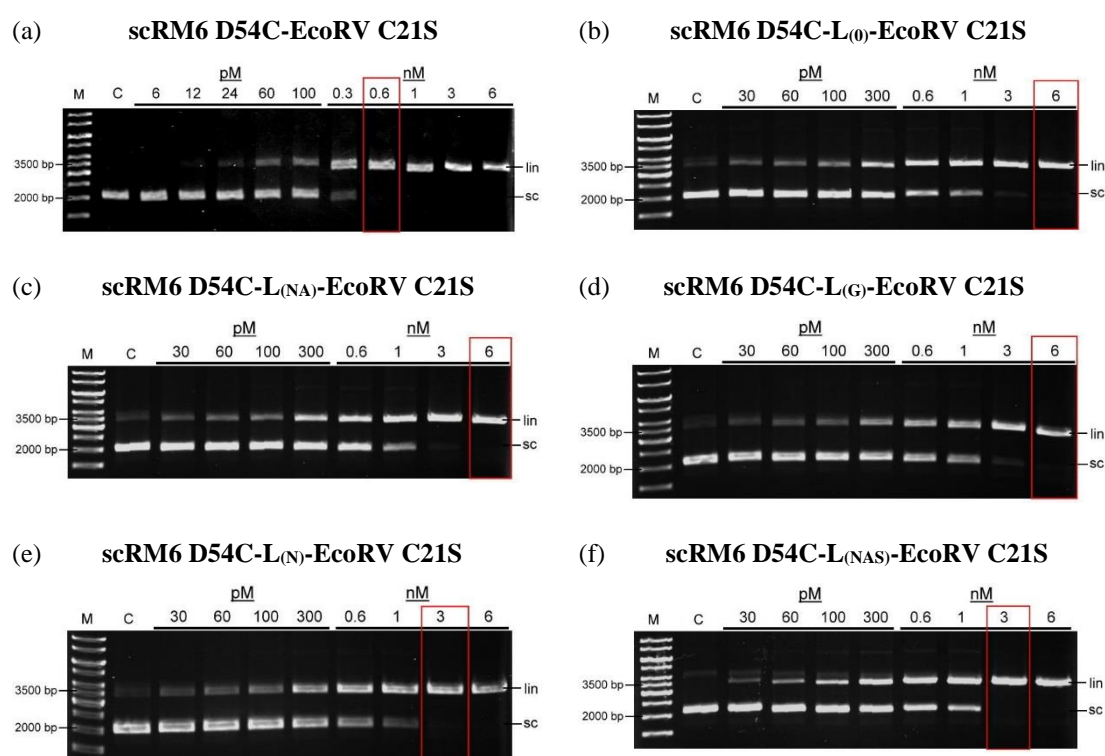


Figure 28: Activity assay of different scRM6-EcoRV fusion protein variants. (a) scRM6 D54-EcoRV C21S, (b) scRM6 D54-L₍₀₎-EcoRV C21S, (c) scRM6 D54-L_(NA)-EcoRV C21S, (d) scRM6 D54-L_(G)-EcoRV C21S, (e) scRM6 D54-L_(N)-EcoRV C21S, (f) scRM6 D54-L_(NAS)-EcoRV C21S. Different concentrations of enzyme were incubated with 6 nM plasmid-DNA (pAT-PEB) and separated on a 0.8 % agarose gel. Gels were stained with ethidium bromide. M = marker (GeneRuler™ 1kb DNA ladder, Fermentas), C = control (uncleaved), lin = linearized plasmid-DNA, sc = supercoiled plasmid-DNA.

It can be seen for all scRM6-EcoRV fusion protein variants that the higher the concentration of the enzyme the more linearized plasmid-DNA appears while the supercoiled plasmid-DNA disappears. The activity assay shows that full cleavage (indicated by the red box) occurs at a concentration of 600 pM for the variant with the original 15 aa linker (scRM6 D54-EcoRV C21S), at a concentration of 6 nM for the variants with the linker L_0 , L_G and L_{NA} and at a concentration of 3 nM for the variants with the linker L_N and L_{NAS} . In contrast, the wild type EcoRV C21S cleaved the plasmid-DNA already at a concentration of 100 pM completely (Figure 37c). This reveals that all scRM6-EcoRV fusion protein variants have a reduced cleavage activity compared to the wild type EcoRV. The cleavage activity of the variant with the original 15 aa linker is reduced by a factor of 6, whereas the cleavage activity of the variants with the shorter linkers is reduced by a factor of 60 (L_0 , L_G and L_{NA}) or 30 (L_N and L_{NAS}).

3.1.2.2 Determination of binding activity

The binding activity of wild type EcoRV C21S and different scRM6-EcoRV fusion protein variants was tested using fluorescence anisotropy as described in chapter 2.2.3.1. The protein was titrated in the presence of 5 mM CaCl_2 to a specific 16 bp oligonucleotide, labeled at the 5'-end with a HEX-fluorophore (1 nM for wild type EcoRV and 2 nM for scRM6-EcoRV fusion protein variants). Representative binding curves are shown in Figure 29 for the wild type EcoRV C21S and the variants scRM6 D54-EcoRV C21S and scRM6 D54- $L_{(0)}$ -EcoRV C21S. The dissociation constants (K_D) of all variants are summarized in Table 23.

Table 23: K_D values for wild type EcoRV and different scRM6-EcoRV fusion protein variants.

Protein variant	K_D [nM]
EcoRV C21S	8 ± 1
scRM6 D54C-EcoRV C21S	78 ± 6
scRM6 D54C-$L_{(0)}$-EcoRV C21S	37 ± 3
scRM6 D54C-$L_{(NA)}$-EcoRV C21S	58 ± 4
scRM6 D54C-$L_{(G)}$-EcoRV C21S	31 ± 3
scRM6 D54C-$L_{(N)}$-EcoRV C21S	27 ± 3
scRM6 D54C-$L_{(NAS)}$-EcoRV C21S	23 ± 2

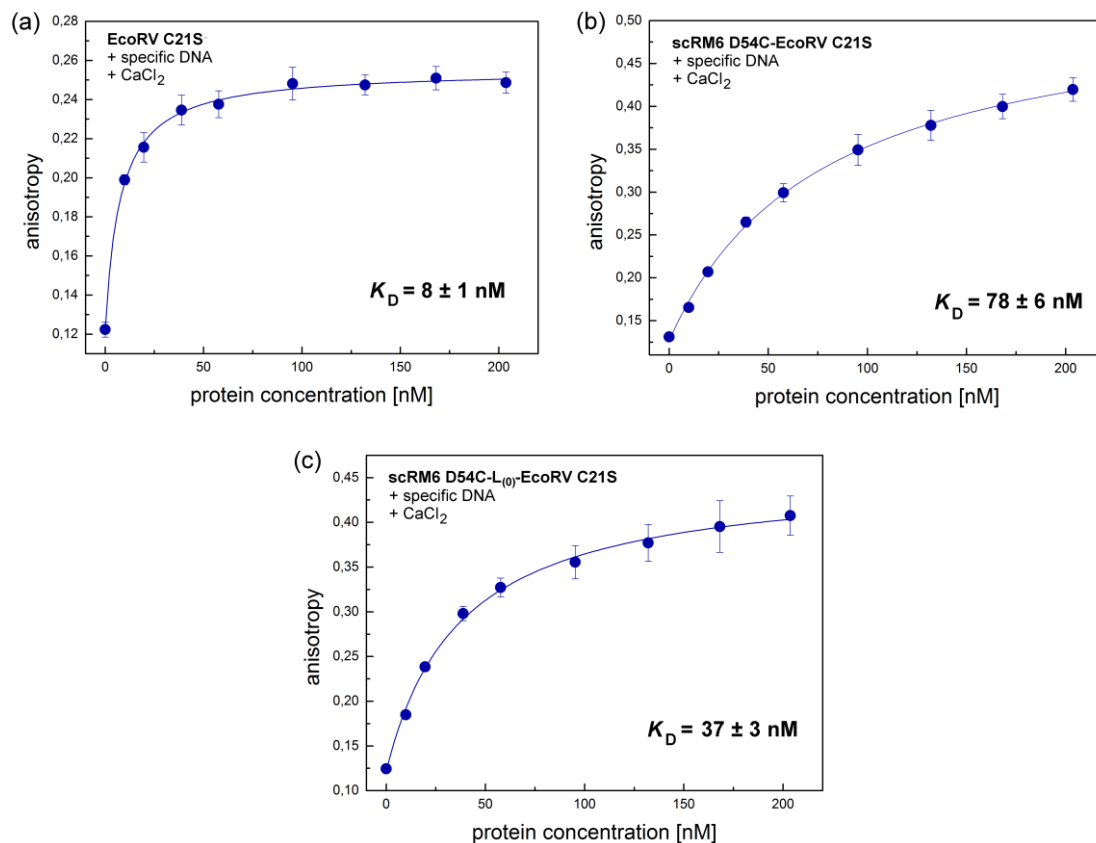


Figure 29: Representative binding curves for wild type EcoRV and different scRM6-EcoRV fusion protein variants. (a) Wild type EcoRV C21S, (b) fusion protein scRM6 D54C-EcoRV C21S and (c) fusion protein scRM6 D54C-L₍₀₎-EcoRV C21S. Binding was tested with a 16 bp oligonucleotide containing a central specific recognition site for EcoRV (1 nM or 2 nM). The anisotropy was measured for different protein concentrations. A simple bimolecular binding model was fitted by non-linear regression to the data points. The results are the average of at least three independent experiments.

The binding curves in Figure 29 show that with increasing protein concentration also the anisotropy increases, indicative of binding of the protein to the DNA. The K_D -values presented in Table 23 show that all scRM6-EcoRV fusion protein variants have a reduced binding activity compared to the wild type EcoRV. The binding activity of the variant with the original 15 aa linker (scRM6 D54C-EcoRV C21S) is reduced by a factor of 10, whereas the binding activity of the variants with the shorter linkers is reduced by a factor of 3 (L_{NAS} and L_N), 4 (L_G), 5 (L₀) and 7 (L_{NA}), respectively.

3.1.2.3 Michaelis-Menten kinetics

Michaelis-Menten kinetics were performed with wild type EcoRV C21S and different scRM6-EcoRV fusion protein variants as described in chapter 2.2.3.2. Each protein variant was incubated in the presence of 10 mM MgCl₂ with different concentrations of a 5'-HEX-labeled molecular beacon, containing a specific recognition site for EcoRV. Cleavage of the beacon was monitored via an increase in the fluorescence over time. Representative Michaelis-Menten curves are shown in Figure 30 for wild type EcoRV C21S and the variants scRM6 D54-EcoRV C21S and scRM6 D54-L₍₀₎-EcoRV C21S. The Michaelis-Menten constants (K_M), the turnover numbers (k_{cat}) and the catalytic efficiencies (k_{cat}/K_M) of all variants are summarized in Table 24.

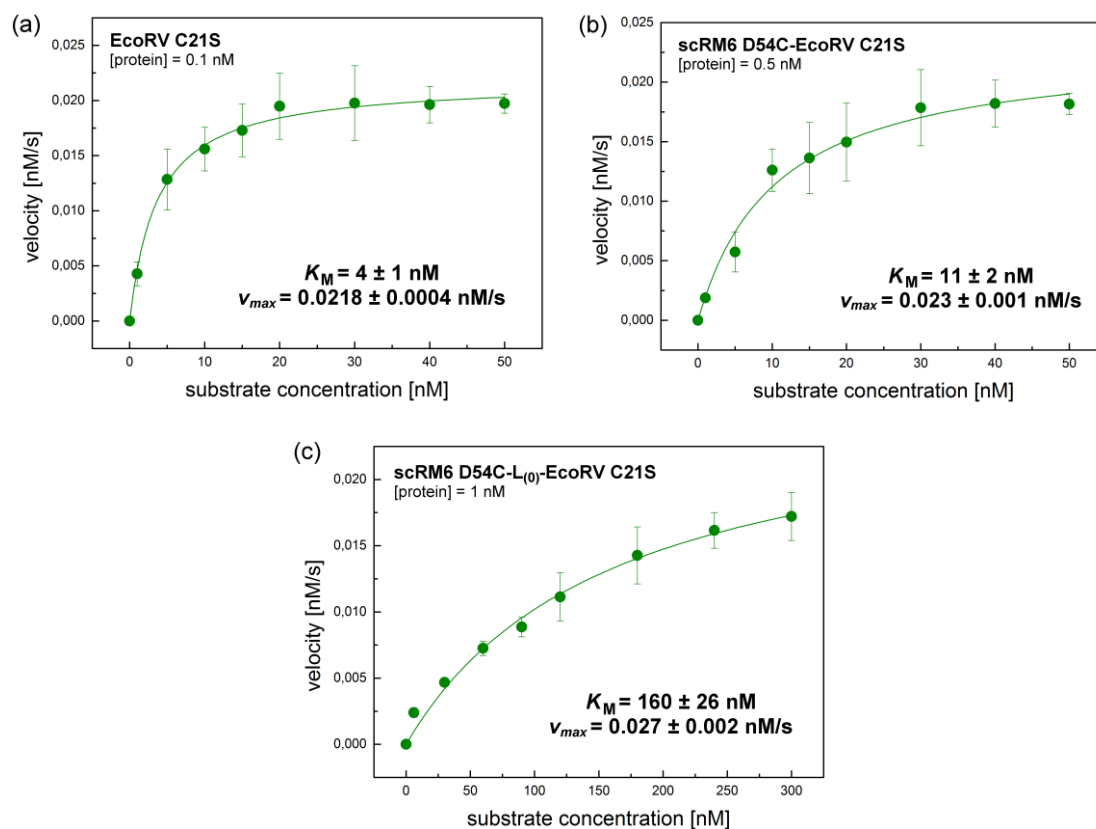


Figure 30: Representative Michaelis-Menten curves for wild type EcoRV and different scRM6-EcoRV fusion protein variants. (a) Wild type EcoRV C21S, (b) fusion protein scRM6 D54-EcoRV C21S and (c) fusion protein scRM6 D54-L₍₀₎-EcoRV C21S. The cleavage assay was performed with a 5'-HEX-labeled molecular beacon, containing a specific recognition site for EcoRV (GATATC). The increase in fluorescence over time was monitored for different substrate concentrations. The Michaelis-Menten equation was fitted by non-linear regression to the data points. The results are the average of at least three independent experiments.

Table 24: K_M , k_{cat} and k_{cat}/K_M values for wild type EcoRV and different scRM6-EcoRV fusion protein variants.

Protein variant	K_M [nM]	k_{cat} [s^{-1}]	k_{cat}/K_M [$s^{-1}\mu M^{-1}$]
EcoRV C21S	4 ± 1	0.218 ± 0.004	54.25
scRM6 D54C-EcoRV C21S	11 ± 2	0.046 ± 0.001	4.16
scRM6 D54C-L₍₀₎-EcoRV C21S	160 ± 26	0.027 ± 0.002	0.17
scRM6 D54C-L_(NA)-EcoRV C21S	116 ± 21	0.024 ± 0.002	0.20
scRM6 D54C-L_(G)-EcoRV C21S	137 ± 19	0.022 ± 0.001	0.16
scRM6 D54C-L_(N)-EcoRV C21S	78 ± 14	0.031 ± 0.002	0.40
scRM6 D54C-L_(NAS)-EcoRV C21S	86 ± 13	0.039 ± 0.002	0.46

The Michaelis-Menten curves in Figure 30 show that with increasing substrate concentration also the velocity of the cleavage reaction increases up to a characteristic maximum velocity (v_{max}). The Michaelis-Menten parameters presented in Table 24 show that all scRM6-EcoRV fusion protein variants have a reduced cleavage activity compared to the wild type EcoRV. The K_M of the variant with the original 15 aa linker (scRM6 D54-EcoRV C21S) is reduced by a factor of 3, whereas K_M of the variants with the shorter linkers was reduced by a factor between 20 (L_N) and 40 (L_0). Interestingly, the k_{cat} is reduced in a comparable manner for all fusion protein variants by a factor between 5 (scRM6 D54-EcoRV C21S) and 10 (L_G). Whereas the k_{cat}/K_M value of the variant with the original 15 aa linker is reduced by a factor of 13, the k_{cat}/K_M values of the variants with the shorter linkers are reduced by a factor between 120 (L_{NAS}) and 340 (L_G).

3.1.3 Studying the spatial expansion via FRET

In order to resolve a rotational movement of the scRM6-EcoRV fusion protein in single-molecule experiments, it is of fundamental importance that the extension component scRM6 is stretched out as modeled in Figure 24. Only when the distance between the DNA axis and the fluorophore is sufficiently large, the transverse position of the fluorescent spot can be distinguished in a rotational movement. Ideally this would mean that the extension component scRM6 is positioned all perpendicular to the DNA axis. Because scRM6 is directly fused to the N-terminal α -helix of EcoRV it can be assumed that the spatial orientation of the N-terminal α -helix (Figure 31) determines the spatial orientation of the extension component scRM6, if the fusion leads to a continuous elongated α -helix.

A first analysis based on the co-crystal structure of EcoRV revealed that the N-terminal α -helix is not maximally stretched out (or all perpendicular) but rather directed towards the DNA molecule from a top view (Figure 31a) and rather oriented upwards from a side view (Figure 31b).

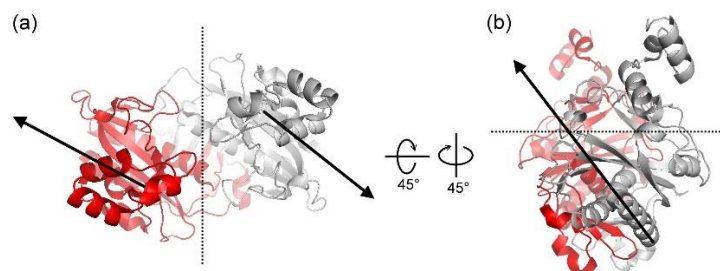


Figure 31: Spatial orientation of the N-terminal α -helix of EcoRV. (a) Top view, (b) Side view. The two subunits of the homodimeric restriction enzyme EcoRV are colored in red and grey, respectively (4RVE). The black dashed lines indicate the position of the DNA and the black arrows indicate the position and direction of the N-terminal α -helices.

To determine the spatial orientation of the extension component scRM6 in more detail and to find out whether it is stretched out sufficiently, a FRET analysis was performed as described in 2.2.3.6. To this end, different scRM6-EcoRV fusion protein variants were randomly double-labeled with donor and acceptor fluorophore at the single-cysteine position at the outside of scRM6 and the FRET efficiency was determined. The rational design of the FRET measurements is illustrated in Figure 32. Ideally the extension component is stretched out in a way that the distance between the donor and the acceptor fluorophore is in the range of 20 nm. Since energy transfer from donor to acceptor fluorophore can only take place if the distance is smaller than 10 nm, the expectation would be that no FRET signal can be measured, if scRM6 is stretched out sufficiently (Figure 32, middle). As positive control, the FRET efficiency has also been measured for the double-labeled single-cysteine variant EcoRV C21S N154C (Figure 32, left). Since the distance between the two symmetry related cysteine residues in each subunit of the homodimeric protein is smaller than 10 nm, a FRET signal should be measurable. As negative control, the FRET efficiency has also been measured for a 97 bp long DNA substrate, double-labeled at each terminal end with a donor and an acceptor fluorophore, respectively (Figure 32, right). Since the distance between the two terminal ends is larger than 10 nm, a FRET signal should not be measurable.

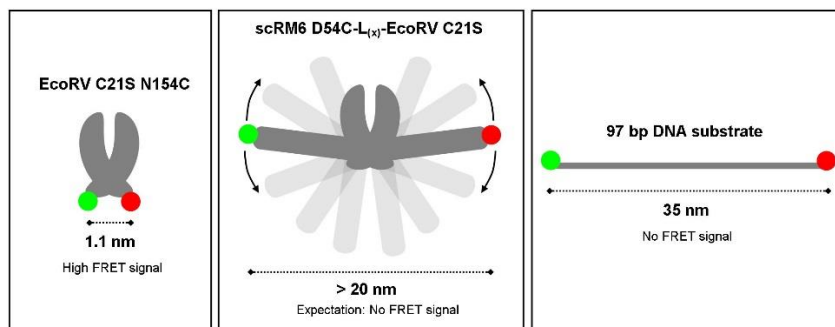


Figure 32: Rational design of FRET measurements to study the spatial expansion of the fusion protein scRM6-EcoRV. Different protein variants and a DNA substrate were double-labeled with a donor (green sphere) and an acceptor (red sphere) fluorophore, respectively and the FRET efficiency was determined. *Left:* single-cysteine variant EcoRV C21S N154. The distance of donor and acceptor is < 10 nm and a FRET signal should be measurable. *Right:* DNA substrate. The distance of donor and acceptor is > 10 nm and a FRET signal should not be measurable. *Middle:* scRM6-EcoRV fusion protein variant. The optimal orientation of the extension component scRM6 is indicated in dark grey, other possible orientations are indicated in light grey. Dependent on the spatial orientation, a FRET signal can be measured or not.

The spatial expansion of the 97 bp DNA substrate, EcoRV C21S N154C and different scRM6-EcoRV fusion protein variants was analyzed by diluting the double-labeled protein or DNA in buffer containing 5 mM CaCl_2 to result in a final concentration of 50 nM (protein) or 25 nM (DNA). After excitation at 470 nm the emission spectrum was recorded, normalized to the maximum donor fluorescence and the FRET efficiency was calculated by dividing the fluorescence intensity of the acceptor at 664 nm by the fluorescence intensity of the donor at 520 nm. In a control experiment, either a 16 bp or 60 bp oligonucleotide was added to the double-labeled protein in the cuvette and the measurement was repeated. In a further control experiment, proteins labeled with only donor or acceptor fluorophore were mixed to result a final concentration of 50 nM and the measurement was repeated. Representative emission spectra of the 97 bp DNA substrate (negative control), EcoRV C21S N154C (positive control) and the fusion protein variant scRM6 D54C-L_(NA)-EcoRV C21S are shown in Figure 33, the corresponding FRET efficiency values of all protein variants are summarized in Table 25.

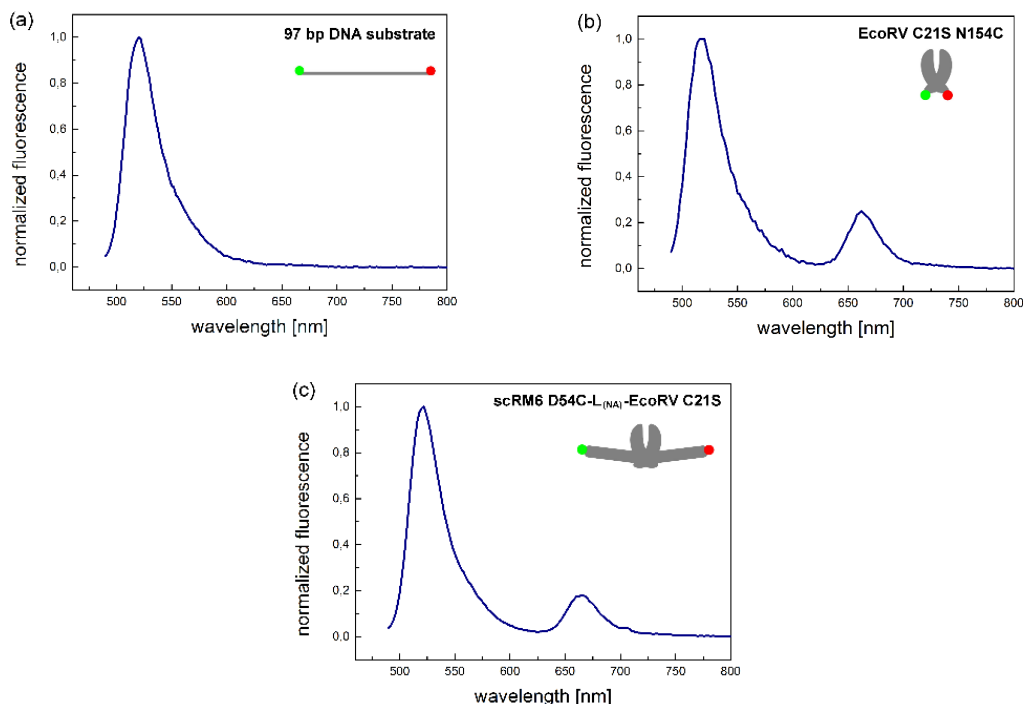


Figure 33: Emission spectra of double-labeled proteins or DNA molecules. (a) Emission spectrum of the double-labeled 97 bp DNA substrate (b) Emission spectrum of double-labeled EcoRV C21S N154C (c) Emission spectrum of double-labeled fusion protein variant scRM6 D54C-L_(NA)-EcoRV C21S. Spectra were normalized to the maximum of donor fluorescence at 520 nm.

The emission spectrum of the double-labeled 97 bp DNA substrate shows only one peak at 520 nm (Figure 33a) whereas the emission spectrum of the double-labeled protein variant EcoRV C21S N154C shows two peaks at 520 nm and 664 nm (Figure 33b) with a corresponding FRET efficiency of 0.23 ± 0.01 (Table 25). Surprisingly, also the double-labeled fusion protein variant scRM6 D54C-L_(NA)-EcoRV C21S (Figure 33c) as well as all other fusion protein variants show an emission spectrum with two peaks at 520 nm and 664 nm. The FRET efficiency values range from 0.17 ± 0.01 for the variant scRM6 D54C-L_(NA)-EcoRV C21S to 0.28 ± 0.01 for the variant scRM6 D54C-L₍₀₎-EcoRV C21S (Table 25). The addition of a 16 bp or 60 bp oligonucleotide to the double-labeled protein results in the same FRET efficiency as for the double-labeled protein alone (0.20 ± 0.01). The mixture of donor and acceptor only labeled proteins instead results in a FRET efficiency of 0.03 which is lower than that of the double-labeled protein (Table 25).

Table 25: FRET efficiencies (E) of different double-labeled protein variants.

Protein variant	FRET efficiency (E)
97 bp DNA substrate	0.01
EcoRV C21S N154C	0.23 ± 0.01
scRM6 D54C-EcoRV C21S	0.20 ± 0.01
+ 16 bp oligonucleotide	0.20 ± 0.01
+ 60 bp oligonucleotide	0.20 ± 0.01
Single labeled protein mix	0.03
scRM6 D54C-L₍₀₎-EcoRV C21S	0.28 ± 0.01
scRM6 D54C-L_(G)-EcoRV C21S	0.22 ± 0.01
scRM6 D54C-L_(N)-EcoRV C21S	0.24 ± 0.01
scRM6 D54C-L_(NA)-EcoRV C21S	0.17 ± 0.01
scRM6 D54C-L_(NAS)-EcoRV C21S	0.21 ± 0.01

3.1.4 Single-molecule experiments

To determine the one-dimensional diffusion coefficient (D_1) of the fusion protein scRM6 D54C-EcoRV C21S and to verify a rotational movement by comparing D_1 with theoretical models, single-molecule experiments were performed as described in 2.2.3.7. The determination of D_1 for the fusion protein was part of a study performed by Dikic et al. [90] which can be considered as an extension of a study performed by Bonnet et al. [77].

In the latter study, D_1 was determined for EcoRV coupled to different fluorescent labels of varying size. The fluorescent label was either a small organic fluorophore (Cy3B with $r = 0.5$ nm) or a small streptavidin organic fluorophore conjugate (savCy3B with $r = 2.1$ nm) or a large quantum dot (QD655 with $r = 15.4$ nm). All fluorescent labels were attached to the protein via a flexible polyethylene glycol linker. In the study performed by Dikic et al. [90] two further quantum dots of varying size coupled to EcoRV via a flexible linker (QD605 with $r = 10.0$ nm via a polyethylene glycol linker and QDEO6 with $r = 7.2$ nm via the N-terminal polyhistidine tag) and the fusion protein scRM6 D54C-EcoRV C21S were investigated. The special feature of the fusion protein is that it represents a conjugation strategy in which the fluorescent label (Cy3B) is coupled to EcoRV via a rigid linker (scRM6). For two reasons scRM6 can be considered as a rigid linker.

On the one hand, scRM6 is a homotetramer with a heptad sequence periodicity and forms a stable coiled-coil structure [91], on the other hand scRM6 was directly fused via its C-terminal α -helix to the N-terminal α -helix of EcoRV, thereby forming an extended α -helix. The scRM6-EcoRV fusion protein can therefore be modeled as EcoRV (with $r = 3.9$ nm) with two spherical labels (scRM6-Cy3B with $r = 3.1$ nm) rigidly attached to the enzyme.

Based on the different conjugation strategies (flexible or rigid linker) and based on the different types of motion (linear diffusion or rotation-coupled diffusion), 5 theoretical models have been established:

- (1) linear diffusion, rigid linker
- (2) rotation-coupled diffusion, rigid linker (one label)
- (3) linear diffusion, flexible linker
- (4) rotation-coupled diffusion, flexible linker
- (5) rotation-coupled diffusion, rigid linker (two labels)

To elucidate the type of motion of scRM6 D54C-EcoRV C21S, D_1 was determined in a first step (see Figure 34a). Subsequently, the friction coefficient (ξ) was derived from D_1 using the Stokes-Einstein relation, normalized to that obtained with EcoRV-Cy3B (considered as unlabeled) and plotted against the radius of the label (see Figure 34b). Finally, the experimental results were compared to the theoretical models.

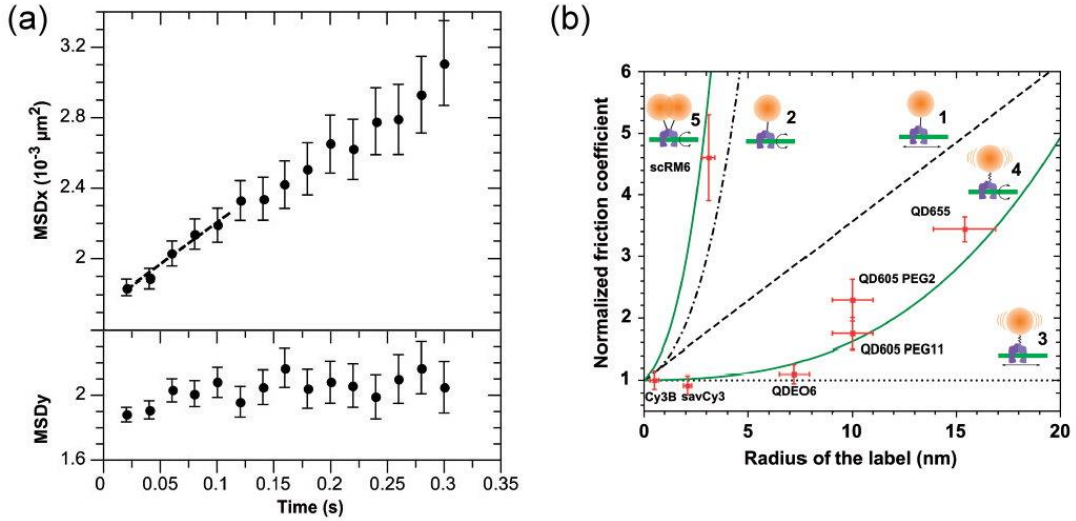


Figure 34: Results of single-molecule experiments. (a) Mean-squared displacement (MSD) of the fusion protein scRM6 D54C-EcoRV C21S. *Upper:* Longitudinal mean-squared displacement (MSD_x). The one-dimensional diffusion coefficient (D_1) is derived from the slope of the curve using the relation $\text{slope} = 2D$. The dashed line indicates the linear fit of the first five data points. *Lower:* Transversal mean-squared displacement (MSD_y). (b) Dependence of the normalized friction coefficient on the label radius. Experimental data are indicated in red. Theoretical data of five different models are indicated by the green or black dashed lines (note that model 5 is the same as model 2 with two labels). EcoRV is represented in magenta, the DNA in green and the label in orange. (Figures adopted from [90]).

The one-dimensional diffusion coefficient of scRM6 D54C-EcoRV C21S, derived from the longitudinal MSD (Figure 34a), was found to be $D_1 = 0.0024 \mu\text{m}^2\text{s}^{-1}$, which is 4-times slower than the one-dimensional diffusion coefficient found for EcoRV labeled with Cy3B ($D_1 = 0.01 \mu\text{m}^2\text{s}^{-1}$) [67]. The normalized friction coefficient showed a significant dependence on the label radius. The experimental data for EcoRV coupled to a fluorescent label via a rigid linker (scRM6-Cy3B) are in agreement with model (5), demonstrating that the diffusion of scRM6 D54C-EcoRV C21S is coupled to rotation (Figure 34b).

3.2 Comparison of structurally different restriction enzymes

Proteins that have to locate their specific recognition site within a high excess of non-specific DNA depend on particular mechanisms to find their target site fast enough to fulfil their biological function. It could be shown in single-molecule experiments [67] that restriction enzymes stay in close contact with the DNA while searching for their recognition site, thereby complementing the 3D-search by a 1D-search (sliding). It would be interesting to know whether the mechanism of sliding is supported by the structure of a restriction enzyme and whether one can derive from the structure of a restriction enzyme to what extent it can slide along the DNA.

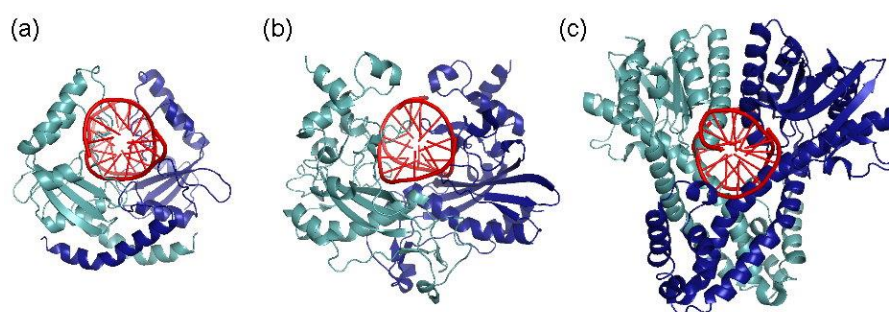


Figure 35: Co-Crystal structures of structurally different type IIP restriction enzymes in complex with specific DNA. (a) PvuII (1PVI), (b) EcoRV (4RVE) and (c) BsoBI (1DC1).

To this end, the structurally different type IIP restriction enzymes PvuII, EcoRV and BsoBI were compared regarding their conformation of the apoenzyme and in complex with specific and non-specific DNA as well as in their ability to make use of linear diffusion to speed up target site location. As it can be seen in Figure 35 that PvuII forms a more open complex with DNA [35] whereas the complexes of EcoRV [30] and BsoBI [36] are partially or fully closed, respectively.

3.2.1 Preparation of single-cysteine variants

In order to study the conformation of the structurally different restriction enzymes alone or in complex with non-specific or specific DNA by FRET measurements, the restriction enzymes PvuII, EcoRV and BsoBI had to be labeled specifically with fluorophores (2.2.3.4). For this purpose a single-cysteine residue had to be introduced into the protein at a defined position. The position was chosen according to the following criteria:

i) no interference with the catalytic center of the restriction enzyme, ii) located at the surface to be accessible, iii) optimal distance for FRET measurements (close to the Förster radius (R_0) of the selected FRET-pair, see 2.2.3.6) and iv) located at a region that is supposed to move upon DNA binding (e.g. close to the DNA-binding domain). The selected positions for each restriction enzyme are shown in Figure 36.

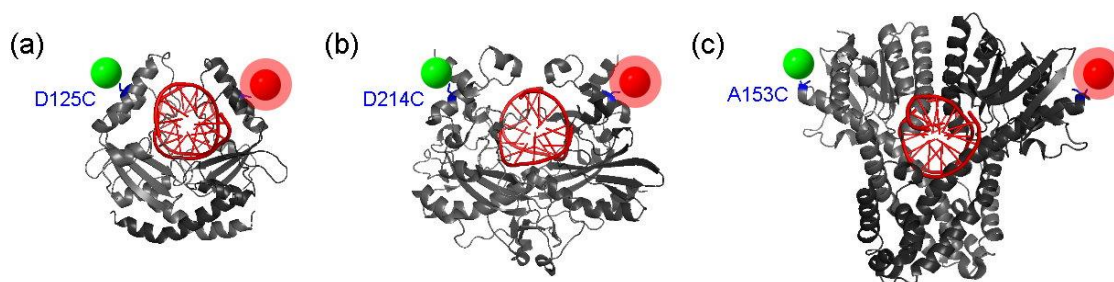


Figure 36: Positions of the single-cysteine substitutions, represented in the co-crystal structure. (a) PvuII D125C, (b) EcoRV D214C and (c) BsoBI A153C. The amino acid residues, which were mutated to cysteine residues are indicated in blue. The proteins were double labeled at the newly introduced cysteine residue with a donor (green sphere) and an acceptor (red sphere) fluorophore.

The plasmid containing the gene coding for the cysteine-free variant of EcoRV and PvuII respectively, was used as a template and site-directed mutagenesis was conducted as described in 2.2.2.6. The aspartic acid residue at position 125 in the PvuII restriction enzyme and the aspartic acid residue at position 214 in the EcoRV restriction enzyme were exchanged for cysteine residues and the success of the substitution was confirmed by sequencing. The single cysteine variant A153C of the BsoBI restriction enzyme had been prepared by Jasmina Dikic [105].

3.2.1.1 Determination of binding and cleavage activity

To test whether the binding and cleavage activity is impaired by the substitution, the activity of the enzyme variants was compared to that of the wild type enzyme. The cleavage activity was tested as described in 2.2.2.13. The plasmid pAT-PEB contains a single recognition site for PvuII and EcoRV, thereby the conversion from supercoiled to linearized plasmid is correlated with cleavage and can be detected on a gel. The results of the activity assay are shown in Figure 37.

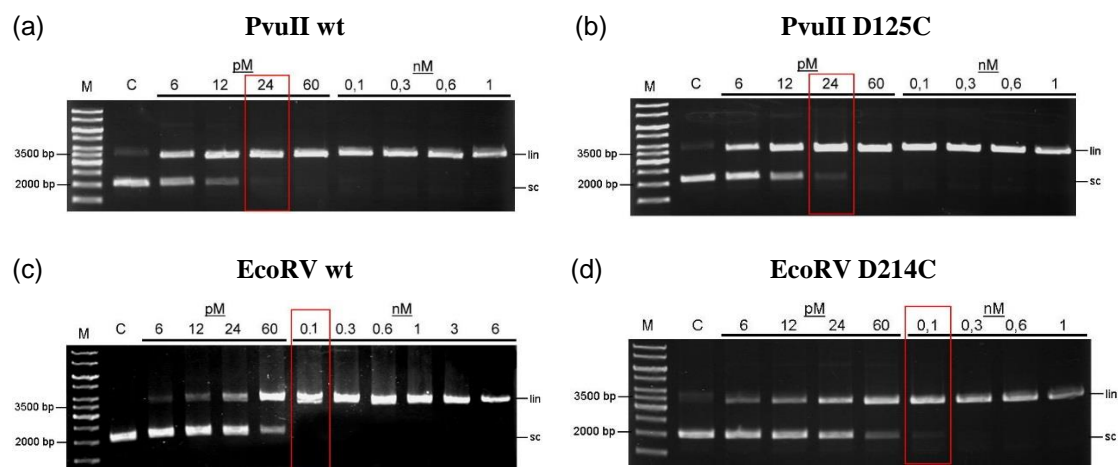


Figure 37: Activity assay of wild type and single cysteine variant. (a) PvuII wild type (wt), (b) PvuII mutant D125C, (c) EcoRV wild type, (d) EcoRV mutant D214C. Different concentrations of enzyme were incubated with 6 nM plasmid DNA (pAT-PEB) and separated on a 0.8 % agarose gel. Gels were stained with ethidium bromide. M = marker (Gene-Ruler™ 1kb DNA ladder, Fermentas), C = control (uncleaved), lin = linearized plasmid-DNA, sc = supercoiled plasmid-DNA.

It can be seen for all restriction enzymes that the higher the concentration of the enzyme the more linearized plasmid-DNA appears while the supercoiled plasmid-DNA disappears. The activity assay shows that full cleavage occurs for wild type PvuII at a concentration of 24 pM (indicated by the red box). The mutant D125C of PvuII shows a negligible lower activity, since at a concentration of 24 pM a weak band for the supercoiled plasmid-DNA can still be seen. The wild type EcoRV cleaves the plasmid-DNA at a concentration of 100 pM completely. As for PvuII also the D214C mutant of EcoRV shows a negligible lower activity than the wild type enzyme. In summary, the single-cysteine variants of EcoRV and PvuII have a similar cleavage activity as their wild type enzymes. The cleavage activity of BsoBI A153C in comparison to the wild type BsoBI had been determined by Jasmina Dikic [105]. Also in this case the substitution at position 153 did not significantly influence the activity.

3.2.1.2 Testing the accessibility of single-cysteine residues

To be accessible for labeling, the cysteine residue had to be introduced on the surface of the protein. Before labeling a protein with a fluorophore, the accessibility was tested by modifying the protein with polyethylene glycol (PEG) as described in chapter 2.2.2.14. Proteins were incubated with PEG maleimide and analyzed on a SDS-polyacrylamide gel. The results of the PEG-modification are shown in Figure 38.

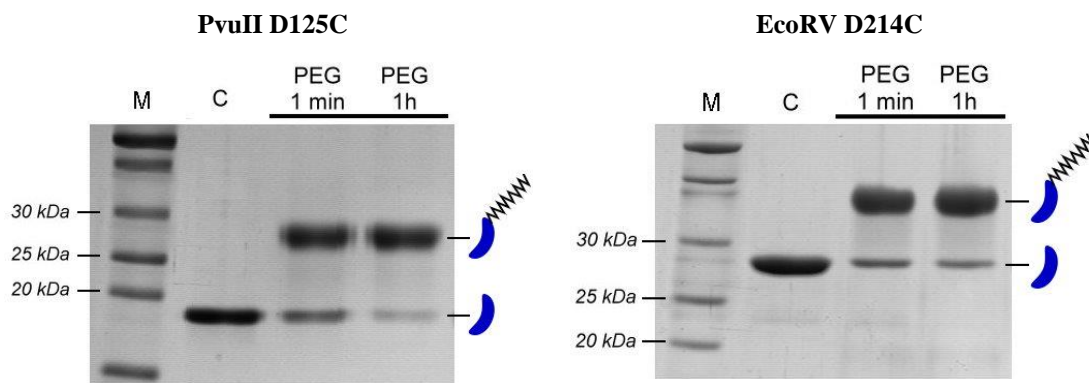


Figure 38: PEG-modification of PvuII D125C and EcoRV D214C. Single-cysteine variants were incubated with a 10-fold molar excess of PEG-maleimide and analyzed on a 15 % (PvuII) or 12 % (EcoRV) SDS-polyacrylamide gel. Gels were stained with Coomassie Brilliant Blue. M = marker (PageRuler™ Protein Ladder, Fermentas), C = control (unmodified), PEG = Polyethylene glycol. The blue half-moon represents one subunit of the protein, the black zigzag chain represents one polyethylene glycol molecule.

Figure 38, left shows the results for PvuII D125C. A single band below 20 kDa can be seen in the second lane which corresponds to one subunit of PvuII D125C which has a size of 18 kDa. The third and the fourth lane show an additional band between 25 and 30 kDa, whereas the intensity of the 18 kDa band decreases. The additional band corresponds to one subunit of PvuII modified with PEG. This band is shifted due to a higher mass and hydrodynamic radius of the protein. More proteins are modified after 1 h ($\approx 91\%$) compared to after 1 min ($\approx 73\%$).

Figure 38, right shows the results for EcoRV D214C. A single band below 30 kDa can be seen in the second lane which corresponds to one subunit of EcoRV D214C which has a size of 29 kDa. The third and the fourth lane show an additional band below 40 kDa, whereas the intensity of the 29 kDa band decreases. The additional band corresponds to one subunit of EcoRV modified with PEG. Slightly more proteins are modified after 1 h ($\approx 85\%$) compared to after 1 min ($\approx 80\%$).

3.2.1.3 Site-specific labeling of single-cysteine variants

To study the conformation (at the entrance to the DNA-binding site) of different type IIP restriction enzymes in the absence and presence of specific and non-specific DNA (3.2.2), enzymes had to be labeled with a donor (Cy3) and an acceptor (Cy5) fluorophore at the single-cysteine residue (in both – identical – subunits of the homodimeric protein). Labeling was performed randomly by incubating the protein first with donor and then with acceptor as described in 2.2.3.4.

The acceptor was added in molar excess in order to minimize the amount of proteins labeled with donor fluorophore only (in both subunits). The free fluorophore was removed and the degree of labeling (DOL) was calculated as described in 2.2.3.5. The calculated labeling degree of the double-labeled variants EcoRV D214C, PvuII D125C and BsoBI A153 is shown in Table 26.

Table 26: Labeling degree for different double labeled protein variants

	Protein monomer conc.	Donor conc.	Acceptor conc.	DOL donor / acceptor	DOL ratio	DOL total
PvuII D125C	15,0 μ M	3,1 μ M	8,9 μ M	21 % / 59 %	2.8	80 %
EcoRV D214C	22,6 μ M	5,9 μ M	9,5 μ M	26 % / 42 %	1.6	68 %
BsoBI A153C	11,9 μ M	1,5 μ M	5,2 μ M	13 % / 44 %	3.4	57 %

Each protein monomer carries one cysteine residue. It can be seen that none of the proteins is completely labeled. The total labeling degree (DOL total) per subunit varies from 57 % for BsoBI, over 68 % for EcoRV to 80 % for PvuII. The amount of protein-bound acceptor fluorophore is always higher than the amount of donor fluorophore. The ratio between the donor and the acceptor fluorophore varies between 1.6 and 3.4. The purity of the labeled proteins and the success of the labeling reaction was confirmed by SDS-PAGE. A representative gel is shown in Figure 39 for EcoRV D214C.

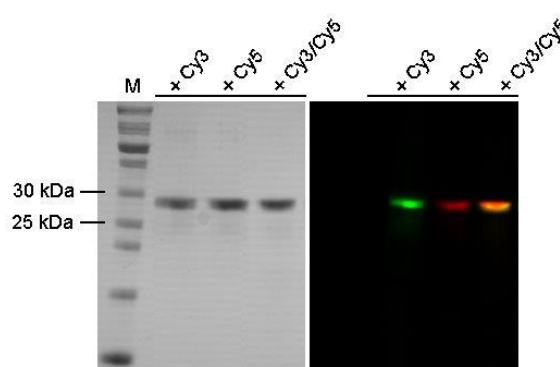


Figure 39: SDS-PAGE of single and double labeled EcoRV D214C. *Left:* Proteins stained with Coomassie Brilliant Blue. *Right:* Merged fluorescent image visualized with the VersaDoc™ Imaging System (Bio-Rad). EcoRV D214C was either single labeled with Cy3 or Cy5 or double labeled with Cy3/Cy5. M = Marker (PageRuler™ Protein Ladder, Fermentas).

The gel shows that labeling was successful for EcoRV D214C (similar results were obtained for PvuII and BsoBI). The green band corresponds to the protein single-labeled with Cy3, the red band corresponds to the protein single-labeled with Cy5 and the yellowish band (merged from green and red) corresponds to the protein double-labeled with Cy3 and Cy5. To test whether the binding and cleavage activity is impaired by the attachment of the fluorophores, the activity of the enzyme variants was compared to that of the wild type enzyme in the same way as it has been described in 3.2.1.1. Also the labeled protein variants showed a comparable activity to their wild-type enzymes.

3.2.2 Studying the conformation of structurally different restriction enzymes

In order to find out which conformation the restriction enzymes EcoRV, PvuII and BsoBI adopt while sliding along the DNA, FRET measurements were performed (2.2.3.6). Restriction endonucleases first bind non-specifically and move along the DNA molecule before they bind specifically to their recognition site. Accordingly, the conformation the enzyme adopts while bound to non-specific DNA is presumably the conformation it uses for sliding [29]. Only for the restriction enzyme EcoRV all relevant crystal structures are available: the apoenzyme, the complex with specific and the complex with non-specific DNA [30] (see Figure 3). By comparing the crystal structures of the specific and non-specific complex one can realize that the DNA-binding cleft of EcoRV in complex with specific DNA is more closed than in complex with non-specific DNA, similarly as it has been reported for BamHI [29]. This can also be derived by measuring the distance between the positions in which cysteine residues in each subunit of the homodimeric protein had been introduced (see Table 27). The distance of the symmetry-related residues in EcoRV at position 214 is smaller in complex with specific DNA than in complex with non-specific DNA (48 Å vs. 57 Å).

Table 27: PDB codes of available crystal structures and distances of single-cysteine residues.*

	Apoenzyme	Non-specific complex	Specific complex
EcoRV	1RVE (47 Å)	2RVE (57 Å)	4RVE (48 Å)
PvuII	1PVU (67 Å)	-	1PVI (48 Å)
BsoBI	-	-	1DC1 (70 Å)

*Distances are indicated in green and were measured from the SH-group of the cysteine residues at position 125 (PvuII), 214 (EcoRV) and 153 (BsoBI) in each subunit of the homodimer using the program PyMOL.

For PvuII only the crystal structures of the apoenzyme and the complex with specific DNA (see Figure 4) and for BsoBI only the crystal structure of the complex with specific DNA are available (see Figure 5). The structure of interest, i.e. the structure of the non-specific complex is missing for both enzymes. For this reason, a comparison between the specific and the non-specific complex on the basis of a distance measurement in the crystal structures, as described above for EcoRV, is not possible. In order to predict the conformation of the enzyme in the non-specific complex, the extent of DNA-binding cleft opening was studied using FRET. To this end a single cysteine residue was introduced into a region close to the DNA-binding domain. Proteins were double-labeled at the defined position with donor and acceptor fluorophore and the FRET efficiency was determined for the apoenzyme, the complex with non-specific and the complex with specific DNA (see 2.2.3.6). The rational design of FRET measurements is shown in Figure 40.

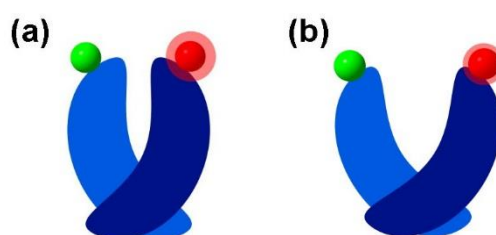


Figure 40: Rational design of FRET measurements to analyze the conformation of a restriction enzyme. (a) The restriction enzyme adopts a closed conformation, thereby donor (green sphere) and acceptor (red sphere) are close together and the FRET efficiency (E) is high. (b) The restriction enzyme adopts an open conformation, thereby donor and acceptor are more separated and the FRET efficiency (E) is low.

The conformation of EcoRV D214C, PvuII D125C and BsoBI A153C was analyzed in steady-state ensemble measurements by mixing double labeled enzyme with either specific or non-specific unlabeled DNA (see Table 14). Experiments were performed in the presence of either Ca^{2+} - or Mg^{2+} -ions or in the presence of EDTA.

Firstly, double labeled EcoRV D214C was diluted in buffer containing either 5 mM CaCl_2 , 10 mM MgCl_2 or 1 mM EDTA to result in a final protein concentration of 50 nM. After excitation at 546 nm the emission spectrum was recorded (emission spectrum of the apoenzyme). Then a 20-fold molar excess of either a specific or a non-specific 16 bp oligonucleotide was added to the cuvette and the measurement was repeated.

As reference, the emission spectrum of donor only labeled EcoRV D214C was recorded. Emission spectra were normalized to the maximum donor fluorescence and the FRET efficiency was calculated by dividing the fluorescence intensity of the acceptor at 666 nm (A) by the fluorescence intensity of the donor at 546 nm (D).

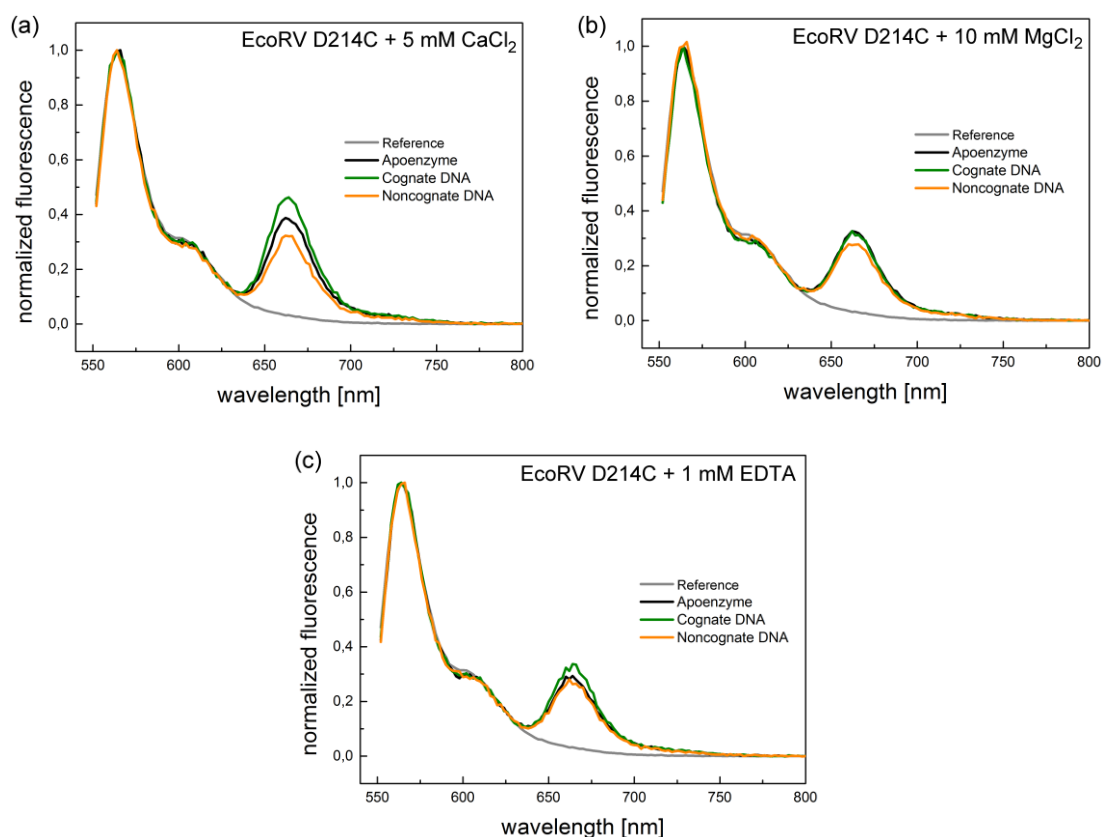


Figure 41: Emission spectra of double-labeled EcoRV D214C. (a) Conformational changes in the presence of CaCl_2 (b) Conformational changes in the presence of MgCl_2 (c) Conformational changes in the presence of EDTA. Donor only labeled enzyme (grey line), double-labeled apoenzyme (black line), double-labeled specific complex (green line), double-labeled non-specific complex (orange line). Spectra were normalized to the maximum of donor fluorescence.

The emission spectra show that in the presence of Ca^{2+} -ions the addition of the specific DNA causes an increase in the acceptor signal, which reflects a movement of the two fluorophores towards each other (Figure 41a). In contrast, the addition of the non-specific DNA causes a decrease in the acceptor signal, which reflects a movement of the two fluorophores away from each other. This shows that the conformation of EcoRV bound to specific DNA is more closed compared to that of the apoenzyme and that the conformation of EcoRV bound to non-specific DNA is more open than that of the apoenzyme and that of EcoRV bound to specific DNA.

In the presence of Mg^{2+} -ions the addition of the specific DNA causes only a slight increase in the acceptor signal (Figure 41b). Because most of the DNA is cleaved in the presence of Mg^{2+} -ions, only the free enzyme can be detected. The addition of the non-specific DNA in the presence of Mg^{2+} -ions causes a slight decrease in the acceptor signal. In the presence of EDTA the addition of either specific or non-specific DNA causes only a slight increase and decrease in the acceptor signal, respectively (Figure 41c).

Table 28: FRET efficiencies (E) of double-labeled *EcoRV D214*.

Metal ion	Protein status	FRET efficiency (E)
Ca^{2+}	Apoenzyme	0.37 ± 0.02
	Non-specific complex	0.32 ± 0.00
	Specific complex	0.46 ± 0.00
Mg^{2+}	Apoenzyme	0.31 ± 0.01
	Non-specific complex	0.29 ± 0.01
	Specific complex	0.33 ± 0.01
EDTA	Apoenzyme	0.30 ± 0.00
	Non-specific complex	0.28 ± 0.00
	Specific complex	0.33 ± 0.01

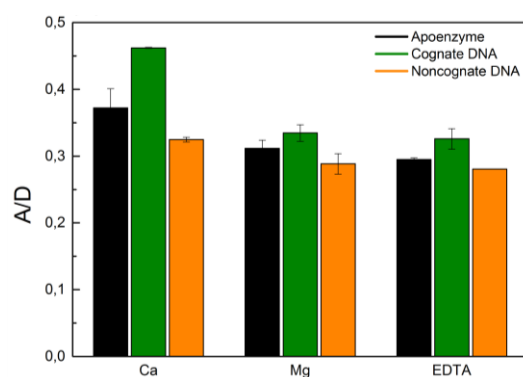


Figure 42: FRET efficiencies (E) of double-labeled *EcoRV D214*. Double-labeled apoenzyme (black bar), addition of specific 16 bp oligonucleotide (green bar), addition of nonspecific 16 bp oligonucleotide (orange bar). The FRET efficiency (A/D) was calculated by dividing the maximum fluorescence of the acceptor signal at 666 nm (A) by the maximum fluorescence of the donor signal at 564 nm (D). The error bars refer to two (specific, non-specific complex) and four (apoenzyme) independent experiments.

The calculated FRET efficiencies are summarized in Table 28 and Figure 42. It can be seen that the complex with specific DNA has always a higher FRET efficiency than the complex with non-specific DNA, which means that the specific complex is more closed than the non-specific complex.

This effect is most prominent in the presence of Ca^{2+} -ions (0.46 vs. 0.32). The FRET efficiency of the apoenzyme is always between that of the complex with specific and non-specific DNA. It can also be seen that the presence of different divalent metal ions has an influence on the conformation of the apoenzyme. In the presence of Ca^{2+} -ions the FRET efficiency of the apoenzyme is higher than in the presence of Mg^{2+} -ions or EDTA (0.37 vs. 0.31 and 0.30), thus the apoenzyme shows a more closed conformation in the presence of Ca^{2+} -ions.

Secondly, double-labeled PvuII D125C was diluted in buffer containing either 5 mM CaCl_2 , 10 mM MgCl_2 or 1 mM EDTA to result in a final protein concentration of 50 nM. After excitation at 546 nm the emission spectrum was recorded. Then a 100-fold excess of either the specific or non-specific 16 bp oligonucleotide was added to the cuvette and the measurement was repeated. As reference, the emission spectrum of donor only labeled PvuII D125C was recorded.

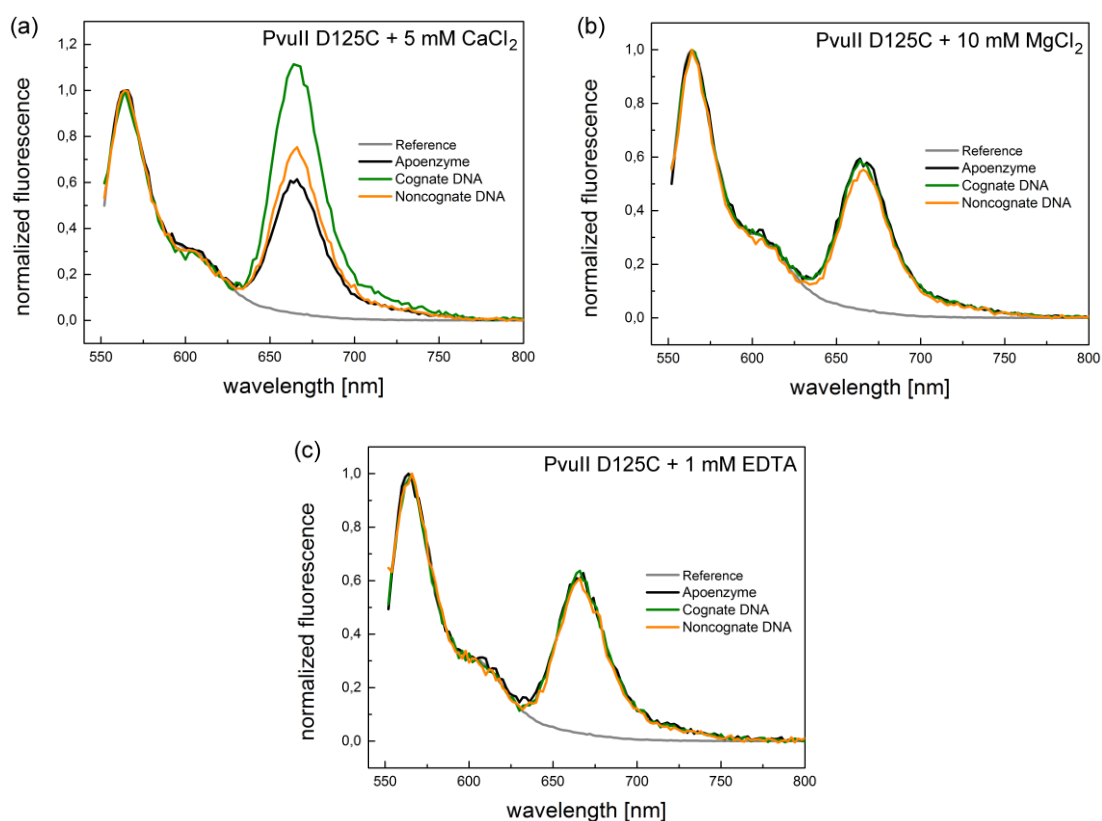


Figure 43: Emission spectra of double-labeled PvuII D125C. For details see legend to Figure 41.

The emission spectra show that in the presence of Ca^{2+} -ions the addition of the specific and the non-specific DNA causes an increase in the acceptor signal, which reflects a movement of the two fluorophores towards each other (Figure 43a). This effect is more pronounced in the presence of specific DNA. It shows that the conformation of PvuII bound to non-specific DNA is more closed compared to that of the apoenzyme and that the conformation of PvuII bound to specific DNA is again more closed than that of the apoenzyme and that of the non-specific complex. In the presence of Mg^{2+} -ions the addition of the specific DNA causes only a slight increase in the acceptor signal (Figure 43b). The addition of the non-specific DNA in the presence of Mg^{2+} -ions induce no change in the acceptor signal. In the presence of EDTA the addition of specific and non-specific DNA causes only a slight increase or no change in the acceptor signal (Figure 43c).

Table 29: FRET efficiencies (E) of double-labeled PvuII D125C.

Metal ion	Protein status	FRET efficiency (E)
Ca^{2+}	Apoenzyme	0.61 ± 0.01
	Non-specific complex	0.74 ± 0.01
	Specific complex	1.12 ± 0.01
Mg^{2+}	Apoenzyme	0.57 ± 0.01
	Non-specific complex	0.56 ± 0.01
	Specific complex	0.60 ± 0.01
EDTA	Apoenzyme	0.60 ± 0.02
	Non-specific complex	0.60 ± 0.00
	Specific complex	0.65 ± 0.01

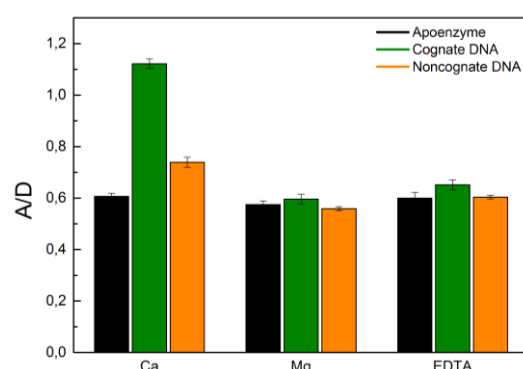


Figure 44: FRET efficiencies (E) of double-labeled PvuII D125C. Double-labeled apoenzyme (black bar), addition of specific 16 bp oligonucleotide (green bar), addition of nonspecific 16 bp oligonucleotide (orange bar). The FRET efficiency (A/D) was calculated by dividing the maximum fluorescence of the acceptor signal at 666 nm (A) by the maximum fluorescence of the donor signal at 564 nm (D). The error bars refer to two (specific, non-specific complex) and four (apoenzyme) independent experiments.

The calculated FRET efficiencies are summarized in Table 29 and Figure 44. It can be seen that the complex with specific DNA has always a higher FRET efficiency than the complex with non-specific DNA, which means that the specific complex is more closed than the non-specific complex. This effect is most prominent in the presence of Ca^{2+} -ions (1.12 vs. 0.74). The FRET efficiency of the apoenzyme is always smaller than that of the complex with specific DNA and smaller or identical with that of the complex with non-specific DNA. It can also be seen that the presence of different divalent metal ions has no influence on the conformation of the apoenzyme, because the FRET efficiency is nearly identical under all conditions (0.61, 0.57 and 0.60).

Thirdly, double labeled BsoBI A153C was diluted in buffer containing either 5 mM CaCl_2 , 10 mM MgCl_2 or 1 mM EDTA to result in a final protein concentration of 50 nM. After excitation at 546 nm the emission spectrum was recorded. Then a 20-fold excess of either the specific or non-specific 16 bp oligonucleotide was added to the cuvette and the measurement was repeated. As reference, the emission spectrum of donor only labeled BsoBI A153C was recorded.

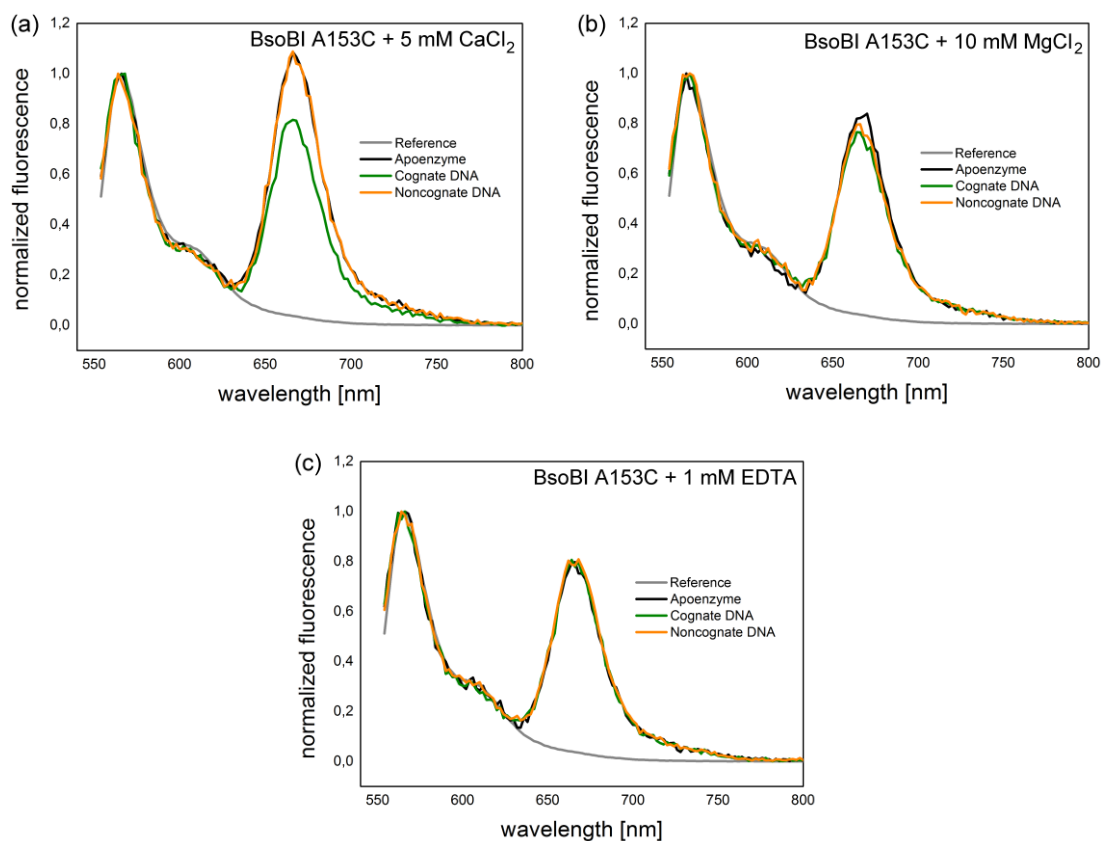


Figure 45: Emission spectra of double labeled BsoBI A153C. For details see legend to Figure 41.

The emission spectra show that in the presence of Ca^{2+} -ions the addition of the specific DNA causes a decrease in the acceptor signal, which reflects a movement of the two fluorophores away from each other (Figure 45a). In contrast, the addition of the non-specific DNA does not induce a change in the acceptor signal. This implies that the conformation of BsoBI bound to specific DNA is apparently more open compared to that of the apoenzyme and that the conformation of BsoBI bound to non-specific DNA is identical to that of the apoenzyme. In the presence of Mg^{2+} -ions the addition of the specific and the non-specific DNA causes only a slight decrease in the acceptor signal, respectively (Figure 45b). The same could be observed in the presence of EDTA (Figure 45c).

Table 30: FRET efficiencies (E) of double-labeled BsoBI A153C.

Metal ion	Protein status	FRET efficiency (E)
Ca^{2+}	Apoenzyme	1.10 ± 0.06
	Non-specific complex	1.10 ± 0.07
	Specific complex	0.82 ± 0.01
Mg^{2+}	Apoenzyme	0.82 ± 0.07
	Non-specific complex	0.79 ± 0.06
	Specific complex	0.76 ± 0.06
EDTA	Apoenzyme	0.80 ± 0.07
	Non-specific complex	0.78 ± 0.06
	Specific complex	0.77 ± 0.03

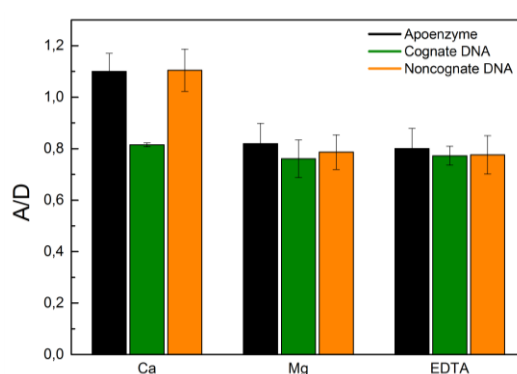


Figure 46: FRET efficiencies (E) of double-labeled BsoBI A153C. Double labeled apoenzyme (black bar), addition of specific 16 bp oligonucleotide (green bar), addition of nonspecific 16 bp oligonucleotide (orange bar). The FRET efficiency (A/D) was calculated by dividing the maximum fluorescence of the acceptor signal at 666 nm (A) by the maximum fluorescence of the donor signal at 564 nm (D). The error bars refer to three (specific, nonspecific complex) and six (apoenzyme) independent experiments.

The calculated FRET efficiencies are summarized in Table 30 and Figure 46. It can be seen that the complex with specific DNA has always a lower FRET efficiency than the complex with non-specific DNA, which means that the specific complex is apparently more open than the non-specific complex (see discussion). This effect is most prominent in the presence of Ca^{2+} -ions (0.82 vs. 1.10). The FRET efficiency of the apoenzyme is identical or slightly higher than that of the complex with non-specific DNA and higher than that of the complex with specific DNA. It can also be seen that the presence of different divalent metal ions has an influence on the conformation of the apoenzyme. In the presence of Ca^{2+} -ions, the FRET efficiency of the apoenzyme is higher than in the presence of Mg^{2+} -ions or EDTA (1.10 vs. 0.82 and 0.80), thus the apoenzyme shows a more closed conformation in the presence of Ca^{2+} ions.

Because the addition of the specific and non-specific DNA in the presence of Mg^{2+} -ions and EDTA did not lead to a pronounced change in the acceptor signal, the binding affinity to these substrates was investigated. The aim was to ensure that the amount of DNA substrate used in the FRET experiments led to binding and that the absence of a change in the acceptor signal was not due to non-binding. The DNA-binding activity of PvuII D125C, EcoRV D214C and BsoBI A153 was tested using fluorescence anisotropy measurements as described in chapter 2.2.3.1. The protein was titrated with either a specific or a non-specific 16 bp oligonucleotide, labeled at the 5'-end with the HEX-fluorophore (2 nM). The sequence of these oligonucleotides has been identical to that of the unlabeled oligonucleotides added in the FRET experiments. The binding was tested in the presence of different divalent metal ions (5 mM CaCl_2 or 10 mM MgCl_2) and in the presence of EDTA. Whereas Ca^{2+} -ions support specific binding but no cleavage, Mg^{2+} -ions support specific binding and cleavage of the DNA substrate. Thus, the combination of specific oligonucleotide and Mg^{2+} -ions was not investigated. Representative binding curves are shown in Figure 47 for PvuII D125C, EcoRV D214C and BsoBI A153C in the presence of non-specific DNA and buffer containing 10 mM MgCl_2 . The dissociation constants (K_D) are summarized in Table 31 for different substrates and different divalent metal ions.

Table 31: K_D values for *PvuII* D125C, *EcoRV* D214C and *BsoBI* A153C.

	Sequence	Metal ion	K_D
PvuII D125C	5'-GTCCG <u>CAGCTG</u> ACCTA-3'	Ca^{2+}	$54 \pm 7 \text{ nM}$
	(specific)	EDTA	$492 \pm 49 \text{ nM}$
	5'-GTCCG <u>GTCGAC</u> ACCTA-3'	Ca^{2+}	$169 \pm 9 \text{ nM}$
	(nonspecific)	EDTA	$605 \pm 13 \text{ nM}$
		Mg^{2+}	$2.0 \pm 0.1 \text{ }\mu\text{M}$
EcoRV D214C	5'-CAGAC <u>GATATC</u> CGTAC-3'	Ca^{2+}	$21 \pm 4 \text{ nM}$
	(specific)	EDTA	$32 \pm 3 \text{ nM}$
	5'-CAGAC <u>CTATAG</u> CGTAC-3'	Ca^{2+}	$17 \pm 4 \text{ nM}$
	(nonspecific)	EDTA	$30 \pm 6 \text{ nM}$
		Mg^{2+}	$69 \pm 8 \text{ nM}$
BsoBI A153C	5'-CGTTG <u>CTCGAG</u> ACATC-3'	Ca^{2+}	$52 \pm 5 \text{ nM}$
	(specific)	EDTA	$99 \pm 6 \text{ nM}$
	5'-CGTTG <u>GAGCTC</u> ACATC-3'	Ca^{2+}	$62 \pm 2 \text{ nM}$
	(nonspecific)	EDTA	$146 \pm 7 \text{ nM}$
		Mg^{2+}	$374 \pm 42 \text{ nM}$

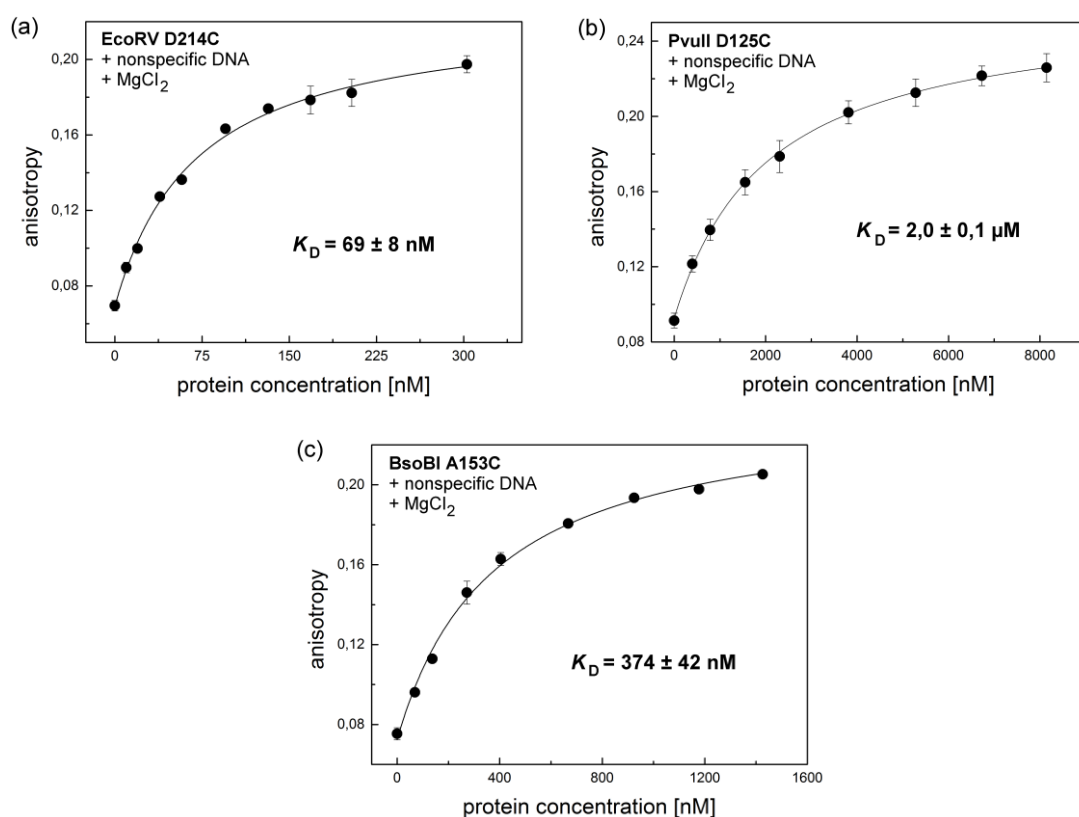


Figure 47: Determination of binding affinity to non-specific DNA in the presence of Mg^{2+} -ions. (a) *EcoRV* D214C, (b) *PvuII* D125C and (c) *BsoBI* A153C. The anisotropy was measured for different protein concentrations. A simple bimolecular binding model was fitted by non-linear regression to the data points. The results are the average of at least three independent experiments.

The binding curves in Figure 47 show that with increasing protein concentrations also the anisotropy increases, indicative of binding of the protein to the DNA. The K_D -values presented in Table 31 show a broad distribution, from the low nanomolar range (17 nM) to the low micromolar range (2 μ M). The highest affinities to the specific and non-specific DNA could be found in the presence of Ca^{2+} -ions. The absence of divalent metal ions as well as the presence of Mg^{2+} -ions decreased the binding affinity.

In order to finally evaluate the extent of DNA-binding cleft opening in the non-specific complex, the corrected FRET efficiencies (E_{corr}) were calculated (for the Ca^{2+} conditions only) as described in chapter 2.2.3.6. The results are presented in Table 32. The corrected values take into consideration that the acceptor signal at 666 nm is not only caused by energy transfer from the donor to the acceptor fluorophore but to a certain extent also by direct excitation of the acceptor fluorophore and signal bleed through from the donor fluorophore.

Table 32: Corrected FRET efficiencies (E_{corr}) in the presence of Ca^{2+} -ions

Restriction enzyme	Protein status	FRET efficiency (E_{corr})
PvuII	Apoenzyme	0.22 ± 0.01
D125C	Non-specific complex	0.31 ± 0.02
	Specific complex	0.59 ± 0.00
EcoRV	Apoenzyme	0.19 ± 0.02
D214C	Non-specific complex	0.14 ± 0.01
	Specific complex	0.26 ± 0.00
BsoBI	Apoenzyme	0.46 ± 0.04
A153C	Non-specific complex	0.45 ± 0.06
	Specific complex	0.26 ± 0.00

It can be seen that the corrected FRET efficiencies (E_{corr}) are in total lower than the uncorrected FRET efficiencies (E) (see Table 28, Table 29 and Table 30). However, the proportions between apoenzyme, non-specific and specific protein-DNA complex are maintained.

3.2.3 Studying linear diffusion of structurally different restriction enzymes

To find out to which extent the structurally different restriction enzymes EcoRV, PvuII and BsoBI make use of linear diffusion, a competitive cleavage assay (2.2.3.3) was employed [31,44,45]. In this assay a short oligonucleotide is cleaved in competition with a long PCR fragment. The oligonucleotide is too short to support linear diffusion to significant extent. The PCR fragments in contrast are long enough to allow the enzyme sliding along the DNA which will accelerate target site location and speed up cleavage. Since the specific recognition site is embedded in an identical sequence context, differences in the cleavage rates of the oligonucleotide and the PCR fragment can only be due to the different length of the two substrates and are correlated with linear diffusion [45]. The ratio of the cleavage rates (k_{long}/k_{short}) is a measure of the ability of the enzyme to make use of linear diffusion and allows comparing different restriction enzymes. The rational design of the competitive cleavage assay is shown in Figure 48.

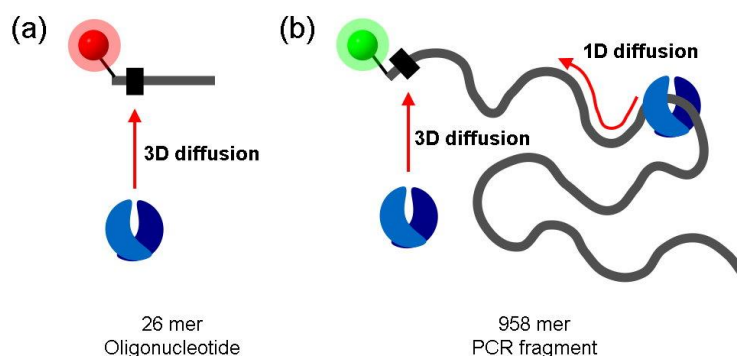


Figure 48: Rational design of the competitive cleavage assay. (a) The target site (black bar) on the short oligonucleotide, 5'-labeled with Atto647N (red dot) can only be reached directly from solution (3D diffusion). (b) The target site on the long PCR fragment, 5'-labeled with Atto488 (green dot) can be reached either directly from solution (3D diffusion) or after non-specific binding and subsequent sliding along the DNA (1D diffusion), which accelerates the location of the target site. Restriction enzymes and DNA fragments are not drawn to scale.

3.2.3.1 Substrate length dependence of linear diffusion

In the first set of experiments, the dependence of the cleavage rate ratio (k_{long}/k_{short}) on the substrate length was investigated. For that purpose, a 26mer oligonucleotide was cleaved in competition with a PCR fragment of 153, 498, 958 or 1488 bp in length. For control, the 26mer was also cleaved in competition with another 26mer.

600 pM of each restriction enzyme were incubated together with 20 nM of the 5'-Atto647N-labeled oligonucleotide and 20 nM of one of the 5'-Atto488-labeled PCR fragments. After appropriate time intervals, samples were withdrawn and analyzed on a denaturing polyacrylamide gel (2.2.2.1). Fluorescent bands were quantified, the amount of substrate cleavage was plotted against the time and cleavage rates of the short oligonucleotide (k_{short}) and the long PCR fragment (k_{long}) were determined independently.

The results of the substrate length dependence of linear diffusion are shown in Figure 49 for EcoRV D214C, in Figure 50 for PvuII D125C and in Figure 51 for BsoBI A153C, respectively. On the polyacrylamide gels, it can be seen that the substrate bands for the 26 bp fragment labeled with Atto647N (red fluorescence) and for the 26, 153, 498, 958 and 1488 bp fragments labeled with Atto488 (green fluorescence) disappear over time, whereas the product bands of a 10 bp fragment (in case of EcoRV and PvuII) or 8 bp fragment (in case of BsoBI) appear over time. Although the cleavage products of the short and the long fragment have the same size, they run with different velocity through the gel, which can be attributed to the different fluorophores. It can also be seen that the PCR fragments were cleaved almost completely (90 - 95 %) whereas the 26 bp oligonucleotides were cleaved only by 40 – 70 %, which can be attributed to the synthetic nature of short oligonucleotides. The cleavage rates for the long PCR fragment and the short oligonucleotide as well as their ratios (k_{long}/k_{short}) and their sum (k_{total}) are summarized in Table 33 for EcoRV D214C, in Table 34 for PvuII D125C and in Table 35 for BsoBI A153C, respectively.

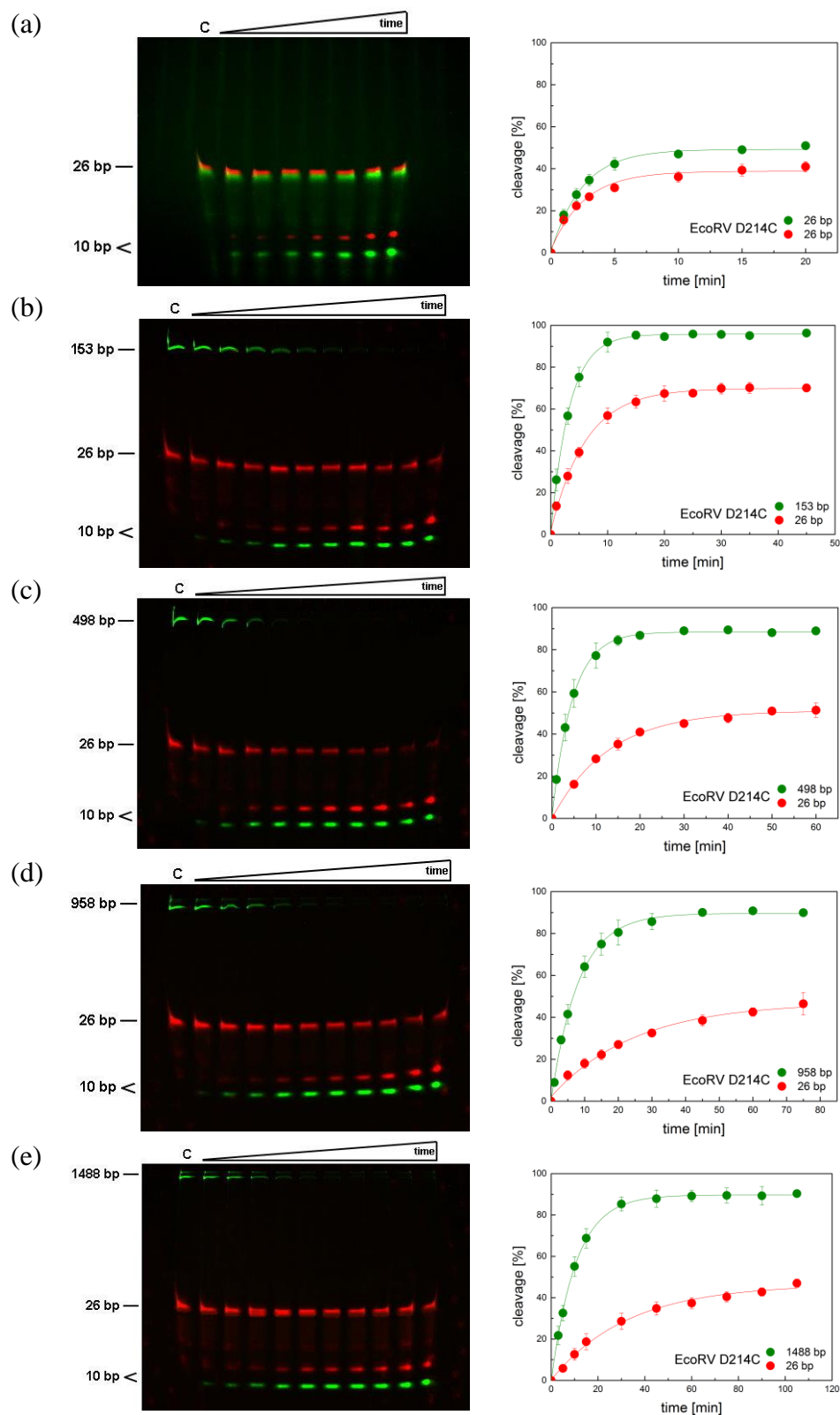


Figure 49: Substrate length dependence for DNA cleavage by EcoRV D214C. Cleavage of a 5'-Atto647N-labeled 26mer in competition with a 5'-Atto488-labeled (a) 26mer, (b) 153mer, (c) 498mer, (d) 958mer and (e) 1488mer. *Left:* Merged fluorescent images of the polyacrylamide gel (red = Atto647N, green = Atto488, C = uncleaved control). *Right:* Time course of the competitive cleavage of the long PCR fragment (green) and the short 26mer oligonucleotide (red). Data points are the average of at least three independent experiments and a single exponential function was fitted to the data.

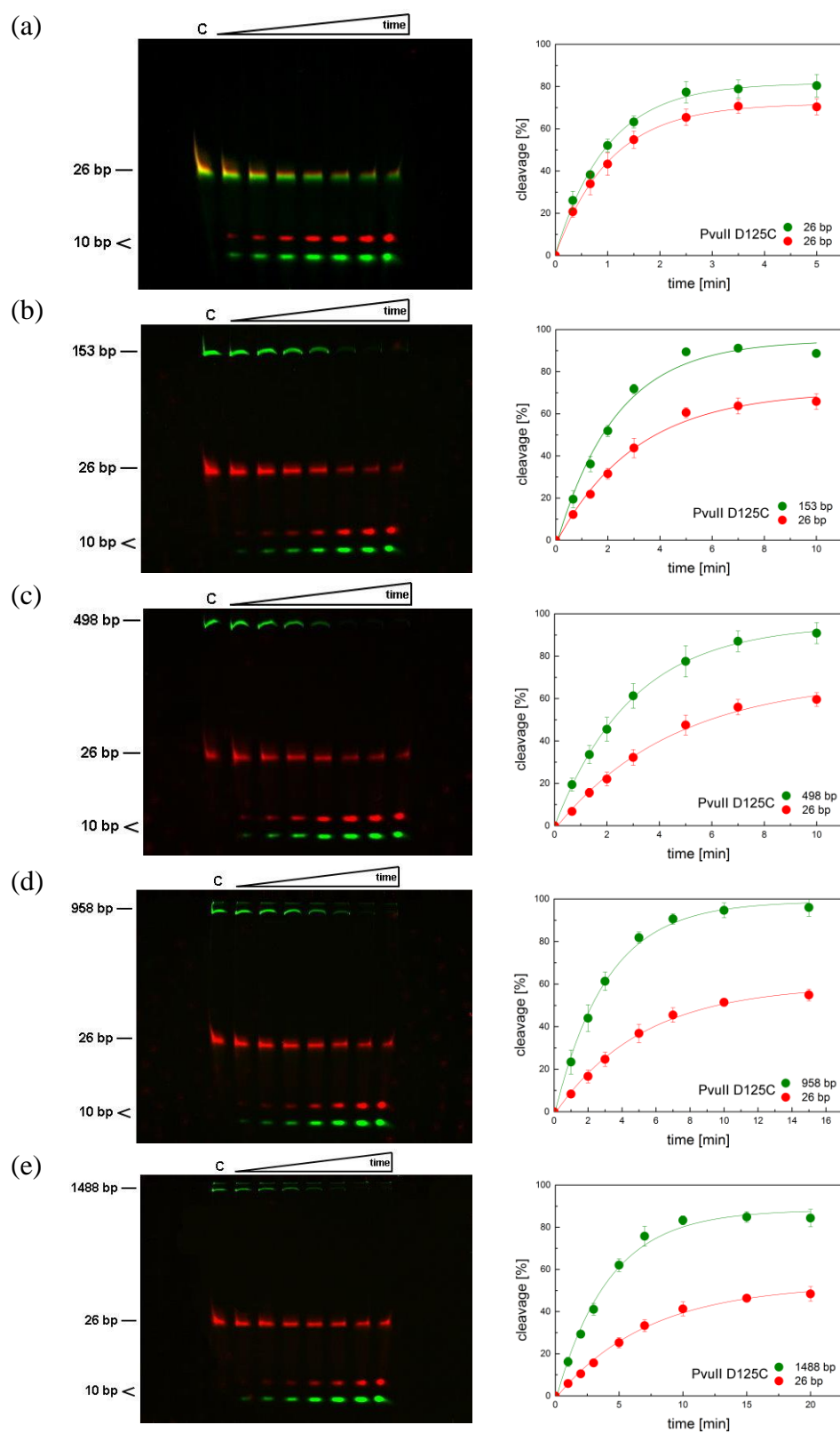


Figure 50: Substrate length dependence for DNA cleavage by PvuII D125C. For details see legend to Figure 49.

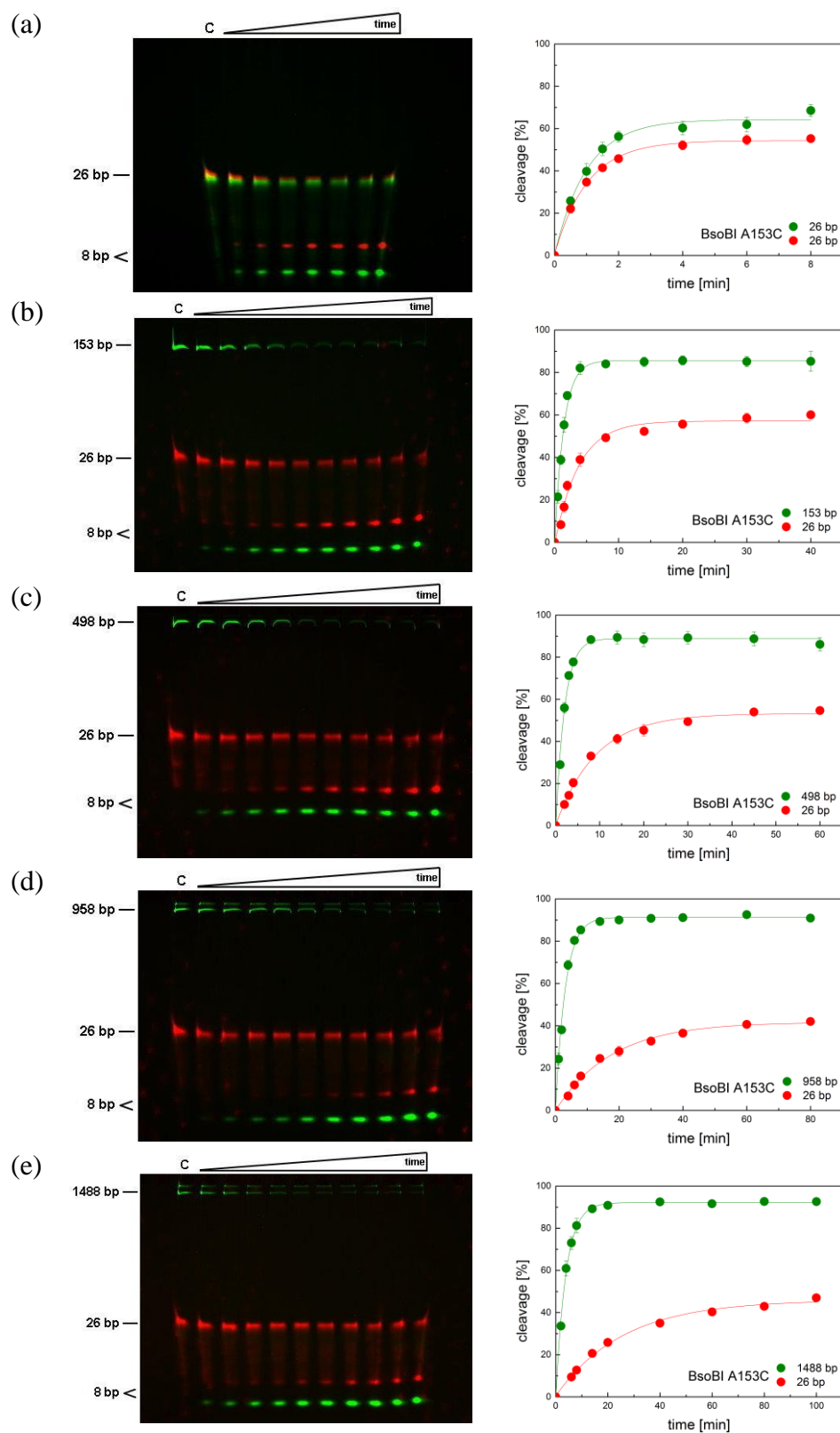


Figure 51: Substrate length dependence for DNA cleavage by BsoBI A153C. For details see legend to Figure 49.

Table 33: Cleavage rates of different PCR-fragments (k_{long}) and the 26mer oligonucleotide (k_{short}), their ratio (k_{long}/k_{short}) and their sum (k_{total}) for the restriction enzyme *EcoRV D214C*.

	$k_{long} [min^{-1}]$	$k_{short} [min^{-1}]$	k_{long}/k_{short}	$k_{total} [min^{-1}]$
26 bp	0.40 ± 0.02	0.38 ± 0.05	1.05	0.78
153 bp	0.306 ± 0.005	0.16 ± 0.05	1.87	0.47
498 bp	0.217 ± 0.005	0.078 ± 0.003	2.78	0.295
958 bp	0.123 ± 0.004	0.040 ± 0.005	3.08	0.163
1488 bp	0.095 ± 0.002	0.031 ± 0.003	3.06	0.126

Table 34: Cleavage rates of different PCR-fragments (k_{long}) and the 26mer oligonucleotide (k_{short}), their ratio (k_{long}/k_{short}) and their sum (k_{total}) for the restriction enzyme *PvuII D125C*.

	$k_{long} [min^{-1}]$	$k_{short} [min^{-1}]$	k_{long}/k_{short}	$k_{total} [min^{-1}]$
26 bp	1.01 ± 0.06	0.95 ± 0.03	1.06	1.96
153 bp	0.44 ± 0.06	0.33 ± 0.04	1.33	0.77
498 bp	0.34 ± 0.01	0.22 ± 0.03	1.55	0.56
958 bp	0.33 ± 0.02	0.19 ± 0.02	1.74	0.52
1488 bp	0.24 ± 0.02	0.14 ± 0.01	1.71	0.38

Table 35: Cleavage rates of different PCR-fragments (k_{long}) and the 26mer oligonucleotide (k_{short}), their ratio (k_{long}/k_{short}) and their sum (k_{total}) for the restriction enzyme *BsoBI A153C*.

	$k_{long} [min^{-1}]$	$k_{short} [min^{-1}]$	k_{long}/k_{short}	$k_{total} [min^{-1}]$
26 bp	0.99 ± 0.09	1.02 ± 0.04	0.97	2.01
153 bp	0.71 ± 0.04	0.27 ± 0.03	2.63	0.98
498 bp	0.50 ± 0.03	0.109 ± 0.008	4.59	0.609
958 bp	0.33 ± 0.02	0.057 ± 0.004	5.79	0.387
1488 bp	0.26 ± 0.01	0.039 ± 0.003	6.67	0.299

It can be seen for all restriction enzymes that the cleavage rates of the PCR fragments (k_{long}) and the oligonucleotide (k_{short}) decrease with increasing length of the PCR fragment. The effect is more pronounced for the short oligonucleotide. Consequently, also the sum of the cleavage rates (k_{total}) decreases with increasing length of the PCR fragment. In contrast the ratio of the cleavage rates (k_{long}/k_{short}) increases with increasing length of the PCR fragment. Furthermore the cleavage of the long PCR fragment is always faster than the cleavage of the short oligonucleotide, whereas the differently labeled 26mers are cleaved with the same rate.

The dependence of the cleavage rate ratios (k_{long}/k_{short}) on the substrate length is again summarized in Figure 52. For each substrate length, BsoBI A153C shows the highest ratio of k_{long}/k_{short} , EcoRV D214C the second highest ratio of k_{long}/k_{short} and PvuII D125C shows the lowest ratio of k_{long}/k_{short} .

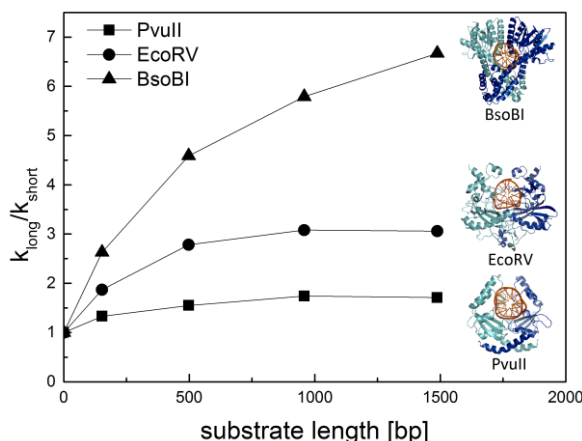


Figure 52: Length dependence of DNA cleavage rates. The relative rates of cleavage (k_{long}/k_{short}) of the long PCR fragment and the short 26mer oligonucleotide were determined in competition cleavage experiments for BsoBI A153C (\blacktriangle), EcoRV D214C (\bullet) and PvuII D125C (\blacksquare) and plotted versus the substrate length. Cartoons of the co-crystal structures in complex with specific DNA are depicted on the right: 1DC1 (BsoBI), 4RVE (EcoRV) and 1PVI (PvuII).

The experiments above showed that a specific recognition site on a long PCR fragment is cleaved much faster than on a short oligonucleotide. In a further experiment it was therefore tested whether this effect can be prevented by fragmentation of the long PCR fragment prior to the competitive cleavage reaction, similarly as described by Ehbrecht et al. [40]. This procedure has the advantage that the same amount of unspecific DNA is present in the reaction mixture. The experimental design is illustrated in Figure 53.

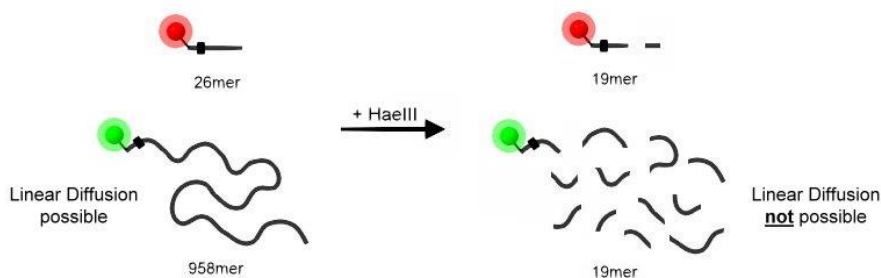


Figure 53: Experimental design to prevent linear diffusion. The 26mer oligonucleotide, containing one HaeIII recognition site (GGCC) and the 958mer PCR fragment, containing 11 HaeIII recognition sites, were predigested with HaeIII resulting in two 19mers, each containing the specific recognition site for either EcoRV, PvuII or BsoBI (black bar) and carrying a 5'-Atto647N (red) or 5'-Atto488 (green) modification, respectively (DNA fragments are not drawn to scale).

For that purpose, a mixture of the 26mer oligonucleotide and the 958mer PCR fragment have been digested with the 4 bp cutter HaeIII, which produces two 19mers fragments (which harbor the recognition site and carry two different fluorescent label) and twelve other fragments ranging from 7 – 234 bp in size. Subsequently, the digested fragments were cleaved in competition as described above.

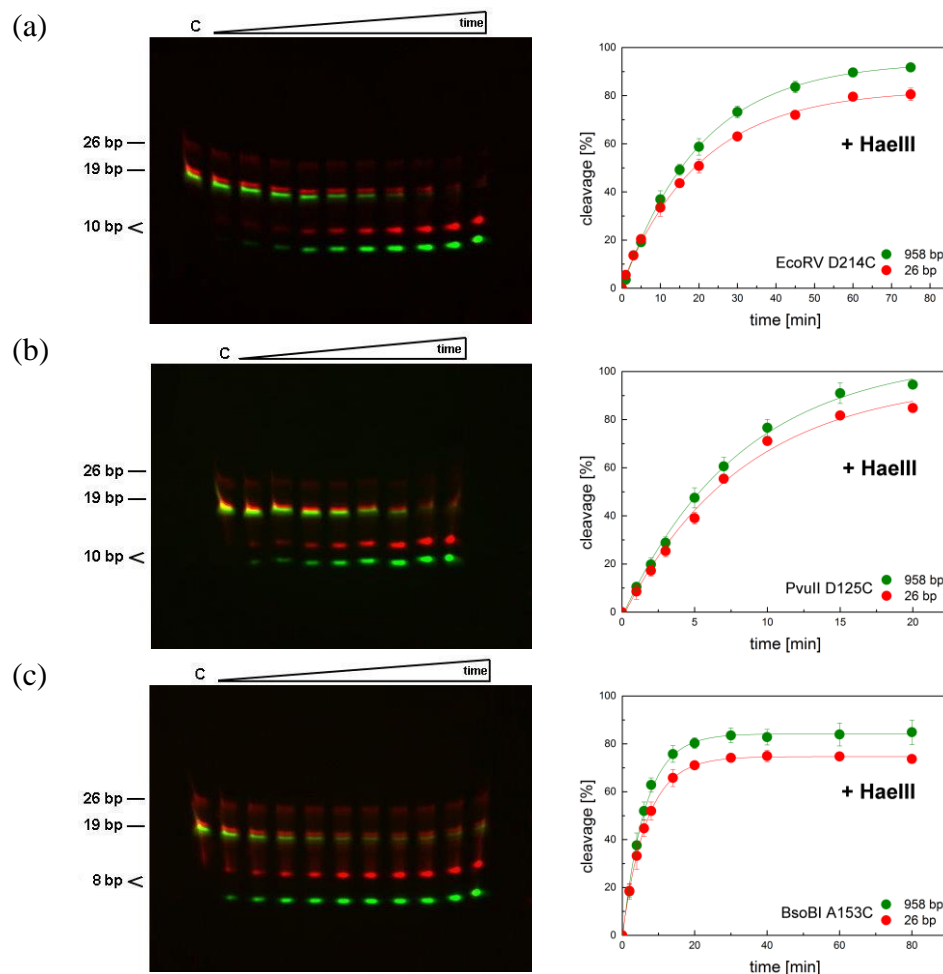


Figure 54: Preventing linear diffusion by destroying the continuity of the DNA double strand. The 5'-Atto647N-labeled 26mer oligonucleotide and the 5'-Atto488-labeled 958mer PCR fragment were predigested with HaeIII and subsequently cleaved in competition by (a) EcoRV D214C, (b) PvuII D125C and (c) BsoBI A153C. *Left:* Merged fluorescent images of the polyacrylamide gel (red = Atto647N, green = Atto488, C = uncleaved control). *Right:* Time course of the competitive cleavage of the predigested 958mer PCR fragment (green) and 26mer oligonucleotide (red). Data points are the average of at least three independent experiments and a single exponential function was fitted to the data.

Figure 54 shows the results of the competitive cleavage assay after digestion with HaeIII. On the polyacrylamide gel, it can be seen that the band for the 5'-Atto488-labeled 958 bp fragment (green fluorescence) is no longer present, whereas the band for the 5'-Atto647N-labeled 26 bp fragment (red fluorescence) is barely recognizable.

This shows that the pre-digestion with HaeIII has been completed for the 958 bp fragment and almost completed for the 26 bp fragment. Instead, two 19 bp fragments (red and green fluorescence) became visible on the gel. The substrate bands of these two 19 bp fragments disappear over time, whereas the product bands of a 10 bp fragment (in case of EcoRV and PvuII) or 8 bp fragment (in case of BsoBI) appear over time. The cleavage rates for the predigested (pd) long PCR fragment and the predigested short oligonucleotide as well as their ratios ($k_{long(pd)}/k_{short(pd)}$) and their sum ($k_{total(pd)}$) are summarized in Table 36.

Table 36: Cleavage rates of the predigested 958mer PCR-fragment ($k_{long(pd)}$) and the predigested 26mer oligonucleotide ($k_{short(pd)}$), their ratio ($k_{long(pd)}/k_{short(pd)}$) and their sum ($k_{total(pd)}$) for different restriction enzymes.

Enzyme	$k_{long(pd)} [min^{-1}]$	$k_{short(pd)} [min^{-1}]$	$k_{long(pd)}/k_{short(pd)}$	$k_{total(pd)} [min^{-1}]$
EcoRV D214C	0.049 ± 0.001	0.048 ± 0.002	1.02	0.097
PvuII D125C	0.12 ± 0.01	0.12 ± 0.01	1.00	0.24
BsoBI A153C	0.161 ± 0.007	0.150 ± 0.002	1.07	0.311

It can be seen that the predigested long and short fragments were cleaved with almost the same rate, consequently the ratio of the cleavage rates ($k_{long(pd)}/k_{short(pd)}$) became 1. Without pre-digestion the long PCR fragment was cleaved much faster than the short oligonucleotide (see Table 33 for EcoRV, Table 34 for PvuII and Table 35 for BsoBI, respectively). By comparing the cleavage rates of the substrates with and without pre-digestion, one can realize that the predigested PCR fragments were cleaved much slower than the undigested PCR fragments. Interestingly, the predigested oligonucleotides were either cleaved with approximately the same rate as the undigested oligonucleotides in case of EcoRV ($0.048 \pm 0.002 \text{ min}^{-1}$ vs. $0.040 \pm 0.005 \text{ min}^{-1}$) and PvuII ($0.12 \pm 0.01 \text{ min}^{-1}$ vs. $0.19 \pm 0.02 \text{ min}^{-1}$) or they were cleaved 3-times faster in case of BsoBI ($0.150 \pm 0.002 \text{ min}^{-1}$ vs. $0.057 \pm 0.004 \text{ min}^{-1}$). Also the total cleavage rates ($k_{total(pd)}$) of the predigested fragments were found to be slower compared to the undigested fragments.

3.2.3.2 Salt dependence of linear diffusion

In a second set of experiments, the dependence of the cleavage rate ratios (k_{long}/k_{short}) on the salt concentration was investigated. For that purpose, a 26mer oligonucleotide was cleaved in competition with a 958mer PCR fragment in the presence of either 20 mM, 100 mM or 200 mM NaCl. The assay was carried out as described above.

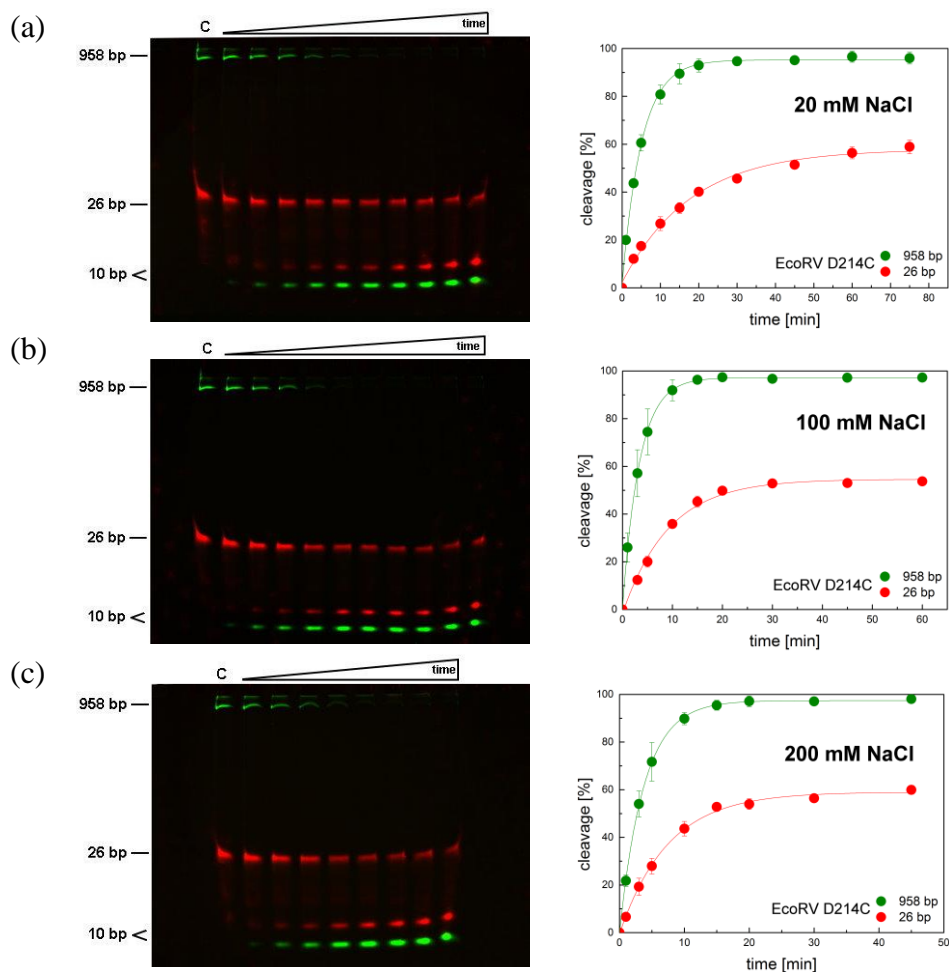


Figure 55: Salt dependence for DNA cleavage by EcoRV D214C. Cleavage of a 5'-Atto647N 26mer in competition with a 5'-Atto488 958mer in the presence of (a) 20 mM NaCl, (b) 100 mM NaCl and (c) 200 mM NaCl. *Left:* Merged fluorescent images of the polyacrylamide gel (red = Atto647N, green = Atto488, C = uncleaved control). *Right:* Time course of the competitive cleavage of the long PCR fragment (green) and the short 26mer oligonucleotide (red). Data points are the average of at least three independent experiments and a single exponential function was fitted to the data.

Table 37: Cleavage rates of the 958mer PCR-fragment (k_{long}) and the 26mer oligonucleotide (k_{short}), their ratio (k_{long}/k_{short}) and their sum (k_{total}) for the restriction enzyme EcoRV D214C under different NaCl concentrations.

[NaCl]	$k_{long} [min^{-1}]$	$k_{short} [min^{-1}]$	k_{long}/k_{short}	$k_{total} [min^{-1}]$
20 mM	0.197 ± 0.006	0.056 ± 0.005	3.52	0.253
50 mM*	0.123 ± 0.004	0.040 ± 0.005	3.08	0.163
100 mM	0.294 ± 0.005	0.109 ± 0.008	2.70	0.403
200 mM	0.266 ± 0.004	0.134 ± 0.007	1.99	0.400

*Results for 50 mM NaCl were taken from Table 33.

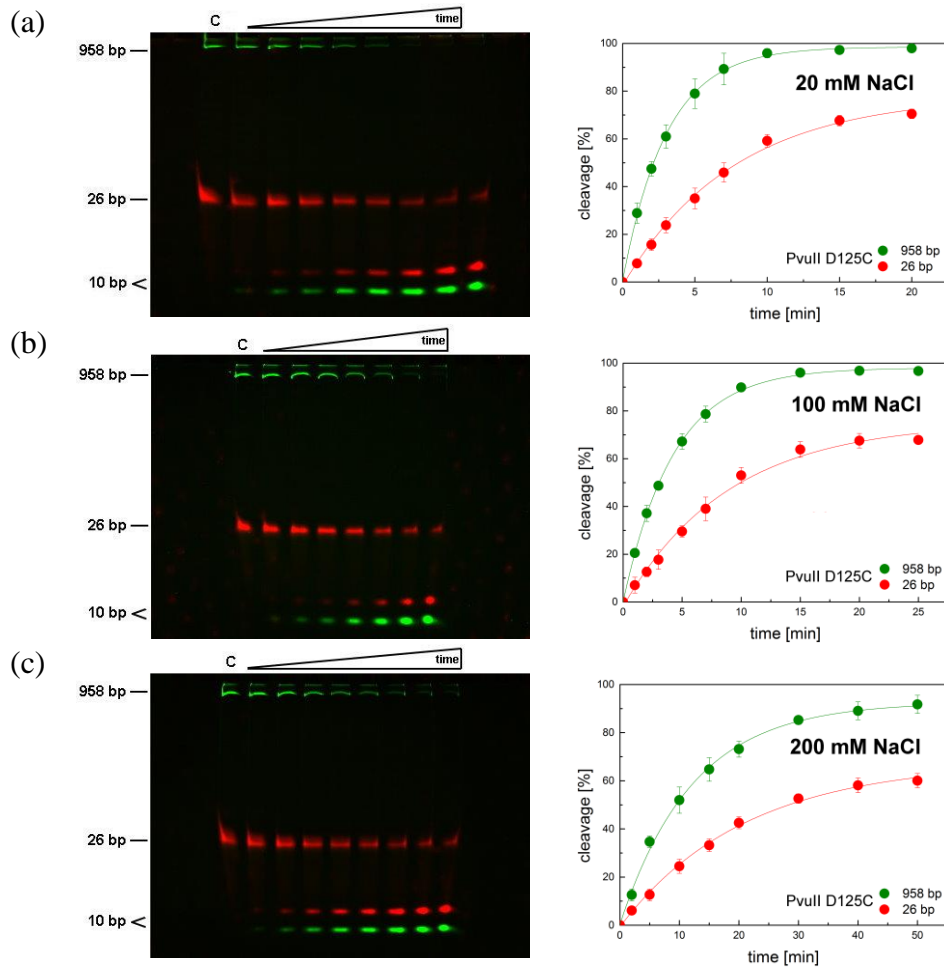


Figure 56: Salt dependence for DNA cleavage by PvuII D125C. For details see legend to Figure 55.

Table 38: Cleavage rates of the 958mer PCR-fragment (k_{long}) and the 26mer oligonucleotide (k_{short}), their ratio (k_{long}/k_{short}) and their sum (k_{total}) for the restriction enzyme PvuII D125C under different salt concentrations.

[NaCl]	$k_{long} [min^{-1}]$	$k_{short} [min^{-1}]$	k_{long}/k_{short}	$k_{total} [min^{-1}]$
20 mM	0.328 ± 0.007	0.13 ± 0.01	2.52	0.341
50 mM*	0.33 ± 0.02	0.19 ± 0.02	1.74	0.52
100 mM	0.234 ± 0.005	0.134 ± 0.009	1.75	0.368
200 mM	0.082 ± 0.004	0.048 ± 0.003	1.71	0.130

*Results for 50 mM NaCl were taken from Table 34.

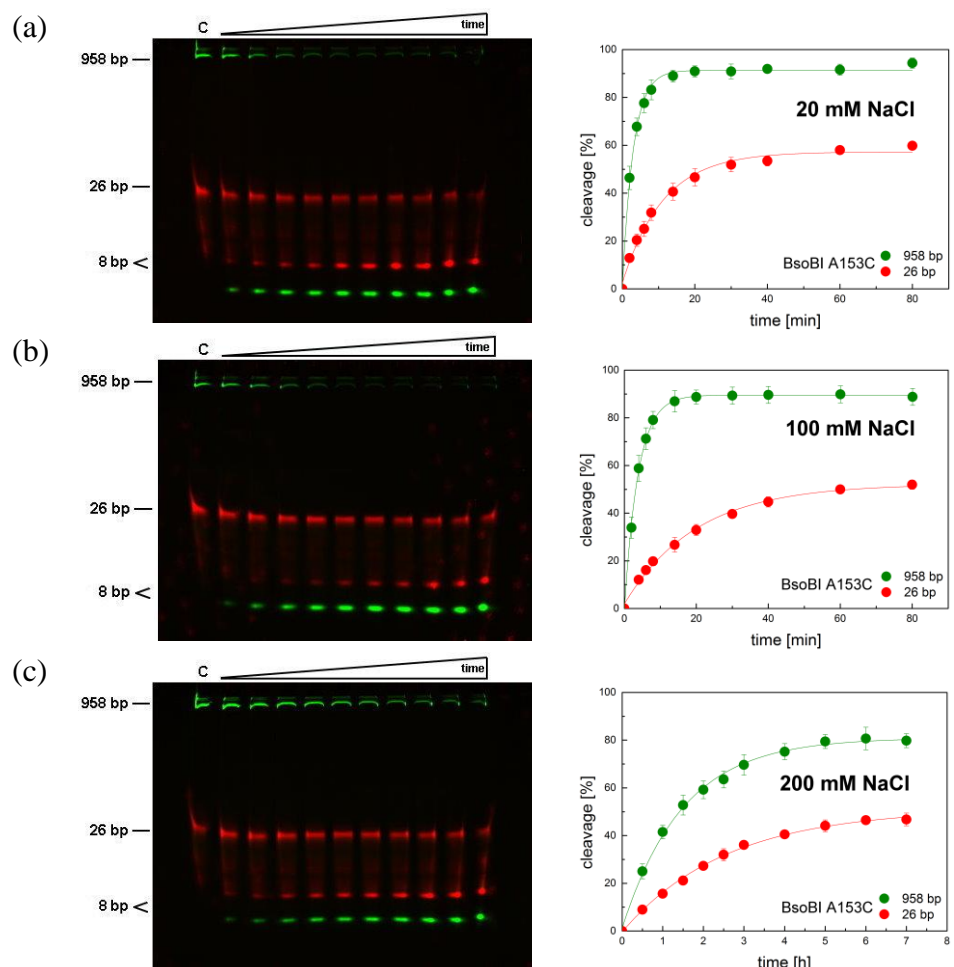


Figure 57: Salt dependence for DNA cleavage by BsoBI A153C. For details see legend to Figure 55.

Table 39: Cleavage rates of the 958mer PCR-fragment (k_{long}) and the 26mer oligonucleotide (k_{short}), their ratio (k_{long}/k_{short}) and their sum (k_{total}) for the restriction enzyme BsoBI A153C under different salt concentrations.

[NaCl]	$k_{long} [min^{-1}]$	$k_{short} [min^{-1}]$	k_{long}/k_{short}	$k_{total} [min^{-1}]$
20 mM	0.33 ± 0.01	0.089 ± 0.007	3.73	0.419
50 mM*	0.33 ± 0.02	0.057 ± 0.004	5.79	0.387
100 mM	0.262 ± 0.008	0.050 ± 0.003	5.24	0.312
200 mM	0.0112 ± 0.0005	0.0065 ± 0.0003	1.72	0.0177

*Results for 50 mM NaCl were taken from Table 35.

The results of the salt dependence of linear diffusion are shown in Figure 55 for EcoRV D214C, in Figure 56 for PvuII D125C and in Figure 57 for BsoBI A153C. Explanations of the images and graphs can be found in Figure 49. The cleavage rates for the long PCR fragment and the short oligonucleotide as well as their ratios (k_{long}/k_{short}) and their sum (k_{total}) are shown in Table 37 for EcoRV D214C, in Table 38 for PvuII D125C and in Table 39 for BsoBI A153C, respectively.

For EcoRV D214C it can be seen that the cleavage rate of the 958mer (k_{long}) first decreased, then increased and then again slightly decreased with increasing NaCl concentration. The cleavage rate of the 26mer (k_{short}) first decreased slightly and then increased with increasing NaCl concentration. The total velocity (k_{total}) showed the same trend as for the 958mer. In contrast the ratio of the cleavage rates (k_{long}/k_{short}) continuously decreased with increasing NaCl concentration from 3.52 to 1.99.

For PvuII D125C it can be seen that the cleavage rate of the 958mer (k_{long}) first remained the same and then decreased with increasing NaCl concentration. The cleavage rate of the 26mer (k_{short}) first increased and then decreased with increasing NaCl concentration. The total velocity (k_{total}) showed the same trend as for the 26mer. In contrast the ratio of the cleavage rates (k_{long}/k_{short}) first decreased from 2.52 to 1.74 by increasing the NaCl concentration from 20 mM to 50 mM and remained at the almost the same value of k_{long}/k_{short} even after a further increase of the NaCl concentration up to 200 mM.

For BsoBI A153C it can be seen that the cleavage rate of the 958mer (k_{long}) first remained the same and then decreased with increasing NaCl concentration. The cleavage rate of the 26mer (k_{short}) continuously decreased with increasing NaCl concentration. The total velocity (k_{total}) showed the same trend as for the 26mer. In contrast the ratio of the cleavage rates (k_{long}/k_{short}) first increased from 3.73 to 5.79 by increasing the NaCl concentration from 20 mM to 50 mM and then slightly decreased k_{long}/k_{short} to 5.24 at a NaCl concentration of 100 mM. A further increase of the NaCl concentration up to 200 mM considerably decreased k_{long}/k_{short} to 1.72.

The dependence of the cleavage rate ratios (k_{long}/k_{short}) on the NaCl concentration is again summarized in Figure 58.

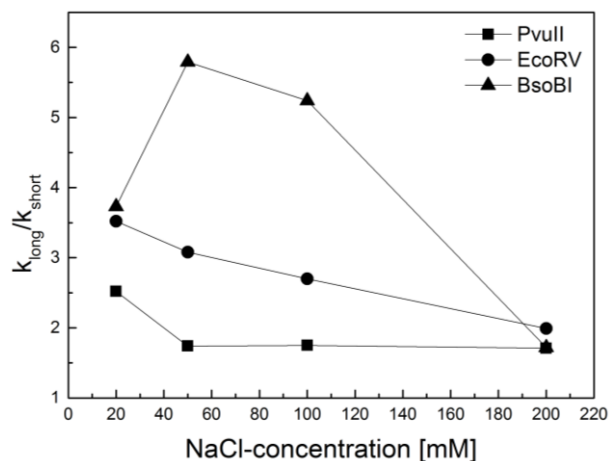


Figure 58: Salt dependence of DNA cleavage rates. The relative rates of cleavage (k_{long}/k_{short}) of the 958 bp long PCR fragment and the short 26 bp oligonucleotide were determined in competition for BsoBI (\blacktriangle), EcoRV (\bullet) and PvuII (\blacksquare) in the presence of different salt concentrations and plotted versus the NaCl-concentration.

3.2.3.3 Structure dependence of linear diffusion

In a third set of experiments, the dependence of the cleavage rate ratios (k_{long}/k_{short}) on the structure was studied by comparing enzymes in which a defined structural change had been introduced (see Figure 59). A large structural change that increases the size of a protein was introduced by fusing EcoRV with the elongated protein scRM6 (see 3.1 and Figure 24). A small structural change that affects the geometry of the DNA-binding cleft was introduced in scPvuII by connecting the two identical subunits of PvuII with a short peptide [93].

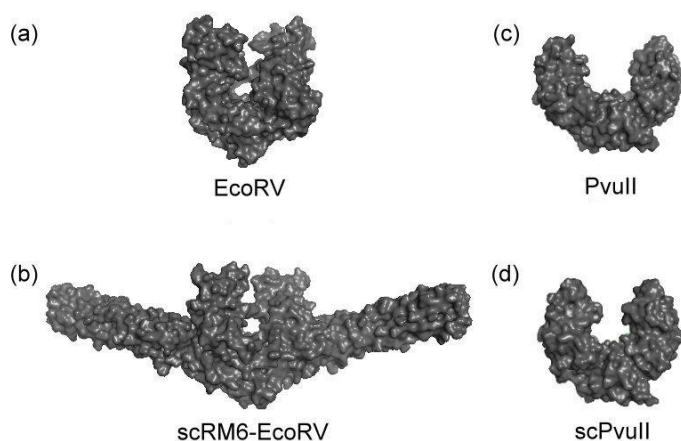


Figure 59: Comparison of different crystal structures. EcoRV (a) has a compact globular structure compared to the fusion protein (b), consisting of scRM6 and EcoRV, which has an elongated shape (model based on the structures of EcoRV and scRM6). The conformation of PvuII (c) is more open than the structure of scPvuII (d). Crystal structures were 1RVE for EcoRV, 1PVU for PvuII and 3KSK for scPvuII. Since the crystal structure of scRM6-EcoRV doesn't exist, it was modeled with the structures of EcoRV (1RVE) and scRM6 (1QX8).

For that purpose, a 26mer oligonucleotide was cleaved in competition with a 958mer PCR fragment by scRM6-EcoRV C21S or scPvuII. The assay was carried out as described above with the exception that of scRM6-EcoRV C21S 10 nM instead of 600 pM were used (attributed to the lower activity of the fusion protein).

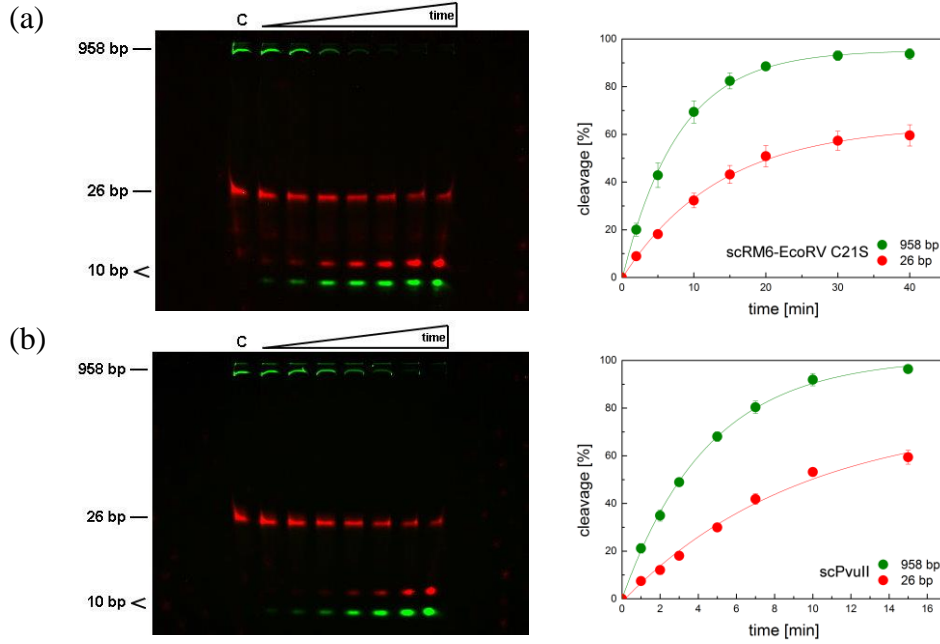


Figure 60: Structure dependence. Cleavage of a 5'-Atto647N 26mer in competition with a 5'-Atto488 958mer by (a) scRM6-EcoRV C21S and (b) scPvuII. *Left:* Merged fluorescent images of the polyacrylamide gel (red = Atto647N, green = Atto488, C = uncleaved control). *Right:* Time course of the competitive cleavage of the long PCR fragment (green) and the short 26mer oligonucleotide (red). Data points are the average of at least three independent experiments and were fitted to a single exponential function.

The results of the competitive cleavage assay are shown in Figure 60. Explanations of the images and graphs can be found in Figure 49. The cleavage rates for the long PCR fragment and the short oligonucleotide as well as their ratios (k_{long}/k_{short}) and their sum (k_{total}) are summarized in Table 40.

Table 40: Cleavage rates of the 958mer PCR-fragment (k_{long}) and the 26mer oligonucleotide (k_{short}), their ratio (k_{long}/k_{short}) and their sum (k_{total}) for the restriction enzymes scRM6-EcoRV and scPvuII.

Enzyme	$k_{long} [min^{-1}]$	$k_{short} [min^{-1}]$	k_{long}/k_{short}	$k_{total} [min^{-1}]$
scRM6-EcoRV	0.128 ± 0.005	0.074 ± 0.005	1.73	0.202
scPvuII	0.223 ± 0.009	0.11 ± 0.02	2.03	0.333

It can be seen that the cleavage rate ratio (k_{long}/k_{short}) of the scRM6-EcoRV fusion protein is lower compared to that of wild type EcoRV (1.73 vs. 3.08, see Table 33), indicating that the linear diffusion behavior of scRM6-EcoRV C21S is reduced. On the contrary, the cleavage rate ratio (k_{long}/k_{short}) for scPvuII is higher compared to that of wild type PvuII (2.03 vs. 1.74, see Table 34), indicating that scPvuII is using linear diffusion to a higher extent.

4 Discussion

4.1 Preparation of an elongated restriction enzyme to study rotational motion

It is known that restriction enzymes slide along the DNA while searching for their recognition site [67]. Their detailed path of motion however, remains unclear. The question arises whether these proteins undergo simple translational diffusion corresponding to a linear path, parallel to the DNA axis ('non-helical' sliding mechanism) or whether they undergo a rotation-coupled translational diffusion corresponding to a helical path, following the DNA axis ('helical' sliding mechanism). The latter path appears more reasonable since it allows the protein to maintain correct register with the DNA molecule and to sense the base pair sequence in the major groove directly.

A helical sliding mechanism of restriction enzymes has already been proposed from bulk ensemble measurements [44,45]. The fact that restriction enzymes do not overlook a specific recognition site implied that the enzyme stays in continuous contact with the DNA and follows the helical pitch during sliding, thereby rotating around the DNA molecule. A helical sliding mechanism has also been confirmed indirectly by single-molecule experiments [75-77]. The one-dimensional diffusion coefficient is expected to be orders of magnitude smaller, if rotation is involved in the mechanism of sliding [74]. Most of the reported D_1 values from single-molecule experiments so far are consistent with a model that involves rotation-coupled sliding.

What is still outstanding and has been addressed in this work is the direct visualization of such a rotation-coupled translational diffusion of restriction enzymes. To this end, a fusion protein consisting of the restriction enzyme EcoRV and the quasi linear protein scRM6 has been prepared and purified (3.1.1). It was tested extensively with regard to binding and cleavage activity (3.1.2) and the spatial expansion was investigated applying FRET measurements (3.1.3). At the end, the fusion protein has been subjected to single-molecule experiments to determine the one-dimensional diffusion coefficient (3.1.4)

4.1.1 Preparation of the scRM6-EcoRV fusion protein

First attempts to prepare the scRM6-EcoRV fusion protein were made with the original eight-cysteine variant of scRM6, in order to determine whether the activity of EcoRV in general will be preserved after fusing it to scRM6 (data not shown in this work). The cloning procedure proved to be extremely difficult. The gene coding for scRM6 had to be amplified via PCR to transfer it subsequently into the vector plasmid pET28a. Because 'single chain' RM6 is a homotetramer which consists of four identical subunits aligned in one polypeptide chain, annealing of the PCR primers has been possible at more than one position. Thereby, not only the desired PCR fragment but also undesired smaller fragments were amplified. For the purification of the eight-cysteine fusion protein variant, the same buffers as for EcoRV could be used (see Table 2). Nevertheless, a second purification step via Heparin column, similar as it has been shown for the single-cysteine fusion protein variant (Figure 27), had to be established as well. Despite of several complications with regard to the cloning and purification procedure, it has finally been possible to prepare a scRM6-EcoRV fusion protein, whose activity could be been shown to be preserved (data not shown in this work), a prerequisite for all further experiments. Since the fusion protein should be labeled specifically with a fluorophore at the tip of the scRM6 helix bundle, the scRM6-EcoRV fusion protein harboring eight cysteine residues could not be used for these studies. To circumvent unspecific labeling, a single-cysteine variant was prepared (3.1.1). As a consequence to the difficulties using the scRM6 gene as a template in a PCR reaction as mentioned above, a stepwise mutagenesis would have been too time-consuming and a modified synthetic gene of scRM6 coding for a single-cysteine variant has been synthesized by GeneArt. This modified gene encoded for a scRM6 variant in which all eight native cysteine residues had been exchanged by alanine residues and a single cysteine residue had been introduced at position 54. For the synthesis of the modified gene it has furthermore been considered that identical amino acids in the four subunits were encoded by different base triplets to prevent the annealing of PCR primers at multiple positions and to facilitate the cloning procedure. Additionally, five different linker variants of the scRM6-EcoRV fusion protein have been prepared, which differ in the number of amino acids between the C-terminal α -helix of scRM6 and the N-terminal α -helix of EcoRV. The peptide linker of the original single-cysteine variant (scRM6 D54C-EcoRV C21S) consists of 15 amino acids whereas the linkers of the different single-cysteine linker variants consists of either zero ($L_{(0)}$), one ($L_{(G)}$ and $L_{(N)}$), two ($L_{(NA)}$) or three ($L_{(NAS)}$) amino acids.

Optimally, the fusion of the two proteins leads to the formation of an elongated, continuous α -helix and thereby to a rigid connection (Figure 24). For that purpose, hydrogen bonds have to be formed across the junction of the C-terminal α -helix of scRM6 and the N-terminal α -helix of EcoRV. Because it is not known in which orientation one α -helix ends and the other α -helix starts and based on the fact, that α -helices have 3.6 amino acids per helical turn, the linker length was varied between 0 and 3 amino acids. Asparagine, alanine, and serine are amino acids, which can be typically found in α -helices and are supposed to promote the formation of an elongated α -helix. Glycine on the other hand is known as helix breaker and is supposed to kink the α -helix, thereby preventing the formation of an elongated α -helix. It should be evaluated which of the different linker variants shows an optimal spatial orientation of the extension components scRM6 (3.1.3) and thereby is suited for the direct visualization of rotational motion in single-molecule experiments. To purify the single-cysteine and the different single-cysteine linker variants of the fusion protein, other buffers as for EcoRV or the eight-cysteine fusion protein variant had to be used (compare Table 2 and Table 3). The main problem was the poor stability in consequence of the low salt and DTT concentration of the previously used purification buffers. For this reason buffers have been changed by increasing the salt concentration of the Ni-NTA elution buffer from 0 mM to 500 mM, the salt concentration of Heparin low salt buffer from 0 mM to 250 mM and the DTT concentration of all buffers from 1 mM to 5 mM (see Table 3). A sufficiently high concentration of DTT was necessary to prevent the formation of disulfide bridges between the exposed single-cysteine residues of the protein. The chromatogram of the Heparin purification (Figure 27) showed that after injection of the protein sample, the conductivity shortly increased up to a value of 40 mS/cm. This observation is attributed to the fact that the injected protein sample is composed of a mixture of 50 % Ni-NTA elution buffer and 50 % low salt buffer. Since the Ni-NTA elution buffer has a higher salt concentration than the low salt buffer (500 mM vs. 250 mM), the injection of the protein sample led to an increase in the salt concentration and thereby to an increase in the conductivity. This conductivity increase led to the elution of undesired proteins, but also to a partially elution of the desired fusion protein (Figure 27). However, the largest part of the fusion protein eluted after further increasing the salt concentration and could successfully be separated from the undesired proteins (Figure 27).

4.1.2 Biochemical characterization of the scRM6-EcoRV fusion protein

After the successful preparation of different scRM6-EcoRV fusion protein variants it was evaluated whether the extension component scRM6 has any influence on the binding or cleavage activity of the restriction enzyme component EcoRV (3.1.2). By looking at the model in Figure 24, one can imagine that the large extensions will handicap the interaction between EcoRV and the DNA molecule, thereby leading to a reduced activity. To analyze in more detail to what extent the activity is influenced, which step of the protein-DNA interaction is influenced most and to find out whether differences among the different scRM6-EcoRV fusion protein variants exist, various activity assays were performed, which either investigated only binding (3.1.2.2) or cleavage in a concentration- (3.1.2.1) or time-dependent (3.1.2.3) manner.

As expected, all performed activity assays demonstrated that the overall activity of the different scRM6-EcoRV fusion protein variants was reduced compared to the wild type EcoRV. Differences among the different interaction steps and linker variants could be detected as well. The binding activity was reduced by a factor between 3 and 10 compared to the wild type EcoRV ($L_{(NAS)}/L_{(N)} \sim 3x$, $L_{(G)} \sim 4x$, $L_{(0)} \sim 5x$, $L_{(NA)} \sim 7x$, $L_{(15)} \sim 10x$) which is in the order of one magnitude (Table 23). All variants with short peptide linkers showed a slightly better binding activity than the variant with the long peptide linker. This observation could be explained by the fact that the long linker permits too much flexibility of the extension component, which makes a proper binding to the DNA molecule more difficult. The shorter linkers instead keep the extension component more fixed, thereby less influencing the binding procedure. The concentration-dependent cleavage assay revealed that the cleavage activity was reduced by a factor between 6 and 60 compared to the wild type EcoRV ($L_{(15)} \sim 6x$, $L_{(NAS)}/L_{(N)} \sim 30x$, $L_{(NA)}/L_{(0)}/L_{(G)} \sim 60x$) which is in the order of one to two magnitudes (Figure 28). Interestingly, this assay revealed that the variant with the long linker showed a much better cleavage activity than the variants with the short linkers. Since the cleavage assay was performed with a plasmid, the protein-DNA interaction involved several steps such as non-specific binding, linear diffusion, conformational changes, specific binding, catalysis and product release (see also Figure 6). Because binding alone has been shown to be better for the variants with the short linkers (Table 23), necessarily one of the other interaction steps must have been worse for the variants with the short linkers.

This for example would make sense for the linear diffusion step, considering that a short linker forms a more rigid connection between the two proteins which causes a higher friction for linear diffusion than a long, flexible linker (see also 3.1.4). It is also conceivable that conformational changes are harder to perform if the linker between the two proteins is shorter, because the extension component needs to be moved as well. A longer linker instead allows EcoRV to perform conformational changes independent from scRM6. The time-dependent cleavage assay revealed that k_{cat} was reduced by a factor between 6 and 10 compared to the wild type EcoRV, which is in the order of one magnitude (Table 24). The different linker variants showed comparable values, indicating that the linker length has no influence on the catalysis. K_M values were found to be reduced by a factor between 3 and 40 compared to the wild type EcoRV (Table 24), which is in the order of one to two magnitudes. In contrast to the K_D values, K_M values showed a different dependency on the linker length. K_D and K_M values are usually expected to be identical, if the k_{cat} is much smaller than the k_{off} . Since k_{cat} has been shown to be comparable for the different linker variants, the k_{off} of the variant with the long linker must have been smaller compared to the variants with short linkers, which can only be achieved if the k_{on} of the variant with the long linker is smaller. A reduced k_{on} for the variant with the long linker would be in agreement with the above mentioned hypothesis that a long linker allows too much flexibility and makes the binding to the DNA more difficult.

Altogether it has been shown that the extension component scRM6 has indeed an influence on the binding and cleavage activity of the restriction enzyme component EcoRV. The reduction of activity was in the order of one to two magnitudes, which can be considered as a small influence. Decreasing the distance between the extension and restriction enzyme component (short linkers) improved binding to the DNA molecule but reduced the overall cleavage activity. Among the different linker variants, scRM6 D54C-L_(N)-EcoRV C21S and scRM6 D54C-L_(NAS)-EcoRV C21S showed the best results, indicating that a peptide linker of one or three amino acids in length leads to a connection of the two proteins that is fewest influencing the binding and cleavage activity.

4.1.3 Studying the spatial expansion via FRET

In addition to the preserved activity of the scRM6-EcoRV fusion protein, the correct spatial orientation of the extension component scRM6 has been another requirement for the investigation of rotational movement by single-molecule experiments. Only if the extension component scRM6 is stretched out maximally, the distance between the DNA axis and the fluorophore is sufficiently large to distinguish the transversal position of the fluorescent spot.

The spatial expansion of the different scRM6-EcoRV fusion protein variants was analyzed using FRET (3.1.3). FRET is a powerful tool to measure distances within biomolecules, since energy can only be transferred if the distance between donor and acceptor fluorophore is smaller than 10 nm. In the fusion protein, two scRM6 proteins are attached to one EcoRV homodimer and the labeling position is located at the tip of the helix bundle of each scRM6 protein (see Figure 24). Random double-labeling ideally leads to the attachment of a donor fluorophore to one scRM6 protein and an acceptor fluorophore to the other scRM6 protein. Considering a length of 7 nm for scRM6 and a diameter of 5 nm for EcoRV, the distance between donor and acceptor fluorophore should be in the range of 20 nm and no FRET signal should be measurable. To ensure, that the FRET assay works in general, two control experiments were performed. As a positive control, the EcoRV variant C21S N154C was used, in which the distance between the two symmetry related residues at position 154 is smaller than 10 nm. As negative control, a 97 bp long DNA substrate was used, in which the distance between the two terminal ends is larger than 10 nm. The length of the DNA substrate is still below the persistence length (~ 150 bp) and it can therefore be considered as rigid molecule. The rational design of the FRET measurements is summarized in Figure 32.

The emission spectrum of the double-labeled 97 bp DNA substrate showed only one peak at 520 nm (Figure 33a), resulting from direct excitation of the donor fluorophore. No second peak could be observed which indicated that no energy transfer took place and that the two fluorophores are separated by more than 10 nm. The calculated FRET efficiency was therefore close to zero ($E = 0.01$). The emission spectrum of the double-labeled protein variant EcoRV C21S N154C on the other hand showed one peak at 520 nm and additional peak at 664 nm (Figure 33b), resulting from energy transfer from the donor to the acceptor fluorophore and indicating that the two fluorophores are closer than 10 nm. The calculated FRET efficiency was found to be $E = 0.23 \pm 0.01$.

The emission spectra of all different double-labeled scRM6-EcoRV fusion proteins variants showed two peaks at 520 nm and 664 nm as well, indicating that energy transfer took place and that the two fluorophores are closer than 10 nm (Figure 33c). FRET efficiencies were found to be in the range of 0.17 ± 0.01 for the variant with the $L_{(NA)}$ linker to 0.28 ± 0.01 for the variant with the $L_{(0)}$ linker. To find out if the spatial orientation of the extension component scRM6 would be different in a DNA-bound state compared to that in solution, a 16 bp oligonucleotide was added to the double-labeled fusion protein variant scRM6 D54C-EcoRV C21S and the measurement was repeated. The FRET efficiency in the presence of DNA was found to be identical to that in the absence of DNA (0.20 ± 0.01). To exclude that the 16 bp oligonucleotide was too short to allow proper binding, the experiment was repeated with a larger 60 bp oligonucleotide. Also in this case, the FRET efficiency remained unchanged. To exclude that aggregation of the proteins due to hydrophobic interactions caused a FRET signal, a mixture of donor and acceptor only labeled protein was measured. This mixture shouldn't lead to any FRET signal, since the single-labeled proteins are sufficiently separated in solution. Aggregation of the proteins would bring the donor fluorophore of one protein closer to the acceptor fluorophore of another protein, thereby causing energy transfer and a FRET signal. The FRET efficiency of the single-labeled protein mixture was found to be 0.03 which indicated that no aggregation contributed to the FRET signal.

The FRET experiments revealed that the two fluorophores are not separated by around 20 nm as assumed but by less than 10 nm because a FRET signal could be measured. This consequently implies that the scRM6 extensions components are not maximally stretched out. No significant differences could be found among the different scRM6-EcoRV linker variants. A reason for the measured FRET signal could be an improper alignment of the two α -helices which allows too much flexibility of the extension component, thereby bringing the terminal ends in close proximity (see Figure 32b, orientations indicated in light grey). It is also possible that the alignment of the two α -helices has been proper but that simply the orientation of the N-terminal α -helix of EcoRV was not optimal to maximally stretch out scRM6. Further, it has to be considered that the FRET efficiency was calculated within bulk ensemble measurements, which can only represent an average value of all subpopulations (population with high and low FRET values). FRET measurements on the single-molecule level could be a solution to this.

4.1.4 Single-molecule experiments

Single-molecule experiments should originally be performed with the fusion protein scRM6 D54C-EcoRV C21S for two different purposes: (i) Indirect proof of a rotational movement by measuring the one-dimensional diffusion coefficient and comparing it to theoretical models (3.1.4) and (ii) direct proof of a rotational movement using super-resolution microscopy.

Indirect proof of rotational movement

The one-dimensional diffusion coefficient of the fusion protein scRM6 D54C-EcoRV C21S labeled with Cy3B was determined in collaboration with the group of Pierre Desbiolles (Laboratoire Kastler Brossel, Paris). By the same group, D_1 was determined previously for EcoRV coupled to fluorescent labels of different size (e.g. Cy3B [67], QD655 [64], sav-Cy3B [77], QD605 and QDEO6 [90]). In case of wild type EcoRV, all fluorescent labels were coupled to the protein via a flexible linker. The fusion protein scRM6 D54C-EcoRV C21S instead represented a conjugation strategy in which the fluorescent label was coupled to EcoRV via a rigid linker, whereby the portfolio of different theoretical models could be extended (see theoretical models in 3.1.4).

The behavior of the fusion protein scRM6 D54C-EcoRV C21S in single-molecule experiments was slightly different from that of wild type EcoRV. The interaction frequency with the DNA molecule was lower and also the interaction time was shorter, which can be explained by the reduced binding affinity observed in bulk ensemble measurements (3.1.2.2). For this reason, buffer conditions had to be changed (from phosphate buffer [90] to KGB buffer (Table 6) to increase the interaction time with the DNA molecule and to allow for an accurate measurement of D_1 . The one-dimensional diffusion coefficient of scRM6 D54C-EcoRV C21S was found to be $D_1 = 0.0024 \mu\text{m}^2\text{s}^{-1}$, which is 4-times slower than the one-dimensional diffusion coefficient of EcoRV labeled with Cy3B ($D_1 = 0.01 \mu\text{m}^2\text{s}^{-1}$) [67]. The reduced sliding velocity of the fusion protein compared to the wild type EcoRV is in agreement with observations from bulk ensemble measurements (see 3.2.3.3). This can be explained by the fact that the scRM6 extension component increased the total hydrodynamic radius of the fusion construct, thereby increasing the friction while sliding along the DNA molecule.

In order to evaluate if rotation is involved in the sliding process of scRM6 D54C-EcoRV C21S, the experimental data were compared to the theoretical models. Two general statements can be derived from the models in Figure 34b. (i) With the same label radius and the same type of motion, a flexibly attached label causes less friction than a rigidly attached label (comparing model 1+3 or model 2+4). This can be explained by the fact that the motion of the label is decoupled from that of the protein if it is flexibly attached, whereas the motion of the label is coupled to that of the protein if it is rigidly attached. (ii) With the same label radius and the same conjugation strategy, linear diffusion causes less friction than rotation-coupled diffusion (comparing model 1+2 or model 3+4). This is attributed to the fact that linear diffusion depends only on translational friction ($\xi = 6\pi\eta r$) and the friction coefficient is expected to increase linearly with the label radius (model 1). In contrast, rotation-coupled diffusion depends on translational and rotational friction ($\xi = 6\pi\eta r + 8\pi\eta r^3$) and the friction coefficient is expected to increase to the power of three with the label radius (model 2) [74]. The friction coefficient of scRM6 D54C-EcoRV C21S calculated from the measured one-dimensional diffusion coefficient showed a fairly high value relative to the small label size (Figure 34b). This can only be explained by the fact that the label is rigidly attached to EcoRV (as assumed) and that linear diffusion is coupled to rotation. Consequently, experimental data were in agreement with model (5).

Direct proof of rotational movement

The single-molecule experiments performed in Paris were suited to confirm a rotational movement indirectly by comparing D_1 with theoretical models. However, a direct visualization based on the theory demonstrated in Figure 23 would not have been possible there, since the spatial and temporal resolution of the detection system was restricted to 30 nm and 20 ms, respectively. For this reason a collaboration with the group of Markus Sauer (Julius-Maximilians University, Würzburg) was started, who established super-resolution fluorescence microscopy imaging techniques (e.g. STORM = Stochastic Optical Reconstruction Microscopy) with superior spatial and temporal resolution [94,95].

Two important prerequisites for the direct visualization of rotational motion by single-molecule experiments were the preserved activity of the scRM6-EcoRV fusion protein and a large distance between the fluorophore and the DNA axis in order to distinguish the transverse position of the fluorescent spot.

The first prerequisite could be met (3.1.2) however, FRET experiments revealed that the scRM6 extension components were not stretched out maximally (3.1.3), which consequently means that the distance between the fluorophore and the DNA axis could not successfully be increased in the fusion protein. Thereby none of the scRM6-EcoRV fusion protein variants was appropriate for the direct visualization of rotational motion.

But even with an optimal spatial expansion of the scRM6-EcoRV fusion protein, a direct visualization would not have been possible. The **spatial resolution** was considered as a problem which can be circumvented with the fusion protein (Figure 23). Theoretically, nanometer precision is possible which would have allowed distinguishing a transversal position change of 20 nm using super-resolution techniques [95]. Effectively, Brownian fluctuations of the DNA molecules take place in the same direction and decrease the spatial resolution by one or two orders of magnitude above the theoretical limitations [62]. An additional problem is the **temporal resolution** (Figure 61). The transverse position of the fluorescent spot is supposed to change by 20 nm after the enzyme turned 180° around the DNA molecule (half-rotation). Therefore the question arises how much time the enzyme needs to perform such a half-rotation. This can be calculated using the equation:

$$\tau = \frac{a^2}{2 \cdot D_1}$$

where τ is the time, a is the covered distance (a half-rotation is performed after sliding over 5 bp, which is equivalent to 1.7 nm) and D_1 is the one-dimensional diffusion coefficient ($D_1 = 0.0024 \mu\text{m}^2\text{s}^{-1}$ for scRM6 D54C-EcoRV C21S). According to the equation, a half-rotation of the scRM6-EcoRV fusion protein is completed after 600 μs . In order to temporally resolve the motion, the exposure time of the camera needs to be in the same order of magnitude. Even with the most sophisticated cameras with exposure times in the range of a few milliseconds, such a fast motion cannot be resolved. During an exposure time of e.g. 10 ms the fusion protein slide already over 7 nm and circled several times around the DNA.

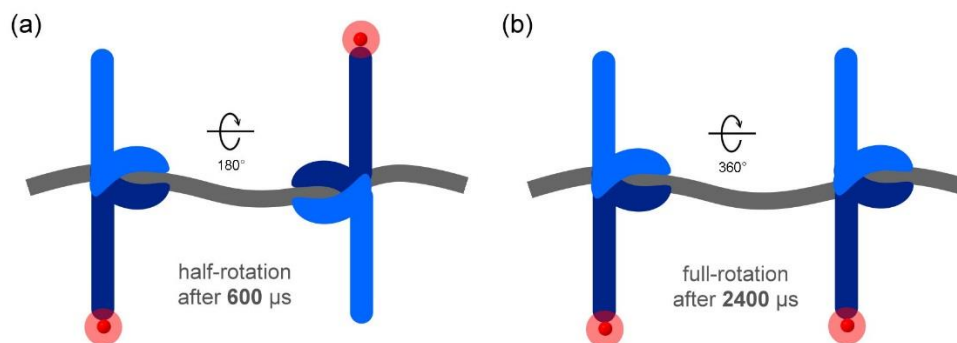


Figure 61: Problem of temporal resolution and rotation speed. The time (τ) that the scRM6-EcoRV fusion protein needs to slide over 1 bp can be calculated using the equation for Brownian motion $\tau = a^2/2D$ where a is the length of 1 bp ($a = 0.34$ nm) and D is the one-dimensional diffusion coefficient of the scRM6-EcoRV fusion protein ($D = 0.0024$ $\mu\text{m}^2\text{s}^{-1}$). According to this, scRM6-EcoRV needs 24 μs to slide over 1 bp. A full-rotation (10 bp based on the length of the helical pitch) is completed after 2400 μs , a half-rotation (5 bp) is completed after 600 μs .

Additionally, spatial and temporal resolution are directly interdependent and mutually determine the localization accuracy of the fluorescent spot. The spatial resolution depends on the number of captured photons accumulated during the exposure time of the camera, whereas the temporal resolution depends on the read-out rate of the camera and thereby on the exposure time. Decreasing the exposure time improves the temporal resolution, because more fluorescent images can be recorded per time, but debase the spatial resolution, because not so many photons can be accumulated within the short exposure time. Increasing the exposure time instead improves the spatial resolution but debase the temporal resolution.

A third problem is the **randomness** of the translocations of Type II restriction enzymes, which means that one-dimensional diffusion oscillates between different directions. Therefore, a change of the transverse position of the fluorescent spot in a periodic manner as described in 3.1 would not have been observable. Because of the randomness it would also be difficult to apply alternative methods for the visualization of rotational movement of Type II restriction enzymes (1.2.1). Fluorescence polarization for example relies on periodically alternating intensities of the vertically and the horizontally polarized light [78,79], which could not be implemented with the scRM6-EcoRV fusion protein. Also torque measurements rely on the fact that the position of the huge labeled tag changes in a clockwise (or anticlockwise) direction which presumes a directed motion of the corresponding protein [80,82]. Presumably for this reason, most of the studies using these techniques have been performed with motor proteins (e.g. myosin, mDia1, RNAP and F₁-ATPase), which undergo directional translocations under energy consumption.

Final conclusion

Despite many difficulties it was finally possible to prepare and to purify the fusion protein consisting of EcoRV and scRM6. The binding and cleavage activity was slightly reduced compared to the wild type EcoRV, however sufficient to study the motion along the DNA molecule by single-molecule techniques. It could successfully be demonstrated by an indirect approach that linear diffusion of the scRM6-EcoRV fusion protein is coupled to rotation [90]. The direct visualization of rotational motion however, was not possible due to the speed and randomness of the diffusional motion. Direct experimental observation of rotation-coupled sliding of restriction enzymes remains a difficult task.

4.2 Comparison of structurally different restriction enzymes

The structurally different restriction enzymes PvuII, EcoRV and BsoBI were compared regarding their conformation and linear diffusion behavior. It was hypothesized that the more open the enzyme-DNA complex, the less linear diffusion is used by the enzyme. To this end, the conformation of the enzyme in complex with non-specific DNA (sliding conformation) was determined in comparison to the conformation of the apoenzyme and the conformation in complex with specific DNA with the aid of FRET measurements (3.2.2). Afterwards the linear diffusion behavior was investigated with conventional kinetic methods (3.2.3). All experiments were performed with the same enzyme mutants under identical buffer condition to ensure the comparability of the results.

4.2.1 Preparation of single-cysteine variants

In order to study the conformation of structurally different restriction enzymes, single-cysteine variants had to be prepared and labeled with fluorophores. The position of the single cysteine residue was chosen according to several criteria, having in mind that the introduction of a cysteine residue in one subunit leads to the introduction at the same position in the other subunit of the homodimer. First of all, the distance of the desired cysteine residues, measured from one subunit to the other, should be different for the apoenzyme and the complexes with specific or non-specific DNA. Consequently, the cysteine residues had to be located in a subdomain, which is supposed to move upon DNA binding. Secondly, the distance of the residues should be in the range of the Förster radius (R_0) (2.2.3.6), which is the distance of donor and acceptor fluorophore at which energy transfer is 50% efficient. Around R_0 , small changes in the distance of donor and acceptor fluorophore cause large changes in the FRET efficiency. In this study the fluorophores Cy3 and Cy5 have been chosen as donor and acceptor fluorophore, respectively. They are the most frequently used and best described FRET pair in the literature [96] with an R_0 of 56 Å. Thirdly, the residue had to be located at the surface of the protein, to be accessible for labeling and finally, the residue had to be located far away from the catalytic subdomain to not influence the binding and cleavage activity of the enzyme. To this end, the three crystal structures of EcoRV (apoenzyme, non-specific complex, specific complex) were compared and the position 214 was found to meet all the criteria.

The residue at position 214 is located on the outside of α -helix D, which belongs to the top of the recognition subdomain of EcoRV which is supposed to move upon DNA binding (Figure 3). The distance changes from 48 Å in the specific complex to 57 Å in the non-specific complex ($\Delta = 9$ Å), which is in the range of the Förster radius. To find an appropriate position for PvuII, the crystal structure of the specific complex was compared to that of the apoenzyme. A residue at position 125, which is located in α -helix D of the recognition subdomain, was chosen (Figure 4). This residue is located at the surface and the distance changes from 67 Å in the apoenzyme to 48 Å in the specific complex ($\Delta = 19$ Å), which is in the range of the Förster radius. For BsoBI it was not possible to choose a position that meet all the criteria, since only the crystal structure of the specific complex is available (Figure 5). From this crystal structure it can only be seen, if the residue is located at the surface of the enzyme and far away from the catalytic center. It cannot be determined, whether this region of the enzyme is supposed to move and if the change of the distance is in the range of the Förster radius. The last two criteria were already investigated by Jasmina Dikic [105] and the residue located at position 153 was found to be appropriate.

The introduction of the mutation and the subsequent labeling should not have an influence on the binding and cleavage activity. By comparing the activity of the wild type enzymes with that of the mutant enzymes (3.2.1.1) or with that of the labeled mutant enzymes (3.2.1.3), it could be shown that neither the mutation nor the attachment of the fluorophore had an influence on the binding or cleavage activity. The PEG-modification (3.2.1.2) confirmed that the cysteine residues are located on the surface of the protein and thus are accessible for labeling. Also the fluorescent labeling (3.2.1.3) was successfully, however to a different extent for the three enzymes. The acceptor was added in excess in order to increase the probability that every enzyme that carries a donor fluorophore carries also an acceptor fluorophore. This strategy minimizes the number of enzymes that carry a donor fluorophore only but it increases the number of enzymes that carry an acceptor fluorophore only. Due to the acceptor crosstalk, the presence of the acceptor only labeled enzymes would lead to a higher acceptor signal and thus to a seemingly higher FRET efficiency. For this reason, the FRET efficiency was corrected as described in 2.2.3.6.

4.2.2 Studying the conformation of structurally different restriction enzymes

Before comparing the linear diffusion behavior of the structurally different restriction enzymes PvuII, EcoRV and BsoBI, it was necessary to elucidate, which conformation the restriction enzymes adopt for sliding. Since linear diffusion takes places on non-specific DNA, the conformation the enzyme adopts in the non-specific complex is the conformation it uses for sliding [29]. Traditionally, X-ray crystallography is used to obtain structural information about an enzyme. However, this technique requires the presence of crystals, which is often hard to achieve and extremely time-consuming. Additionally, one has to keep in mind that crystal structures represent only a snapshot of a particular phase of a dynamic process. So far, structural information about the non-specific complex is available only for EcoRV [30] (and BamHI [29]). Since the non-specific complex structures of PvuII and BsoBI are missing, a new strategy had to be found, which allows determining the conformation of the non-specific complex in comparison to the apoenzyme and the specific complex.

Förster resonance energy transfer (FRET) represents a powerful tool for monitoring distance changes and thereby conformational changes in proteins. It has many advantages over X-ray crystallography since it is cheap, rapid and easy. A disadvantage of FRET is that it is dependent on the photo-physical properties of the fluorophores. Thereby, obtaining quantitative distances and deriving the three-dimensional structures remains extremely challenging. Several approaches for the determination of FRET efficiencies exist in the literature [89,97], which differ in the measured species and the degree of corrections. Among the intensity-based FRET approaches, one can distinguish between (i) approaches which rely on the measurement of the donor emission in the presence and absence of acceptor and (ii) approaches which rely on the measurement of the acceptor emission after excitation of the donor. The first approach requires the presence of two different species (one that carry only a donor fluorophore and another that carry a donor and an acceptor fluorophore), the second requires the presence of only one species (that carries a donor and an acceptor fluorophore). Since in this work donor and acceptor fluorophore were coupled to two different subunits but in one protein, only the second approach turned out to be suitable. FRET measurements were performed with the single-cysteine variants EcoRV D214C, PvuII D125C and BsoBI A153C.

Proteins were single-labeled and randomly double-labeled with donor and acceptor fluorophore (see 3.2.1.3) leading ideally to the introduction of the donor fluorophore in one subunit and the acceptor fluorophore in the other subunit. Emission spectra were recorded for the apoenzyme, the complex with non-specific and the complex with specific DNA in the presence of either Ca^{2+} - or Mg^{2+} -ions or in the presence of EDTA and the FRET efficiency was calculated (see 3.2.2).

First of all, some general statements can be made. The emission spectrum of the donor only labeled protein (reference) showed only one maximum at 564 nm, the emission spectrum of the double-labeled protein (apoenzyme) showed two maxima at 564 nm and 666 nm. Since in both cases only the donor fluorophore was excited, the additional maximum of the double-labeled protein at 666 nm could only result from energy transfer from the donor to the acceptor fluorophore (and to a lower degree also from acceptor crosstalk; see discussion below), indicating that the distance of the two fluorophores is within the Förster distance (< 10 nm). The addition of either specific or non-specific DNA changed the ratio of the two maxima (and thereby the FRET efficiency) to a different extent, indicative of conformational changes of the protein upon DNA binding.

For all restriction enzymes, the effect on the change in FRET efficiency upon DNA binding was most pronounced in the presence of Ca^{2+} -ions and only weak or non-existent for EDTA and Mg^{2+} -ions. The question arose, whether the enzymes are able to bind to the oligonucleotides under the conditions used for the assay. For this reason, the binding affinity to these substrates was tested (3.2.2). The results showed indeed, that the binding affinity in the presence of EDTA or Mg^{2+} -ions is weaker than in the presence of Ca^{2+} -ions (the K_D values for PvuII and non-specific DNA were for example 169 nM in the presence of Ca^{2+} -ions, 605 nM in the presence of EDTA and 2 μM in the presence of Mg^{2+} -ions). Nevertheless, the chosen concentrations of protein (50 nM) and the high excess of oligonucleotide (1 μM for EcoRV and BsoBI and 5 μM for PvuII) should lead to an almost complete binding of the protein to the oligonucleotides under all conditions. The oligonucleotides used in the FRET and binding experiments have exactly the same sequence, the only difference is that the oligonucleotides that were used for binding experiments were labeled with a HEX-fluorophore and the oligonucleotides that were used for the FRET experiments were unlabeled.

It is therefore possible that the presence of the HEX-fluorophore, however increased the affinity to the labeled oligonucleotides and that the real affinity to the unlabeled oligonucleotide was much lower. This would consequently mean that not all proteins were bound in the presence of EDTA and Mg^{2+} -ions, thereby a mixture of bound and unbound species was measured. Since this two kind of species cannot be distinguished in an ensemble measurement, only an average of the FRET efficiencies could be measured, leading to the conclusion that only small conformational changes took place in the presence of EDTA and Mg^{2+} -ions. For this reason only the FRET efficiencies calculated in the presence of Ca^{2+} -ions were considered for the evaluation, since in this case binding surely had occurred.

As described in 2.2.3.6, FRET efficiencies were calculated in two different ways. In a first approach, FRET efficiencies were directly calculated from the emission spectra by dividing the acceptor emission intensity at 666 nm by the donor emission intensity at 564 nm (Table 28, Table 29 and Table 30). Due to the normalization of the emission spectra to the maximum of donor emission at 564 nm, the FRET efficiency could be derived directly from the height of the acceptor peak at 666 nm. For a comparison of the FRET efficiencies instead, it was necessary to correct the acceptor emission intensity at 666 nm, since this emission did not only result from energy transfer of the donor fluorophore. Two other components contributed to the signal at 666 nm as well. On the one hand, the donor itself was able to emit light at the emission maximum of the acceptor fluorophore, because both emission maxima were not sufficiently separated (denoted as ‘donor bleed-through’ [89]). On the other hand, the acceptor could also be directly excited to a certain extent by the excitation wavelength of donor, because of an overlap between the excitation spectrum of the acceptor and the excitation wavelength of the donor (denoted as ‘acceptor crosstalk’ [89]). Thus, in a second approach, FRET efficiencies were calculated by dividing the corrected acceptor emission at 666 nm by the donor emission at 564 nm (Table 32). The results showed that the corrected FRET efficiencies were lower than the directly calculated FRET efficiencies ($E_{\text{corr}} < E$). This was expected, since a subtraction of the donor bleed through and acceptor crosstalk from the acceptor emission intensity led to a decrease of the acceptor emission intensity and thereby to a decrease of the FRET efficiency. The tendency or rather the proportions between apoenzyme, non-specific and specific protein-DNA complex remained the same.

In order to finally evaluate the extent of DNA-binding cleft opening in the non-specific complex, the corrected FRET efficiency of the non-specific complex was compared with the corrected FRET efficiencies of the apoenzyme and the specific complex. Furthermore it was examined if and to which extent the results of FRET measurements correspond with the available crystal structures and the conformational changes described so far in the literature.

PvuII D125C

The measurements revealed corrected FRET efficiencies of 0.22 for the apoenzyme, 0.31 for the non-specific complex and 0.59 for the specific complex, respectively (see Table 32 and Figure 62, orange numbers). By comparing apoenzyme and non-specific complex, it can be seen that the FRET efficiency increased by 0.09, which means that the enzyme closes its DNA-binding cleft slightly upon non-specific binding. Comparing apoenzyme and specific complex, the FRET efficiency increased by 0.37, which means that the enzyme closes its DNA-binding cleft considerably upon specific binding. The difference between non-specific and specific complex was found to be 0.28, which means that the enzyme closes the DNA-binding cleft when switching from the non-specific to the specific binding mode and that the specific complex is more closed than the non-specific complex. This first comparison showed that for sliding PvuII adopts a conformation which is between the conformation of the apoenzyme and the specifically bound enzyme. Since the difference between the non-specific complex and the apoenzyme (0.09) is much smaller than the difference between the non-specific and the specific complex (0.28), it can be concluded that the conformation of PvuII during sliding is more related to the conformation of the apoenzyme. Since the conformation of the apoenzyme is extremely open, it is assumed that PvuII uses also an open conformation for sliding.

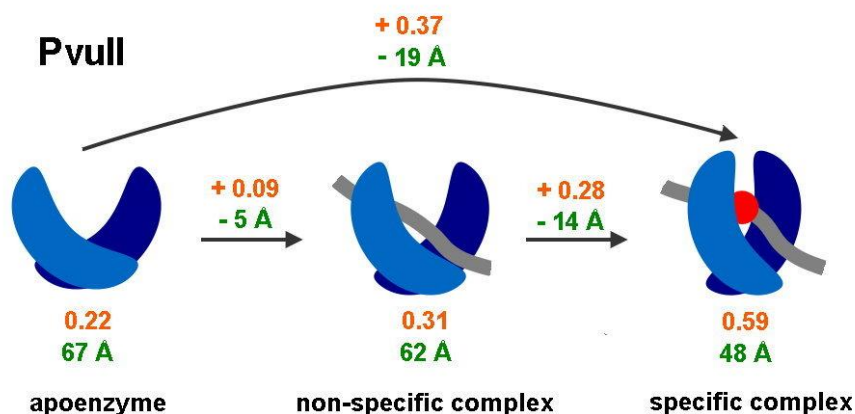


Figure 62: Summary of FRET efficiencies and distances for the restriction enzyme PvuII. FRET efficiencies and FRET efficiency changes are indicated in orange, distances and distance changes are indicated in green. Note that the distances of the apoenzyme (67 Å) and the specific complex (48 Å) are derived from crystal structures and that the distance of the non-specific complex (62 Å) is estimated based on FRET efficiency comparison.

The results of the FRET measurements perfectly fit the available crystal structures of PvuII. The distance in the crystal structure of the apoenzyme was found to be 67 Å [34], whereas it was found to be 48 Å in the co-crystal structure of the specific complex [35](see Table 27). This shows that the apoenzyme closes its DNA-binding cleft by 19 Å upon specific binding, which can be perfectly correlated with an increase in the FRET efficiency of 0.37. If a change of 19 Å can be considered equivalent to a change of 0.37 in the FRET efficiency, a change of 0.09 in the FRET efficiency should be equivalent to 5 Å and a change of 0.28 in the FRET efficiency should be equivalent to 14 Å estimated by the rule of three. This means that the enzyme closes its DNA binding cleft by 5 Å upon non-specific binding and closes by further 14 Å upon specific binding. With this comparative analyses the distance in the non-specific complex can be predicted as 62 Å. The distances and distance changes of PvuII are summarized in Figure 62 (green numbers).

The results of the FRET measurements perfectly fit the conformational changes described so far in the literature for PvuII [23,27,34]. The crystal structure of the apoenzyme implied that the DNA-binding cleft is too open to accommodate DNA with both subunits simultaneously. Therefore, it was postulated that a contact of the L-AB loop with the DNA stimulates closing of the DNA-binding cleft [34]. Indeed, the FRET measurements showed that the enzyme closes the DNA-binding cleft slightly (by 5 Å) upon binding to non-specific DNA. It can further be deduced that the enzyme remains in this relatively open conformation during the sliding process and closes the DNA-binding cleft considerably (by 14 Å) after binding to the specific recognition site.

Furthermore, it can be seen that PvuII undergoes relatively large conformational changes, which can be attributed to the fact that changes in the conformation of PvuII are mainly characterized by quaternary conformational changes rather than by local conformational changes (see 1.1.1.1). The motion of the two subunits occurs in a pure tongue-like motion, which is characterized by a translation of the subunits that is nearly perpendicular to the DNA axis [23]. This translation is characterized by a rotation of 46° around an axis almost completely parallel to the DNA axis [23], which indicates a considerably opening/closing movement around the DNA. This explains the large changes of FRET efficiencies. Local conformational changes were not described for PvuII so far. The order and the degree of conformational changes are summarized in Figure 63.

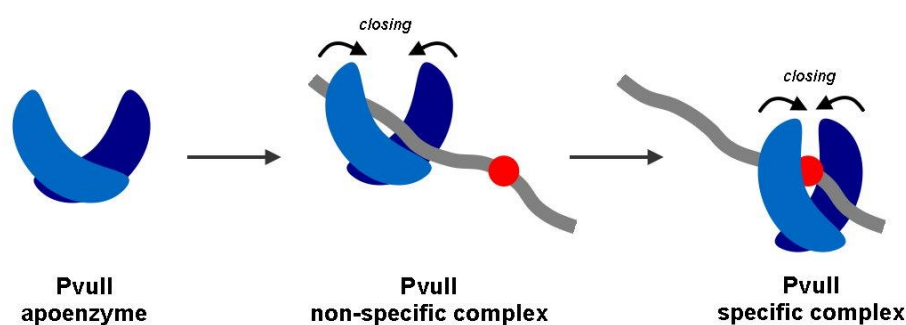


Figure 63: Summary of conformational changes of the restriction enzyme PvuII. The apoenzyme of PvuII has an open conformation, which does not allow accommodating DNA with both subunits simultaneously. The contact of the L-AB loop with the DNA molecule triggers a slight closing of the DNA-binding cleft. PvuII remains in this relatively open conformation to slide along the DNA. The contact with the specific recognition site triggers the two subunits to move toward each other in a tongue-like motion, thereby closing the DNA-binding cleft considerably.

EcoRV D214C

The measurements revealed corrected FRET efficiencies of 0.19 for the apoenzyme, 0.14 for the non-specific complex and 0.26 for the specific complex, respectively (see Table 32 and Figure 64, orange numbers). By comparing apoenzyme and non-specific complex, it can be seen that the FRET efficiency decreased by 0.05, which means that the enzyme slightly opens its DNA-binding cleft upon non-specific binding. Comparing apoenzyme and specific complex, the FRET efficiency increased by 0.07, which means that the enzyme slightly closes its DNA-binding cleft upon specific binding. The difference between non-specific and specific complex was found to be 0.12, which means that the enzyme closes the DNA-binding cleft when switching from the non-specific to the specific binding mode and that the specific complex is more closed than the non-specific complex.

This first comparison showed that for sliding EcoRV adopts a conformation which is more open than the conformation of the apoenzyme and the specifically bound enzyme. Since the differences between the non-specific complex, the apoenzyme and the specific complex are marginal (0.05 - 0.12) and since the conformation of the apoenzyme and the specific complex are both relatively closed, it is assumed that EcoRV uses also a more closed conformation for sliding.

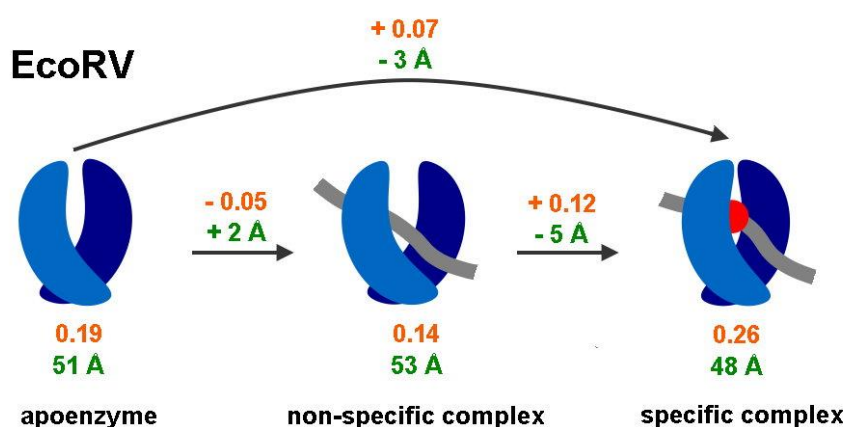


Figure 64: Summary of FRET efficiencies and calculated distances for the restriction enzyme EcoRV. FRET efficiencies and FRET efficiency changes are indicated in orange, distances and distance changes are indicated in green.

At first sight, the results of the FRET measurements did not fit the available crystal structures of EcoRV. The distances in the crystal structures of the apoenzyme, the non-specific and the specific complex were found to be 47 Å, 57 Å and 48 Å, respectively [30] (see Table 27). It can be seen that the distance change between the apoenzyme and the non-specific complex is relatively high (10 Å) whereas the distance change between the apoenzyme and the specific complex is extremely low (1 Å); the change in the FRET efficiency however, was found to be similar (0.05 and 0.07). For this reason, the results of the FRET measurements could not be reconciled with the available crystal structures of Winkler only. Since for EcoRV several different crystal and co-crystal structures exist, they were also measured regarding the distance of the two cysteine residues at position 214. For the apoenzyme, one further crystal structure exists (1AZ3) in which the distance was found to be 51 Å [25], for the non-specific complex, also one further co-crystal structure exists (2BOD) in which the distance was found to be 50 Å [32] and for the specific complex two further co-crystal structures exist (1B94 and 1EOP) in which the distances were found to be 51 Å [98,99].

The biggest difference between all these available structures exists for the non-specific complex (57 Å in the Winkler structure vs. 50 Å in the Hiller structure) which can be attributed to the fact that different non-specific oligonucleotides were used for crystallization (Winkler et al. used two 8mer duplexes, Hiller et al. used one 11mer duplex). The FRET efficiencies could best be reconciled with a distance of 51 Å for the apoenzyme (distance found in the structure of Perona [25]) and a distance of 48 Å for the specific complex (distance found in the structure of Winkler [30]), resulting in a distance of 53 Å for the non-specific complex which is right in the middle of the distances found in the structure of Hiller and Winkler, respectively. Again, one has to keep in mind that a crystal structure only represents a protein which has been frozen in a certain step of a dynamic process, whereas in the FRET measurements the dynamic behavior of the proteins is preserved. Based on the above mentioned assumption, it can further be derived that the enzyme opens its DNA-binding cleft by 2 Å (equivalent to a FRET efficiency change of 0.05) upon non-specific binding and closes again by 5 Å (equivalent to a FRET efficiency change of 0.07) upon specific binding. The distances and distance changes of EcoRV are summarized in Figure 64 (green numbers).

The results of the FRET measurements perfectly fit the conformational changes described so far in the literature for EcoRV [23,25,27,30,32]. The crystal structure of the apoenzyme implied that the DNA-binding cleft is not sufficiently open to allow DNA entry. It was therefore postulated that a contact of the C-terminal α -helices with the DNA stimulates opening of the DNA-binding cleft [33]. Indeed, the FRET measurements showed that the enzyme opens the DNA-binding cleft slightly (by 2 Å) upon binding to non-specific DNA. It can further be deduced that the enzyme remains in this relatively closed conformation during the sliding process and closes the DNA-binding cleft again slightly (by 5 Å) after binding to the specific recognition site. It can be seen that EcoRV undergoes relatively small conformational changes, which can be attributed to the fact that changes in the conformation of EcoRV are mainly characterized by local conformational changes rather than by quaternary conformational changes as it postulated for PvuII. The motion of the two subunits predominantly occurs in a scissor-like motion, which is characterized by a translation of the subunits which is more parallel to the DNA axis [23]. This translation is characterized by a rotation of 23° around an axis more perpendicular to the DNA axis [23], which indicates that the orientation of the subunits changes only slightly. This explains also the small changes of the FRET efficiencies.

The local conformational changes which especially occur in EcoRV (like ordering of the Q- and the R-loop) cannot be detected with the FRET measurements. The order and the degree of conformational changes are summarized in Figure 65.

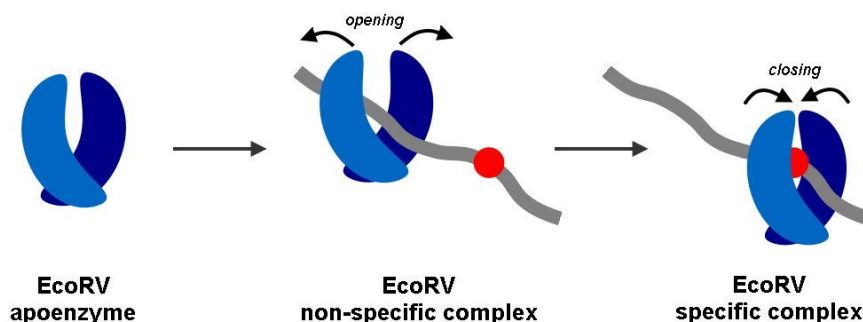


Figure 65: Summary of conformational changes for the restriction enzyme *EcoRV*. The EcoRV apoenzyme has a closed conformation, which does not allow DNA entry. The contact of the C-terminal α -helices with the DNA molecule triggers a slight opening of the DNA-binding cleft. EcoRV remains in this relatively closed conformation to slide along the DNA. The contact with the specific recognition site triggers the two subunits to move toward each other in a more scissor-like motion, thereby closing the DNA-binding cleft again slightly.

BsoBI A153C

The measurements revealed corrected FRET efficiencies of 0.46 for the apoenzyme, 0.45 for the non-specific complex and 0.26 for the specific complex, respectively (see Table 32). By comparing apoenzyme and non-specific complex, it can be seen that the FRET efficiency is almost identical, which suggests that the enzyme does not change its conformation upon non-specific binding. Comparing apoenzyme and specific complex, the FRET efficiency decreased by 0.20, which suggests that the enzyme opens its DNA-binding cleft upon specific binding. It also indicates that the specific complex is apparently more open than the non-specific complex. Although the hypothesis that BsoBI undergoes large conformational changes in order to allow DNA entry [36] could be confirmed (FRET efficiency changed by 0.20 upon specific binding), the direction of the changes was unexpected. It was expected that the FRET efficiency increases upon specific binding, which means that the enzyme closes its DNA-binding cleft, as it could be shown for PvuII and EcoRV. Also previous experiments performed by Jasmina Dikic [105], including steady-state ensemble as well as single-molecule measurements, revealed the same unexpected results. It was concluded that the conformational changes in BsoBI cannot be explained by a simple closing/opening of the DNA-binding cleft in a tongue- or scissor-like movement, as it assumed for PvuII or EcoRV.

The conformational changes could best be explained assuming a twisting-like motion of the two subunits of BsoBI, by which upon specific binding the DNA-binding cleft closes while the residues located at position 153 however move away from each other [105]. If with this explanation, the DNA-binding cleft is considered to be closed in the specific complex and open in the apoenzyme, this would consequently mean that the DNA-binding cleft is also open in the non-specific complex, since the FRET efficiencies of the apoenzyme and the non-specific complex were found to be similar (0.46 vs. 0.45). No change of the FRET efficiency upon binding to a non-specific 12 bp oligonucleotide has been observed also by Jasmina Dikic in single-molecule experiments [105]. Interestingly, the addition of a non-specific 39 bp oligonucleotide induced a decrease of the FRET efficiency, which in a twisting-like motion would mean a closing of the DNA-binding cleft. It was therefore concluded that the conformation BsoBI uses for sliding is more closed than the conformation of the apoenzyme [105]. It can be seen that the conformational changes of BsoBI are more complex and cannot be explained by single FRET measurements. A definitive answer regarding the non-specific complex of BsoBI requires further experiments (e.g. labeling at different sites in the protein) or the solution of the crystal structure. Nevertheless, it is not assumed that BsoBI greatly deviates from its ‘tunnel conformation’, because a tunnel could be a strategy to promote linear diffusion [36]. However, it is assumed that the conformation BsoBI adopts for sliding is ‘tunnel-like’, on the one hand closed enough to prevent falling off the DNA and on the other hand open enough to prevent friction between the protein and the DNA.

Another interesting observation that could be made during the FRET measurements, is that the apoenzyme of BsoBI and EcoRV exist in at least two different conformations in solution, depending on the presence of divalent metal ions. It has been postulated earlier that restriction enzymes oscillate between a ‘closed’ and an ‘open’ state [33,100]. However, these observations could not be made for PvuII. It is therefore possible that only restriction enzymes whose DNA-binding cleft is not open enough to directly bind to DNA (such as EcoRV and BsoBI) switch between different conformations in solution. Since the DNA-binding cleft of PvuII is already open enough, no conformational changes in solution are necessary.

4.2.3 Studying linear diffusion of structurally different restriction enzymes

Linear diffusion has been studied in detail for EcoRI [40,44] and more extensively for EcoRV [31,45](see also 1.1.1.2). In these studies several aspects were investigated such as the influence of the substrate length and the concentration of mono- and divalent cations on linear diffusion, the effect of obstacles and star sites, overlooking of specific sites, reflection at the ends of DNA and the mechanism of product dissociation. So far not under investigation was, whether linear diffusion depends on the structure of a restriction enzyme, especially on the conformation of the DNA-binding cleft. In this work the dependence of linear diffusion on the substrate length and the salt concentration has been examined in a comparative manner for the structurally different restriction enzymes EcoRV, PvuII and BsoBI. All enzymes are homodimeric 6 bp cutter but differ in the conformation of their DNA-binding cleft (Figure 35). It seems reasonable to assume that the structural features of the three enzymes will affect their ability to make use of linear diffusion. It has been hypothesized that the more open the DNA-binding cleft, the smaller the contribution of linear diffusion to target site location.

Substrate length dependence

It has been shown in earlier studies that the degree of linear diffusion depends on the length of the DNA substrate [31,40,45]. To find out whether the substrate length dependence is similar for the three enzymes, competitive cleavage experiments were carried out under identical conditions.

The results showed that the cleavage rates of the long and the short fragment (k_{long} and k_{short}) and consequently the total cleavage rates (k_{total}) decreased with increasing length of the PCR fragment (Table 33, Table 34 and Table 35). This observation can be attributed to the fact that the longer the PCR fragment the more non-specific DNA is present in the reaction mixture, which reduces the concentration of free enzyme and thereby the cleavage rate (so called ‘trapping effect’ of non-specific DNA [101]). This effect was most pronounced for BsoBI (k_{total} was reduced from 2.01 min⁻¹ for the 26mer to 0.299 min⁻¹ for the 1488mer by a factor of 6.7) and less pronounced for EcoRV (factor 6.2) and PvuII (factor 5.2), indicating that BsoBI can be trapped more effectively on non-specific DNA than EcoRV and PvuII, which can be correlated with a longer residence time on non-specific DNA. Further experiments revealed that the trapping effect of non-specific DNA depends on the continuity of the DNA substrate.

The 26mer was cleaved 3-times faster by BsoBI when the 958mer was digested prior to the competitive cleavage reaction, although the same amount of non-specific DNA was present in the reaction mixture (Table 36). Due to the fragmentation of the 958mer, less BsoBI was trapped in a sliding movement on non-specific DNA and thereby more BsoBI was available to cleave the 26mer which increased the cleavage rate. This revealed that BsoBI can be trapped more effectively on long DNA substrates than on shorter ones, suggesting that the residence time on long fragments is longer than on short fragments. In case of EcoRV and PvuII instead, the 26mer was cleaved with nearly the same rate, independent of whether the 958mer was digested prior to the competitive cleavage reaction or not. This revealed that EcoRV and PvuII can be trapped on short and long fragments equally well, suggesting that the residence time on long fragments is comparable to that on short fragments.

Furthermore, the results showed that the cleavage of the long fragment was always faster than the cleavage of the short fragment ($k_{long} > k_{short}$), which can be attributed to a contribution of linear diffusion to the searching process. k_{short} characterizes the rate of cleavage resulting from direct binding to the specific site (3D-diffusion), whereas k_{long} characterizes the rate of cleavage resulting from initial non-specific binding and subsequent sliding to the specific site (1D- and 3D-diffusion) (see also Figure 48). The probability that the protein makes a direct collision with the specific site is low and it is more likely that the initial contact will be non-specific. The following 1D-diffusion along non-specific DNA effectively decreases the search volume of the protein which accelerates the location of the target site. This property of long substrates is also referred to as ‘antenna effect’ of non-specific DNA [101]. Further experiments showed that the antenna effect can be eliminated and linear diffusion thereby prevented. After digestion of the 958mer prior to the competitive cleavage reaction, the short and the (fragmented) long substrate were cleaved with essentially the same rate ($k_{long} = k_{short}$), resulting from the fact that the predigested 958mers were cleaved much slower than the undigested 958mers. Due to the fragmentation of the 958mer, non-specific DNA could no longer serve as antenna and linear diffusion could no longer contribute to the searching process, thereby reducing the rate of cleavage.

The above mentioned preferential cleavage of long substrates over the short ones, which can also be expressed in the ratio of the cleavage rates (k_{long}/k_{short}), was found to increase with increasing length of the long substrate (see Figure 52). However, the dependence on the substrate length was found to be different for the three enzymes, demonstrating that linear diffusion is used to a different extent. The length dependence was most pronounced for BsoBI (e.g. the 958mer was cleaved 5.79-times faster than the 26mer), second most pronounced for EcoRV (e.g. the 958mer was cleaved 3.08-times faster than the 26mer) and least pronounced for PvuII (e.g. the 958mer was cleaved 1.74-times faster than the 26mer), indicating that BsoBI is using the antenna effect of non-specific DNA most effectively to accelerate target location. The length dependence of (k_{long}/k_{short}) is directly relevant to the sliding length, which is the average number of base pairs scanned within one binding event [102](Figure 66). If the length of the substrate is smaller than the sliding length, (k_{long}/k_{short}) is virtually proportional to the length of the substrate, because of the antenna effect. Every binding event would lead to cleavage of the specific site. If the length of the substrate is greater than the sliding length, not every binding event would lead to cleavage of the specific site, since the probability increases that the enzyme dissociates before finding the specific site by linear diffusion, which explains the asymptotical dependence of (k_{long}/k_{short}) on the substrate length. Accordingly, it can be derived from Figure 52 that BsoBI scans more base pairs within one binding event than EcoRV or PvuII.

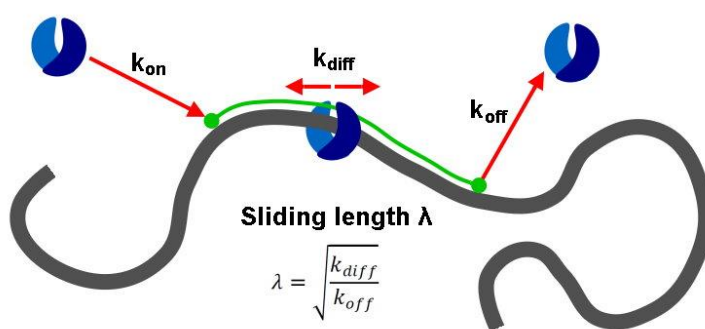


Figure 66: Sliding length. After non-specific association to the DNA molecule (k_{on}), the sliding length λ depends on the probability that the enzyme slides one step (k_{diff}) rather than dissociates from the DNA (k_{off}). The cleavage rate can only be enhanced by linear diffusion, if dissociation is slow (low k_{off}) or/and linear diffusion is fast (high k_{diff}).

The fact that BsoBI is using linear diffusion to a higher degree than EcoRV and PvuII can be attributed to the fact that BsoBI spends more time diffusing along non-specific DNA and thereby is able to scan more base pairs within one binding event. A long residence time (also called dwell time) on non-specific DNA should be reflected in the non-specific binding constant (K_D) of the enzymes.

The dwell time (τ) is related to dissociation rate constant (k_{off}) by $\tau = 1/k_{off}$, which can be calculated by $k_{off} = K_D * k_{on}$ from the non-specific binding constant (K_D) (see Table 31), assuming that the association rate constant (k_{on}) is identical for the three enzymes and diffusion controlled ($k_{on} = 10^8 \text{ M}^{-1}\text{s}^{-1}$). The calculations revealed an expected short dwell time for PvuII (5 ms), the dwell time for BsoBI however, was not as long as expected (27 ms), instead EcoRV showed the longest dwell time (145 ms). There are different possibilities how to explain the discrepancy. One possibility is that the association of BsoBI to non-specific DNA is slower than assumed. This would make sense if one considers that BsoBI has to open the DNA-binding cleft prior to binding. And indeed, it could be shown in pre-steady state experiments that the association to a specific 39mer in the presence of Mg^{2+} -ions was slower than diffusion controlled ($k_{on} = 4.8 \times 10^6 \text{ M}^{-1}\text{s}^{-1}$) [105]. Recalculating the dwell time for BsoBI with this value of k_{on} yields 557 ms, which is longer than the dwell time of EcoRV. Another possibility is that the diffusion along the DNA (k_{diff}) is much faster for BsoBI compared to EcoRV. If the dwell time of BsoBI is shorter than that of EcoRV, BsoBI has to move much faster in order to scan the same amount of base pairs within in one binding event. A third possibility is that the low binding affinity (and thereby the short dwell time) is only valid for short substrates (for the determination of K_D a 16-bp oligonucleotide was used) and would be much higher for long substrates. This theory is consistent with the finding that BsoBI could be trapped much better on long substrates than on short ones (see 3.2.3.1). It would also explain why no conformational changes could be observed in the presence of a non-specific 16mer but in the presence of a non-specific 39mer [105]. Since BsoBI presumably forms a tunnel around non-specific DNA, it is more likely that it falls-off the ends (which would happen faster if the substrate is short) rather than opening the DNA-binding cleft. However, in order to elucidate which of the three options is the correct one, further experiments are necessary to determine for example the association rate constant (k_{on}), the one-dimensional diffusion coefficient (D_1) and the dwell time (τ) on longer DNA substrates for BsoBI. But, regardless of what the correct explanation is, it remains the fact that the sliding length of BsoBI is longer than that of EcoRV and PvuII, indicating that BsoBI uses linear diffusion most effectively.

Salt dependence

In early studies with EcoRI [40,42,43] and EcoRV [31,45] it was shown that the effect of facilitated diffusion on target site location is salt dependent. To find out whether the salt dependence is similar for the three enzymes, competitive cleavage experiments were carried out in the presence of 20, 50, 100 and 200 mM NaCl under otherwise identical conditions.

The salt dependence of linear diffusion can be ascribed to the fact that salt influences both the non-specific binding constant (K_D) and the one-dimensional diffusion coefficient (D_1). Both parameters influence the sliding length (see Figure 66) and thereby the efficiency of linear diffusion. High salt concentrations are expected to increase K_D , mainly by increasing k_{off} since the rate of association (k_{on}) is only moderately affected by salt [38]. A high k_{off} leads to a shorter interaction time (τ) with the DNA, which reduces the sliding length (λ) and thereby the efficiency of linear diffusion. The effect of salt on the one-dimensional diffusion coefficient (D_1) is controversial. It was first assumed that D_1 would be independent of the salt concentration, since the protein remains in contact with the DNA, hopping instead was expected to be dependent, since dissociation and re-association events are involved in the mechanism [71]. However, it could be shown in single-molecule experiments [67] as well as in bulk ensemble measurements [101] that D_1 increased with increasing salt concentration. In the first instance this suggests that increasing the salt concentration would increase the efficiency of linear diffusion, since a high D_1 increases the sliding length. Nevertheless, the experiments also revealed that in total the sliding length and thereby the efficiency of linear diffusion was reduced with increasing salt concentration [67,101], which implies that the negative effect on the interaction time was much more pronounced than the positive effect on D_1 .

The results in Figure 58 showed that only the k_{long}/k_{short} values for EcoRV continuously decreased with increasing NaCl concentration, however Jeltsch et al. [31,45] found a maximum for EcoRV at 50 mM NaCl. The k_{long}/k_{short} values for PvuII only initially decreased (when increasing the NaCl concentration from 20 to 50 mM) and then remained approximately at the same level, indicating that already NaCl concentrations > 50 mM reduce the efficiency of linear diffusion considerably. In contrast, such a low efficiency of linear diffusion ($k_{long}/k_{short} \approx 1.8$) was seen with EcoRV and BsoBI only at a NaCl concentration > 200 mM.

The k_{long}/k_{short} values for BsoBI initially increased (when increasing the NaCl concentration from 20 to 50 mM) and then continuously decreased with increasing NaCl concentration, indicating that the efficiency of linear diffusion is reduced at NaCl concentrations < 50 mM and > 150 mM. Low salt concentrations should normally increase the efficiency of linear diffusion. On the other hand, one has to consider that salt has the function of balancing electrostatic interactions or hydrogen bonds between the protein and the DNA. If they are unbalanced, binding between protein and DNA becomes too strong and increases the friction. In order to move on, interactions have to be broken which reduces the rate of linear diffusion [31,45].

The results showed indeed that the salt dependence of linear diffusion is different for the three enzymes. This was expected since all enzymes have a different protein-DNA interface with different hydrogen bonds and electrostatic interactions. Between 50 and 100 mM NaCl the efficiency of linear diffusion remained mostly the same for each enzyme. Decreasing the NaCl concentration to 20 mM led to either a higher degree of linear diffusion for PvuII or to a lower degree of linear diffusion for BsoBI. At 200 mM NaCl facilitated diffusion is much less effective than at 100 mM NaCl for all enzymes, indicating that ionic strength above the physiological value (150 mM) reduces the effectiveness of facilitated diffusion considerably.

Structure dependence

The structure dependence of linear diffusion can be studied particularly well if one introduces structural changes into the same enzyme. This has been done already for EcoRV, where individual hydrogen bond acceptors or donors and positive charges had been removed from the DNA-binding cleft of the protein, leading to variants for which linear diffusion was impaired or even abolished [31]. In this work the effect of a defined structural change was investigated (see Figure 59).

The results in Table 40 showed that small as well as large structural changes influenced the efficiency of linear diffusion. By fusing EcoRV to the elongated protein scRM6 the hydrodynamic radius was increased. It could be shown in single-molecule experiments that the one-dimensional diffusion coefficient (D_1) of the fusion protein was reduced by a factor of 4 compared to EcoRV (see 3.1.4 and [90]). This observation could now be confirmed by ensemble measurements since the fusion protein showed a lower value of k_{long}/k_{short} compared to wild type EcoRV, indicating that the efficiency of linear diffusion was reduced.

By connecting the two subunits of PvuII with a short peptide linker the DNA-binding cleft became more closed (the distance of the symmetry-related cysteine residues at position 125 decreased from 67 Å in PvuII to 58 Å in scPvuII) [93]. It could be shown that the k_{long}/k_{short} values for scPvuII were larger than for wild type PvuII, indicating that this small change allows scPvuII to make better use of linear diffusion than the wild type. In addition, this observation confirms the above mentioned hypothesis.

Final conclusion

The results of the linear diffusion analysis (3.2.3) perfectly fit the results of the conformation analysis (3.2.2) and confirm the hypothesis that restriction enzymes with a relatively open DNA-binding cleft make less use of linear diffusion than enzymes with a more closed DNA-binding cleft.

PvuII was found to adopt an open conformation while sliding along the DNA and showed the lowest degree of linear diffusion. Conformational changes in PvuII are characterized by rigid body motions in a tongue-like movement, which are supposed to facilitate fast association and dissociation [27]. Additionally, it could be shown for PvuII that only small conformational changes are needed to associate with or dissociate from non-specific DNA (slight closing/opening of the DNA-binding cleft). This suggests that the probability of dissociation is much higher than the probability of linear diffusion, resulting in a shorter interaction time with non-specific DNA (which has been confirmed by a high K_D for PvuII) and consequently in a shorter sliding length and a low degree of linear diffusion. Additionally, a search mechanism consisting of mainly association and dissociation events is supposed to be more impaired by salt than a pure sliding mechanism. This explains why already small salt concentrations (> 50 mM) decreased the interaction time and consequently the degree of linear diffusion.

EcoRV was found to adopt a more closed conformation while sliding along the DNA and showed a higher degree of linear diffusion than PvuII. Conformational changes in EcoRV are characterized mainly by local rearrangements and only few by rigid body motions in a scissor-like movement. Such motions are not supposed to facilitate fast association and dissociation. This suggests that the probability of linear diffusion is much higher than the probability of dissociation, resulting in a longer interaction time with non-specific DNA (which has been confirmed by a low K_D for EcoRV) and consequently in a longer sliding length and a higher degree of linear diffusion. Due to a different mechanism, the degree of linear diffusion was affected only at salt concentrations > 150 mM.

For **BsoBI** it was assumed that it adopts a closed (‘tunnel-like’) conformation while sliding along the DNA and showed the highest degree of linear diffusion. The exact conformational changes in BsoBI are not known so far, since only the crystal structure of the specific complex is available, but it was assumed that changes appear in a twisting-like motion [105]. Nevertheless, these kind of motions are not supposed to facilitate fast association and dissociation. Once wrapped around the DNA, it seems more likely that BsoBI diffuses along the DNA rather changes again the conformation in order to dissociate from the DNA. This results in a longer interaction time with non-specific DNA and consequently in a longer sliding length and a higher degree of linear diffusion. A close contact between protein and DNA also explains the finding that linear diffusion was decreased for BsoBI at low salt concentrations. In this case the reducing effect of low salt concentrations on the one-dimensional diffusion coefficient predominates, leading to a higher friction and a lower degree of linear diffusion.

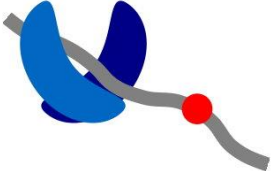
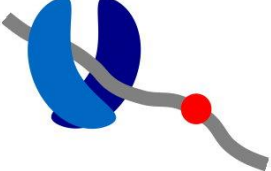
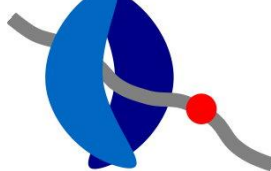
Relation between structure and linear diffusion	PvuII	EcoRV	BsoBI
			
Conformation	Open	Partially closed	Closed
Interaction time (τ)	Short	Intermediate	Long
Sliding length (λ)	Short	Intermediate	Long
Efficiency of linear diffusion	Low	Intermediate	High
Influence of salt	NaCl > 50 mM reduce efficiency	NaCl > 150 mM reduce efficiency	NaCl < 50 mM and NaCl > 150 mM reduce efficiency

Figure 67: Summary of the properties of structurally different restriction enzymes.

It has been proposed that the structural basis for linear diffusion is that the enzyme partly wraps around the DNA and that both components are held together by electrostatic interactions and hydrogen bonds [31]. By the comparison of structurally different restriction enzymes, it can be further assumed that the wrapping around the DNA might be a strategy of the enzyme to stay in longer contact with the DNA. The more pronounced the wrapping, the longer the interaction time and the higher the contribution of linear diffusion to the mechanism of target site location.

5 Summary

Many biological functions depend on interactions between DNA and site-specific DNA-binding proteins, which must locate their specific target site within a high excess of non-specific sites. Several proteins make use of a process called facilitated diffusion, which is based on translocations of the protein along non-specific DNA and accelerates target site location. Different mechanisms involved in facilitated diffusion, such as sliding, hopping or jumping and intersegment transfer, have been discussed. Type II restriction enzymes are model systems for studying protein-DNA interactions and their target search mechanism has been investigated intensively by bulk ensemble as well as by single-molecules experiments. Two open questions related to the sliding (linear diffusion) mechanism of Type II restriction enzymes have been addressed in this work.

The first aim of this work was to investigate whether the sliding mechanism of Type II restriction enzymes is coupled to rotation. To this end, different variants of an 'elongated' restriction enzyme, consisting of EcoRV and the quasi-linear protein scRM6, have been prepared. Two important prerequisites for the visualization of rotational motion are: a preserved activity and a correct spatial orientation. Binding- and cleavage experiments demonstrated that the activity could be preserved, although being reduced by one to two orders of magnitude compared to EcoRV alone. FRET measurements however revealed that the extension component scRM6 is not maximally stretched out and hence the spatial orientation is not optimal. Rotational movement of the fusion protein scRM6-EcoRV could successfully be demonstrated indirectly by measuring the linear diffusion coefficient (D_1) using single-molecule experiments and comparing it to theoretical models. However, direct visualization of rotational movement using super-resolution microscopy has not been possible due to suboptimal spatial orientation of the fusion protein and speed and randomness of the diffusional motion.

The second aim of this work was to investigate whether the structure of a restriction enzyme influences the degree of sliding. To this end, the structurally different Type II restriction enzymes PvuII, EcoRV and BsoBI were compared regarding their conformation in complex with DNA and their ability to make use of linear diffusion. It was hypothesized that the more open the enzyme-DNA complex, the less linear diffusion is used by the enzyme. FRET measurements were performed to elucidate the conformation of the restriction enzyme in complex with non-specific DNA (sliding conformation), especially the extent of opening of the DNA-binding cleft. The measurements revealed that PvuII

adopts an open conformation for sliding, whereas EcoRV and BsoBI adopt a more closed conformation. Conventional kinetic methods were performed to investigate the linear diffusion behavior and revealed that linear diffusion is used most effectively by BsoBI to speed up target site location and less effectively by EcoRV and PvuII. Additionally, it could be demonstrated that the ionic strength dependence of linear diffusion is different for the three enzymes. Enzymes with an open conformation (PvuII) are more affected by salt than enzymes with a more closed conformation (EcoRV, BsoBI). The results of the conformation analysis could be perfectly correlated with the results of the linear diffusion analysis and confirmed the hypothesis that restriction enzymes with a relatively open DNA-binding cleft make less use of linear diffusion than enzymes with a more closed DNA-binding cleft. The hypothesis could be further confirmed by studying the linear diffusion behavior of enzyme variants in which a defined structural change had been introduced.

6 Zusammenfassung

Viele biologische Funktionen hängen von Wechselwirkungen zwischen DNA und spezifischen DNA-Bindungproteinen ab, die ihre spezifische Zielsequenz im hohen Überschuss nicht-spezifischer Sequenzen auffinden müssen. Verschiedene Proteine haben einen Prozess namens ‚erleichterter Diffusion‘ entwickelt, der auf einer Translokation des Proteins entlang nicht-spezifischer DNA beruht und das Auffinden der Zielsequenz beschleunigt. Verschiedene Mechanismen der erleichterten Diffusion, wie z.B. Gleiten, Hüpfen oder Springen und Intersegmenttransfer, wurden diskutiert. Typ II-Restriktionsenzyme dienen als Modellsysteme für die Untersuchung von Protein-DNA Wechselwirkungen und ihr Suchmechanismus wurde bereits intensiv durch ‚Bulk-Ensemble‘ sowie durch Einzelmolekülexperimente untersucht. Zwei offene Fragen im Zusammenhang mit dem Gleitmechanismus (lineare Diffusion) der Typ II-Restriktionsenzyme wurden in dieser Arbeit adressiert.

Das erste Ziel dieser Arbeit war es zu untersuchen, ob der Gleitmechanismus von Typ II-Restriktionsenzymen mit einer Rotationsbewegung verbunden ist. Hierzu sind verschiedene Varianten eines ‚verlängerten‘ Restriktionsenzym, bestehend aus EcoRV und dem quasi-linearen Protein scRM6, hergestellt worden. Zwei wichtige Voraussetzungen für die Visualisierung einer Rotationsbewegung sind: eine konservierte Aktivität und eine korrekte räumliche Orientierung. Bindungs- und Spaltexperimente zeigten, dass die Aktivität bewahrt werden konnte, wenn sie auch im Vergleich zu EcoRV alleine um ein bis zwei Größenordnungen reduziert war. FRET-Messungen zeigten hingegen, dass die ‚Erweiterungskomponente‘ scRM6 nicht maximal ausgestreckt und damit die räumliche Orientierung nicht optimal ist. Die Rotationsbewegung des Fusionsproteins scRM6-EcoRV konnte erfolgreich durch Messung des linearen Diffusionskoeffizienten (D_1) unter Verwendung von Einzelmolekülmessungen und dem Vergleich mit theoretischen Modellen indirekt nachgewiesen werden. Allerdings war die direkte Visualisierung der Rotationsbewegung mittels superhochauflösender Mikroskopie aufgrund der suboptimalen räumlichen Orientierung des Fusionsproteins und der Geschwindigkeit sowie zufälligen Richtung der diffusen Bewegung nicht möglich.

Das zweite Ziel dieser Arbeit war es zu untersuchen, ob die Struktur eines Restriktionsenzym das Ausmaß des Gleitens beeinflussen kann. Zu diesem Zweck wurden die strukturell unterschiedlichen Typ II-Restriktionsenzyme PvuII, EcoRV und BsoBI hinsichtlich

ihrer Konformation im Komplex mit DNA und ihrer Fähigkeit zur Verwendung von linearer Diffusion verglichen. Es wurde angenommen, dass je offener der Enzym-DNA Komplex ist, desto weniger lineare Diffusion durch das Enzym verwendet wird. FRET-Messungen wurden durchgeführt um die Konformation des Restriktionsenzym im Komplex mit nicht-spezifischer DNA (Konformation des Gleitens), insbesondere das Ausmaß der Öffnung der DNA-Bindungsspalte, aufzuklären. Die Messungen ergaben, dass PvuII eine offene Konformation zum Gleiten einnimmt, während EcoRV und BsoBI eine eher geschlossene Konformation einnehmen. Konventionelle kinetische Methoden wurden verwendet, um das lineare Diffusionsverhalten zu untersuchen und zeigten, dass lineare Diffusion am effektivsten von BsoBI zur beschleunigten Auffindung der Zielsequenz verwendet wird und weniger effektiv durch EcoRV und PvuII. Darüber hinaus konnte gezeigt werden, dass die drei Enzyme eine unterschiedliche Ionenstärkeabhängigkeit in Bezug auf lineare Diffusion aufweisen. Enzyme mit einer offenen Konformation (PvuII) werden stärker in ihrem linearen Diffusionsvermögen von Salz beeinflusst als Enzyme mit einer eher geschlossenen Konformation (EcoRV, BsoBI). Die Ergebnisse der Konformationsanalyse konnten perfekt mit den Ergebnissen der linearen Diffusionsanalyse in Einklang gebracht werden und die Hypothese, dass Restriktionsenzyme mit einer relativ offenen DNA-Bindungsspalte mehr Gebrauch von linearer Diffusion machen als Enzyme mit einer geschlossenen DNA-Bindungsspalte, bestätigen. Die Hypothese konnte durch Untersuchungen des linearen Diffusionsverhaltens von Enzymvarianten, in denen eine definierte Strukturänderung eingeführt wurde, weiter bestätigt werden.

7 References

1. Anderson, J.E. (1993) Restriction endonucleases and modification methylases. *Curr. Opin. Struct. Biol.*, **3**, 24-30.
2. Raleigh, E.A. and Brooks, J.E. (1998) In De Bruijn, F. J., Lupski, J. R. and Weinstock, G. M. (eds.), *Bacterial Genomes*. Chapman & Hall, New York, pp. 78-92.
3. Van Etten, J.L. (2003) Unusual life style of giant chlorella viruses. *Annu. Rev. Genet.*, **37**, 153-195.
4. Jeltsch, A. (2002) Beyond Watson and Crick: DNA methylation and molecular enzymology of DNA methyltransferases. *ChemBiochem*, **3**, 274-293.
5. Sistla, S. and Rao, D.N. (2004) S-Adenosyl-L-methionine-dependent restriction enzymes. *Crit. Rev. Biochem. Mol. Biol.*, **39**, 1-19.
6. Bheemanaik, S., Reddy, Y.V. and Rao, D.N. (2006) Structure, function and mechanism of exocyclic DNA methyltransferases. *Biochem. J.*, **399**, 177-190.
7. Smith, H.O. and Nathans, D. (1973) Letter: A suggested nomenclature for bacterial host modification and restriction systems and their enzymes. *J. Mol. Biol.*, **81**, 419-423.
8. Roberts, R.J., Belfort, M., Bestor, T., Bhagwat, A.S., Bickle, T.A., Bitinaite, J., Blumenthal, R.M., Degtyarev, S., Dryden, D.T., Dybvig, K. *et al.* (2003) A nomenclature for restriction enzymes, DNA methyltransferases, homing endonucleases and their genes. *Nucleic Acids Res.*, **31**, 1805-1812.
9. Loenen, W.A., Dryden, D.T., Raleigh, E.A., Wilson, G.G. and Murray, N.E. (2014) Highlights of the DNA cutters: a short history of the restriction enzymes. *Nucleic Acids Res.*, **42**, 3-19.
10. Murray, N.E. (2000) Type I restriction systems: sophisticated molecular machines (a legacy of Bertani and Weigle). *Microbiol. Mol. Biol. Rev.*, **64**, 412-434.
11. Loenen, W.A., Dryden, D.T., Raleigh, E.A. and Wilson, G.G. (2014) Type I restriction enzymes and their relatives. *Nucleic Acids Res.*, **42**, 20-44.
12. Pingoud, A., Wilson, G.G. and Wende, W. (2014) Type II restriction endonucleases--a historical perspective and more. *Nucleic Acids Res.*, **42**, 7489-7527.
13. McClelland, S.E. and Sczcelkun, M.D. (2004) In Pingoud, A. (ed.), *Restriction Endonucleases*. Springer, Berlin, pp. 111-135.
14. Rao, D.N., Dryden, D.T. and Bheemanaik, S. (2014) Type III restriction-modification enzymes: a historical perspective. *Nucleic Acids Res.*, **42**, 45-55.
15. Loenen, W.A. and Raleigh, E.A. (2014) The other face of restriction: modification-dependent enzymes. *Nucleic Acids Res.*, **42**, 56-69.
16. Pingoud, A. and Jeltsch, A. (1997) Recognition and cleavage of DNA by type-II restriction endonucleases. *Eur. J. Biochem.*, **246**, 1-22.
17. Pingoud, A. and Jeltsch, A. (2001) Structure and function of type II restriction endonucleases. *Nucleic Acids Res.*, **29**, 3705-3727.

18. Pingoud, A., Fuxreiter, M., Pingoud, V. and Wende, W. (2005) Type II restriction endonucleases: structure and mechanism. *Cell. Mol. Life Sci.*, **62**, 685-707.
19. Venclovas, C., Timinskas, A. and Siksnys, V. (1994) Five-stranded beta-sheet sandwiched with two alpha-helices: a structural link between restriction endonucleases EcoRI and EcoRV. *Proteins*, **20**, 279-282.
20. Aggarwal, A.K. (1995) Structure and function of restriction endonucleases. *Curr. Opin. Struct. Biol.*, **5**, 11-19.
21. Huai, Q., Colandene, J.D., Chen, Y., Luo, F., Zhao, Y., Topal, M.D. and Ke, H. (2000) Crystal structure of NaeI - an evolutionary bridge between DNA endonuclease and topoisomerase. *EMBO J.*, **19**, 3110-3118.
22. Sussman, J.L., Lin, D., Jiang, J., Manning, N.O., Prilusky, J., Ritter, O. and Abola, E.E. (1998) Protein Data Bank (PDB): database of three-dimensional structural information of biological macromolecules. *Acta Crystallogr D Biol Crystallogr*, **54**, 1078-1084.
23. Little, E.J. and Horton, N.C. (2005) DNA-induced conformational changes in type II restriction endonucleases: the structure of unliganded HincII. *J. Mol. Biol.*, **351**, 76-88.
24. Newman, M., Strzelecka, T., Dorner, L.F., Schildkraut, I. and Aggarwal, A.K. (1995) Structure of Bam HI endonuclease bound to DNA: partial folding and unfolding on DNA binding. *Science*, **269**, 656-663.
25. Perona, J.J. and Martin, A.M. (1997) Conformational transitions and structural deformability of EcoRV endonuclease revealed by crystallographic analysis. *J. Mol. Biol.*, **273**, 207-225.
26. Scheuring-Vanamee, E., Viadiu, H., Lukacs, C.M. and Aggarwal, A.K. (2004) In Pingoud, A. (ed.), *Restriction Endonucleases*. Springer, Berlin, pp. 215-236.
27. Uyar, A., Kurkcuoglu, O., Nilsson, L. and Doruker, P. (2011) The elastic network model reveals a consistent picture on intrinsic functional dynamics of type II restriction endonucleases. *Phys. Biol.*, **8**, 056001.
28. Lukacs, C.M., Kucera, R., Schildkraut, I. and Aggarwal, A.K. (2001) Structure of free BglIII reveals an unprecedented scissor-like motion for opening an endonuclease. *Nat. Struct. Biol.*, **8**, 126-130.
29. Viadiu, H. and Aggarwal, A.K. (2000) Structure of BamHI bound to nonspecific DNA: A model for DNA sliding. *Mol. Cell*, **5**, 889-895.
30. Winkler, F.K., Banner, D.W., Oefner, C., Tsernoglou, D., Brown, R.S., Heathman, S.P., Bryan, R.K., Martin, P.D., Petratos, K. and Wilson, K.S. (1993) The crystal structure of EcoRV endonuclease and of its complexes with cognate and non-cognate DNA fragments. *EMBO J.*, **12**, 1781-1795.
31. Jeltsch, A., Wenz, C., Stahl, F. and Pingoud, A. (1996) Linear diffusion of the restriction endonuclease EcoRV on DNA is essential for the in vivo function of the enzyme. *EMBO J.*, **15**, 5104-5111.
32. Hiller, D.A., Rodriguez, A.M. and Perona, J.J. (2005) Non-cognate enzyme-DNA complex: structural and kinetic analysis of EcoRV endonuclease bound to the EcoRI recognition site GAATTC. *J. Mol. Biol.*, **354**, 121-136.

33. Schulze, C., Jeltsch, A., Franke, I., Urbanke, C. and Pingoud, A. (1998) Crosslinking the EcoRV restriction endonuclease across the DNA-binding site reveals transient intermediates and conformational changes of the enzyme during DNA binding and catalytic turnover. *EMBO J.*, **17**, 6757-6766.
34. Athanasiadis, A., Vlassi, M., Kotsifaki, D., Tucker, P.A., Wilson, K.S. and Kokkinidis, M. (1994) Crystal structure of PvuII endonuclease reveals extensive structural homologies to EcoRV. *Nat. Struct. Biol.*, **1**, 469-475.
35. Cheng, X., Balendiran, K., Schildkraut, I. and Anderson, J.E. (1994) Structure of PvuII endonuclease with cognate DNA. *EMBO J.*, **13**, 3927-3935.
36. van der Woerd, M.J., Pelletier, J.J., Xu, S. and Friedman, A.M. (2001) Restriction enzyme BsoBI-DNA complex: a tunnel for recognition of degenerate DNA sequences and potential histidine catalysis. *Structure (Camb.)*, **9**, 133-144.
37. von Hippel, P.H. and Berg, O.G. (1989) Facilitated target location in biological systems. *J. Biol. Chem.*, **264**, 675-678.
38. Halford, S.E. and Marko, J.F. (2004) How do site-specific DNA-binding proteins find their targets? *Nucleic Acids Res.*, **32**, 3040-3052.
39. Jeltsch, A. and Urbanke, C. (2004) In Pingoud, A. (ed.), *Restriction Endonucleases*. Springer, Berlin, pp. 95-110.
40. Ehbrecht, H.J., Pingoud, A., Urbanke, C., Maass, G. and Gualerzi, C. (1985) Linear diffusion of restriction endonucleases on DNA. *J. Biol. Chem.*, **260**, 6160-6166.
41. Winter, R.B., Berg, O.G. and von Hippel, P.H. (1981) Diffusion-driven mechanisms of protein translocation on nucleic acids. 3. The Escherichia coli lac repressor--operator interaction: kinetic measurements and conclusions. *Biochemistry*, **20**, 6961-6977.
42. Jack, W.E., Terry, B.J. and Modrich, P. (1982) Involvement of outside DNA sequences in the major kinetic path by which EcoRI endonuclease locates and leaves its recognition sequence. *Proc. Natl. Acad. Sci. U. S. A.*, **79**, 4010-4014.
43. Terry, B.J., Jack, W.E. and Modrich, P. (1985) Facilitated diffusion during catalysis by EcoRI endonuclease. Nonspecific interactions in EcoRI catalysis. *J. Biol. Chem.*, **260**, 13130-13137.
44. Jeltsch, A., Alves, J., Wolfes, H., Maass, G. and Pingoud, A. (1994) Pausing of the restriction endonuclease EcoRI during linear diffusion on DNA. *Biochemistry*, **33**, 10215-10219.
45. Jeltsch, A. and Pingoud, A. (1998) Kinetic characterization of linear diffusion of the restriction endonuclease EcoRV on DNA. *Biochemistry*, **37**, 2160-2169.
46. Stanford, N.P., Szczelkun, M.D., Marko, J.F. and Halford, S.E. (2000) One- and three-dimensional pathways for proteins to reach specific DNA sites. *EMBO J.*, **19**, 6546-6557.
47. Halford, S.E. and Szczelkun, M.D. (2002) How to get from A to B: strategies for analysing protein motion on DNA. *Eur. Biophys. J.*, **31**, 257-267.
48. Townson, S.A., Samuelson, J.C., Bao, Y., Xu, S.Y. and Aggarwal, A.K. (2007) BstYI bound to noncognate DNA reveals a "hemispecific" complex: implications for DNA scanning. *Structure*, **15**, 449-459.

49. Singer, P. and Wu, C.W. (1987) Promoter search by Escherichia coli RNA polymerase on a circular DNA template. *J. Biol. Chem.*, **262**, 14178-14189.
50. Ricchetti, M., Metzger, W. and Heumann, H. (1988) One-dimensional diffusion of Escherichia coli DNA-dependent RNA polymerase: a mechanism to facilitate promoter location. *Proc. Natl. Acad. Sci. U. S. A.*, **85**, 4610-4614.
51. Surby, M.A. and Reich, N.O. (1996) Facilitated diffusion of the EcoRI DNA methyltransferase is described by a novel mechanism. *Biochemistry*, **35**, 2209-2217.
52. Surby, M.A. and Reich, N.O. (1996) Contribution of facilitated diffusion and processive catalysis to enzyme efficiency: implications for the EcoRI restriction-modification system. *Biochemistry*, **35**, 2201-2208.
53. Berg, O.G., Winter, R.B. and von Hippel, P.H. (1981) Diffusion-driven mechanisms of protein translocation on nucleic acids. 1. Models and theory. *Biochemistry*, **20**, 6929-6948.
54. Lieberman, B.A. and Nordeen, S.K. (1997) DNA intersegment transfer, how steroid receptors search for a target site. *J. Biol. Chem.*, **272**, 1061-1068.
55. Coleman, R.A. and Pugh, B.F. (1995) Evidence for functional binding and stable sliding of the TATA binding protein on nonspecific DNA. *J. Biol. Chem.*, **270**, 13850-13859.
56. Joo, C., Balci, H., Ishitsuka, Y., Buranachai, C. and Ha, T. (2008) Advances in single-molecule fluorescence methods for molecular biology. *Annu. Rev. Biochem.*, **77**, 51-76.
57. Bustamante, C. (2008) In singulo biochemistry: when less is more. *Annu. Rev. Biochem.*, **77**, 45-50.
58. Orrit, M. and Bernard, J. (1990) Single pentacene molecules detected by fluorescence excitation in a p-terphenyl crystal. *Phys Rev Lett*, **65**, 2716-2719.
59. Haustein, E. and Schwille, P. (2004) Single-molecule spectroscopic methods. *Curr. Opin. Struct. Biol.*, **14**, 531-540.
60. Wozniak, A.K., Schroder, G.F., Grubmuller, H., Seidel, C.A. and Oesterhelt, F. (2008) Single-molecule FRET measures bends and kinks in DNA. *Proc. Natl. Acad. Sci. U. S. A.*, **105**, 18337-18342.
61. Margittai, M., Widengren, J., Schweinberger, E., Schroder, G.F., Felekyan, S., Haustein, E., Konig, M., Fasshauer, D., Grubmuller, H., Jahn, R. *et al.* (2003) Single-molecule fluorescence resonance energy transfer reveals a dynamic equilibrium between closed and open conformations of syntaxin 1. *Proc. Natl. Acad. Sci. U. S. A.*, **100**, 15516-15521.
62. Gorman, J. and Greene, E.C. (2008) Visualizing one-dimensional diffusion of proteins along DNA. *Nat. Struct. Mol. Biol.*, **15**, 768-774.
63. van den Broek, B., Noom, M.C. and Wuite, G.J. (2005) DNA-tension dependence of restriction enzyme activity reveals mechanochemical properties of the reaction pathway. *Nucleic Acids Res.*, **33**, 2676-2684.
64. Biebricher, A., Wende, W., Escude, C., Pingoud, A. and Desbiolles, P. (2009) Tracking of single quantum dot labeled EcoRV sliding along DNA manipulated by double optical tweezers. *Biophys. J.*, **96**, L50-52.

65. Herbert, K.M., Greenleaf, W.J. and Block, S.M. (2008) Single-molecule studies of RNA polymerase: motoring along. *Annu. Rev. Biochem.*, **77**, 149-176.
66. Crut, A., Koster, D.A., Seidel, R., Wiggins, C.H. and Dekker, N.H. (2007) Fast dynamics of supercoiled DNA revealed by single-molecule experiments. *Proc. Natl. Acad. Sci. U. S. A.*, **104**, 11957-11962.
67. Bonnet, I., Biebricher, A., Porte, P.L., Loverdo, C., Benichou, O., Voituriez, R., Escude, C., Wende, W., Pingoud, A. and Desbiolles, P. (2008) Sliding and jumping of single EcoRV restriction enzymes on non-cognate DNA. *Nucleic Acids Res.*, **36**, 4118-4127.
68. Kim, J.H. and Larson, R.G. (2007) Single-molecule analysis of 1D diffusion and transcription elongation of T7 RNA polymerase along individual stretched DNA molecules. *Nucleic Acids Res.*, **35**, 3848-3858.
69. Wang, Y.M., Austin, R.H. and Cox, E.C. (2006) Single molecule measurements of repressor protein 1D diffusion on DNA. *Phys Rev Lett*, **97**, 048302.
70. Graneli, A., Yeykal, C.C., Robertson, R.B. and Greene, E.C. (2006) Long-distance lateral diffusion of human Rad51 on double-stranded DNA. *Proc. Natl. Acad. Sci. U. S. A.*, **103**, 1221-1226.
71. Blainey, P.C., van Oijen, A.M., Banerjee, A., Verdine, G.L. and Xie, X.S. (2006) A base-excision DNA-repair protein finds intrahelical lesion bases by fast sliding in contact with DNA. *Proc. Natl. Acad. Sci. U. S. A.*, **103**, 5752-5757.
72. Gorman, J., Chowdhury, A., Surtees, J.A., Shimada, J., Reichman, D.R., Alani, E. and Greene, E.C. (2007) Dynamic basis for one-dimensional DNA scanning by the mismatch repair complex Msh2-Msh6. *Mol. Cell*, **28**, 359-370.
73. Tafvizi, A., Huang, F., Leith, J.S., Fersht, A.R., Mirny, L.A. and van Oijen, A.M. (2008) Tumor suppressor p53 slides on DNA with low friction and high stability. *Biophys. J.*, **95**, L01-03.
74. Schurr, J.M. (1979) The one-dimensional diffusion coefficient of proteins absorbed on DNA. Hydrodynamic considerations. *Biophys. Chem.*, **9**, 413-414.
75. Bagchi, B., Blainey, P.C. and Xie, X.S. (2008) Diffusion constant of a nonspecifically bound protein undergoing curvilinear motion along DNA. *J Phys Chem B*, **112**, 6282-6284.
76. Blainey, P.C., Luo, G., Kou, S.C., Mangel, W.F., Verdine, G.L., Bagchi, B. and Xie, X.S. (2009) Nonspecifically bound proteins spin while diffusing along DNA. *Nat. Struct. Mol. Biol.*, **16**, 1224-1229.
77. Bonnet, I. and Desbiolles, P. (2011) The diffusion constant of a labeled protein sliding along DNA. *The European physical journal. E, Soft matter*, **34**, 1-10.
78. Sase, I., Miyata, H., Ishiwata, S. and Kinosita, K., Jr. (1997) Axial rotation of sliding actin filaments revealed by single-fluorophore imaging. *Proc. Natl. Acad. Sci. U. S. A.*, **94**, 5646-5650.
79. Mizuno, H., Higashida, C., Yuan, Y., Ishizaki, T., Narumiya, S. and Watanabe, N. (2011) Rotational movement of the formin mDia1 along the double helical strand of an actin filament. *Science*, **331**, 80-83.
80. Sakata-Sogawa, K. and Shimamoto, N. (2004) RNA polymerase can track a DNA groove during promoter search. *Proc. Natl. Acad. Sci. U. S. A.*, **101**, 14731-14735.

81. Harada, Y., Ohara, O., Takatsuki, A., Itoh, H., Shimamoto, N. and Kinoshita, K., Jr. (2001) Direct observation of DNA rotation during transcription by *Escherichia coli* RNA polymerase. *Nature*, **409**, 113-115.
82. Noji, H., Yasuda, R., Yoshida, M. and Kinoshita, K., Jr. (1997) Direct observation of the rotation of F1-ATPase. *Nature*, **386**, 299-302.
83. Nishizaka, T., Oiwa, K., Noji, H., Kimura, S., Muneyuki, E., Yoshida, M. and Kinoshita, K., Jr. (2004) Chemomechanical coupling in F1-ATPase revealed by simultaneous observation of nucleotide kinetics and rotation. *Nat. Struct. Mol. Biol.*, **11**, 142-148.
84. Kirsch, R.D. and Joly, E. (1998) An improved PCR-mutagenesis strategy for two-site mutagenesis or sequence swapping between related genes. *Nucleic. Acids Res.*, **26**, 1848-1850.
85. Gill, S.C. and von Hippel, P.H. (1989) Calculation of protein extinction coefficients from amino acid sequence data. *Anal. Biochem.*, **182**, 319-326.
86. Huang, Q. and Quinones, E. (2008) A spectroscopic method to determine the activity of the restriction endonuclease EcoRV that involves a single reaction. *Anal. Biochem.*
87. Jeltsch, A., Fritz, A., Alves, J., Wolfes, H. and Pingoud, A. (1993) A fast and accurate enzyme-linked immunosorbent assay for the determination of the DNA cleavage activity of restriction endonucleases. *Anal. Biochem.*, **213**, 234-240.
88. Hillisch, A., Lorenz, M. and Diekmann, S. (2001) Recent advances in FRET: distance determination in protein-DNA complexes. *Curr. Opin. Struct. Biol.*, **11**, 201-207.
89. Zeug, A., Woehler, A., Neher, E. and Ponimaskin, E.G. (2012) Quantitative intensity-based FRET approaches--a comparative snapshot. *Biophys. J.*, **103**, 1821-1827.
90. Dikic, J., Menges, C., Clarke, S., Kokkinidis, M., Pingoud, A., Wende, W. and Desbiolles, P. (2012) The rotation-coupled sliding of EcoRV. *Nucleic Acids Res.*, **40**, 4064-4070.
91. Glykos, N.M., Papanikolau, Y., Vlassi, M., Kotsifaki, D., Cesareni, G. and Kokkinidis, M. (2006) Loopless Rop: structure and dynamics of an engineered homotetrameric variant of the repressor of primer protein. *Biochemistry*, **45**, 10905-10919.
92. Han, R., Li, Z., Fan, Y. and Jiang, Y. (2013) Recent advances in super-resolution fluorescence imaging and its applications in biology. *J Genet Genomics*, **40**, 583-595.
93. Simoncsits, A., Tjornhammar, M.L., Rasko, T., Kiss, A. and Pongor, S. (2001) Covalent joining of the subunits of a homodimeric type II restriction endonuclease: single-chain PvuII endonuclease. *J. Mol. Biol.*, **309**, 89-97.
94. Wolter, S., Schuttpelz, M., Tscherepanow, M., S., V.D.L., Heilemann, M. and Sauer, M. (2010) Real-time computation of subdiffraction-resolution fluorescence images. *J Microsc.*, **237**, 12-22.

95. Huang, B., Wang, W., Bates, M. and Zhuang, X. (2008) Three-dimensional super-resolution imaging by stochastic optical reconstruction microscopy. *Science*, **319**, 810-813.
96. Levitus, M. and Ranjit, S. (2011) Cyanine dyes in biophysical research: the photophysics of polymethine fluorescent dyes in biomolecular environments. *Q. Rev. Biophys.*, **44**, 123-151.
97. Berney, C. and Danuser, G. (2003) FRET or no FRET: a quantitative comparison. *Biophys. J.*, **84**, 3992-4010.
98. Thomas, M.P., Brady, R.L., Halford, S.E., Sessions, R.B. and Baldwin, G.S. (1999) Structural analysis of a mutational hot-spot in the EcoRV restriction endonuclease: a catalytic role for a main chain carbonyl group. *Nucleic Acids Res.*, **27**, 3438-3445.
99. Horton, N.C. and Perona, J.J. (2000) Crystallographic snapshots along a protein-induced DNA-bending pathway. *Proc. Natl. Acad. Sci. U. S. A.*, **97**, 5729-5734.
100. Erskine, S.G., Baldwin, G.S. and Halford, S.E. (1997) Rapid-reaction analysis of plasmid DNA cleavage by the EcoRV restriction endonuclease. *Biochemistry*, **36**, 7567-7576.
101. Esadze, A., Kemme, C.A., Kolomeisky, A.B. and Iwahara, J. (2014) Positive and negative impacts of nonspecific sites during target location by a sequence-specific DNA-binding protein: origin of the optimal search at physiological ionic strength. *Nucleic Acids Res.*, **42**, 7039-7046.
102. Esadze, A. and Iwahara, J. (2014) Stopped-flow fluorescence kinetic study of protein sliding and intersegment transfer in the target DNA search process. *J. Mol. Biol.*, **426**, 230-244.
103. Adam, G. and Delbrück, M. (1968) Reduction of dimensionality in biological diffusion processes. *Structural Chemistry and Molecular Biology* (Rich, A. and Davidson, N., Eds.), 198-215, Freeman & Co., San Francisco.
104. Richter, P.H. and Eigen, M. (1974) Diffusion controlled reaction rates in spheroidal geometry: Application to repressor-operator association and membrane bound enzymes. *Biophys. Chem.*, **9**, 255-263.
105. Dikic, J. (2009) The conformational dynamics of BsoBI, analyzed by fluorescence spectroscopy down to the single molecule level. *Inauguraldissertation, Justus-Liebig University Giessen*.